Study of RNA Structure by Affinity Cleaving

Thesis by

Hogyu Han

In Partial Fulfillment of the Requirements

for the Degree of

Doctor of Philosophy

California Institute of Technology

Pasadena, California

1995

(Submitted March 3, 1994)

Acknowledgments

I would like to thank my research advisor Professor Peter B. Dervan for his thoughtful guidance and support in this work. I also thank the members of the Dervan group, past and present, for supporting this work with discussion, suggestions, and friendships. Special thanks go to Dr. Martha G. Oakley, Prof. Laura L. Kiessling, Junhyeong Cho, Scott F. Singleton, Prof. Mark D. Distefano, Prof. David A. Horne, Scott Carter, Matthew Taylor, William Greenberg, Dr. Jongsung Koh, Dr. Stephen Woski, Dr. Ken Turnbull, Prof. Yitzhak Tor, Joe Hacia, and Guido Kruz.

I appreciate the helpful advice offered by my committee: Professors Judith L. Campbell, Carl S. Parker, John N. Abelson. I also thank Professor Chul-Hak Yang at Seoul National University who introduced me to biological chemistry.

The love, support, and encouragement offered by my mother Sookja Oh, wife Nan Woo, and family have been especially helpful throughout my stay at Caltech.

To My Mother

and Wife

Abstract

Chapter 1. Sequence-Specific Recognition of Double Helical RNA and RNA•DNA by Triple Helix Formation.

The stabilities of eight triple helical pyrimidine•purine•pyrimidine structures comprised of identical sequence but different RNA (R) or DNA (D) strand combinations were measured by quantitative affinity cleavage titration. The differences in equilibrium binding affinities reveal the importance of strand composition. For the sequences studied here, the stabilities of complexes containing a pyrimidine third strand D or R and purine•pyrimidine double helical DD, DR, RD, and RR decrease in order: D + DD, R + DD, R + DR, D + DR > R + RD, R + RR » D + RR, D + RD (pH 7.0, 25 °C, 100 mM NaCl / 1 mM spermine). These findings suggest that RNA and DNA oligonucleotides will be useful for targeting *(i)* double helical DNA and *(ii)* RNA•DNA hybrids if the purine Watson-Crick strand is DNA. However, RNA, but not DNA, oligonucleotides will be useful for sequence-specific binding of *(i)* double helical RNA and *(ii)* RNA•DNA hybrids if the purine Watson-Crick strand is RNA. This has implications for the design of artificial ligands targeted to specific sequences of double helical RNA and RNA•DNA hybrids.

Abstract

Chapter 2. Different Conformational Families of Pyrimidine•Purine•Pyrimidine Triple Helices Depending on Backbone Composition.

Different helical conformations of DNA (D), RNA (R), and DNA•RNA (DR) hybrid double and triple helices have been detected using affinity cleavage analysis. Synthetic methods were developed to attach EDTA•Fe to a single nucleotide on RNA as well as DNA oligonucleotides. Cleavage patterns generated by a localized diffusible oxidant in the major groove on the pyrimidine strand of four purine•pyrimidine double helices consisting of all DNA, all RNA, and the corresponding hybrids reveal that the relative cleavage intensity shifts to the 5′ end of the purine strand increasingly in the order: DD<DR<RD<RR. These results are consistent with models derived from structural studies. In six pyrimidine•purine•pyrimidine triple helices, the altered cleavage patterns of the Watson-Crick pyrimidine strands reveal at least two conformational families: (i) D+DD, R+DD, D+DR, and R+DR and (ii) R+RD and R+RR.

Abstract

Chapter 3. Visualization of RNA Tertiary Structure by RNA-EDTA•Fe(II) Autocleavage. Analysis of tRNA(*U47)^{Phe}•Fe(II).

To test whether intramolecular autocleavage of RNA labeled at a single nucleotide position with EDTA•Fe(II) is a useful approach for the investigation of tertiary structures of RNAs, yeast phenylalanine tRNA-EDTA was synthesized by the incorporation of uridine-EDTA (*U) at position U47. Autocleavage of tRNA(*U47)^{Phe} in the presence of $Fe(NH_4)_2(SO_4)_2$ and dithiothreitol produced a set of cleavage fragments which are in general agreement with the three-dimensional structure derived from x-ray analysis.

Abstract

Chapter 4. Mapping Regions in Eukaryotic Ribosomes That Are Accessible to Methidiumpropyl-EDTA•Fe(II) and EDTA•Fe(II).

Methidiumpropyl-EDTA•Fe(II) (MPE•Fe(II)) and EDTA•Fe(II) were used to investigate the structure of *Drosophila melanogaster* ribosomes. Cleavage reactions were performed on intact ribosomes in cell lysates *in vitro* and analyzed by primer extension with reverse transcriptase using oligodeoxynucleotide primers. Regions of 18S and 28S ribosomal RNAs (rRNAs) which are accessible to MPE•Fe(II) and EDTA•Fe(II) are located almost exclusively within expansion segments. The accessibility of these regions to cleavage indicates that they are exposed on the surface of eukaryotic ribosomes. These results provide valuable information about the overall tertiary structure of rRNA in ribosomes.

Table of Contents

Chapter 1

Sequence-Specific Recognition of Double Helical RNA and RNA•DNA by Triple Helix Formation

Introduction

Oligodeoxyribonucleotide-directed triple helix formation is one of the most versatile methods for the sequence-specific recognition of double helical DNA (1, 2). The ability to target a broad range of DNA sequences, the stabilities of deoxyribonucleic acid triple helical complexes, and the sensitivity to single base mismatches allow single site targeting within megabase DNA (3-5). At least two structural classes of DNA triple helices exist that differ in base triplet interactions, sequence compositions of the third strand, relative orientations, and relative positions of the phosphate-deoxyribose backbones. Pyrimidine oligodeoxyribonucleotides bind purine tracts in the major groove of double helical DNA parallel to the purine Watson-Crick strand (1). Sequence specificity is derived from thymine (T) recognition of adenine•thymine (AT) base pairs (T•AT base triplets) and N-3 protonated cytosine (C^+) recognition of guanine•cytosine (GC) base pairs (C+GC base triplets) (6, 7). Purine-rich oligodeoxyribonucleotides bind purine tracts in the major groove of DNA antiparallel to the Watson-Crick purine strand (8, 9). Sequence specificity is derived from guanine (G) recognition of GC base pairs (G•GC base triplets) and from A or T recognition of AT base pairs (A•AT and T•AT triplets) (8-10). The stabilities of triple helical complexes are dependent on the length, sequence composition, and temperature, as well as solution conditions, including pH and cation concentrations (11-13). Dissecting the relative contributions of all factors controlling triple helix stabilites will be pivotal when considering the use of oligonucleotide-directed sequence specific recognition of double helical nucleic acids for *in vivo* applications where temperature, pH, and salt conditions are strictly controlled.

For sequence-specific recognition of double helical RNA or DNA•RNA hybrids by triple helix formation, the importance of strand composition on the stabilities of triple helical complexes must be determined. In a formal sense, there are eight triple helical complexes wherein each strand could consist of DNA or RNA (Figure 1). We report the thermodynamic stabilities of eight triple helical complexes measured by quantitative affinity cleavage titration at pH 7.0 and 25 °C. The results reveal that triple helical stabilities are different depending on backbone composition. Although in qualitative agreement with stabilities reported recently by Roberts and Crothers, there are differences in both order and scale (14).

Materials and Methods

General. Sonicated, deproteinized calf thymus DNA (Pharmacia) was dissolved in H_2O to a final concentration of 2 mM in base pairs (bp). Ribonucleotide triphosphates were Pharmacia ultrapure grade and were used as supplied. [γ-^{32}P]ATP (≥3000 Ci / mmol; 1 Ci = 37 GBq) was obtained from Amersham. Calf intestine alkaline phosphatase was purchased from Pharmacia and T4 polynucleotide kinase was obtained from New England Biolabs. Phosphoramidites were purchased from Applied Biosystems (dA, dG, dC, and T) and from BioGenex Laboratories (San Ramon, CA) (rA, rG, rC, U).

Oligodeoxyribonucleotide-EDTA and Oligoribonucleotide-EDTA Syntheses. Pyrimidine oligodeoxyribonucleotides (D) and oligoribonucleotides (R) were synthesized by standard automated solid-support chemistry using an Applied Biosystems Model 394 DNA/RNA synthesizer and cyanoethyl *N,N*-diisopropyl phosphoramidites for DNA and 2′-*t*-butyldimethylsilyl 3′-cyanoethyl *N,N*-

diisopropyl phosphoramidites for RNA. The synthesis of oligonucleotides D and R containing EDTA at the 5′ end (*T and *U) will be described elsewhere.

Double Helical DNA and RNA Preparation. DNA templates, 36 nt in length, were prepared by chemical synthesis. RNA templates, 36 nt in length, were prepared by enzymatic synthesis using T7 RNA polymerase (Pharmacia) employing a 53-nt single-stranded DNA template (15). DNA and RNA were purified with 15% denaturing polyacrylamide gels and extracted with 0.3 M NaCl or NaOAc, respectively. DNA was 5′-end labeled using [γ-^{32}P]ATP and T4 polynucleotide kinase, precipitated with ethanol, and dissolved in H_2O (16). RNA was dephosphorylated with calf intestine alkaline phosphatase and subsequently 5′-^{32}P labeled with T4 polynucleotide kinase, precipitated, and dissolved in H_2O. The 5′-^{32}P-end-labeled duplex was prepared by mixing labeled strands with their unlabeled complementary strands in hybridization buffer (200 mM NaCl / 1 mM EDTA) at 37 °C and purified with a 15% nondenaturing polyacrylamide gel. The 5′-end labeled duplex was eluted with 200 mM NaCl and filtered through a 0.45-μm filter, followed by ethanol precipitation.

Quantitative Affinity Cleavage Titrations. Cleavage titration experiments were performed in association buffer (50 mM Tris acetate pH 7.0 / 100 mM NaCl / 1 mM spermine / 200 μM bp calf thymus DNA) containing 20,000 cpm of duplex. The DNA and the various concentrations of oligonucleotide-EDTA•Fe were allowed to equilibrate for 24 h at 25 °C. The cleavage reactions were initiated by addition of dithiothreitol (4 mM) and incubated for 8 h at 25 °C. The cleavage reactions were stopped by ethanol precipitation and analyzed by gel electrophoresis.

Quantitation. Gels were exposed to photostimuable storage phosphor imaging plates (Kodak Storage Phosphor Screen S0230 obtained from Molecular Dynamics) in the dark at 25 °C for 24 h. A Molecular Dynamics 400S PhosphorImager was used to obtain data from the phosphorimaging screens. Rectangles of the same dimensions were drawn around the cleavage bands at the target and at the references sites. The ImageQuant v. 3.0 program running on an AST Premium 386/33 computer was used to integrate the volume of each rectangle.

Affinity Cleavage Titration Fitting Procedure. A detailed description of the affinity cleavage titration procedure used has been published (11, 12). The relative cleavage efficiencies at the target site for each oligonucleotide concentration were determined by using the following equation:

$$I_{site} = I_{tot} - \lambda I_{ref} \qquad [1]$$

where I_{tot} and I_{ref} are the intensites of the cleavage bands at the target site and at the reference site, respectively, and λ is a scaling parameter defined as the ratio I_{tot}/I_{ref} at the lowest oligonucleotide concentration. A binding curve, represented by Eq. 2 where I_{sat} is the apparent maximum cleavage, K_T the equilibrium association constant for the oligonucleotide, and $[O]_{tot}$ the oligonucleotide-EDTA concentration, was used to fit the experimental data using I_{sat} and K_T as adjustable parameters:

$$I_{site} = I_{sat} \cdot \frac{K_T [O]_{tot}}{1 + K_T [O]_{tot}} \qquad [2]$$

KaleidaGraph software (version 2.1, Abelweck Software) running on a Macintosh IIfx computer was used to minimize the difference between I_{fit} and I_{site} for all data points. All reported values are the means of three experimental observations ± SEM. For graphical representation and comparision, I_{site} values were converted to fractional occupancies by dividing I_{site} by I_{sat}.

Results

Affinity Cleavage. Two pyrimidine strands, 18 nt in length, consisting of DNA (D) and RNA (R), were synthesized with EDTA on the T or U base at the 5′ end for affinity cleavage reactions. Four 36-nt strands were synthesized to form stable 35-bp duplexes, each containing an 18-bp site for triple helix formation: all DNA (DD), DNA purine strand + RNA pyrimidine strand (DR), RNA purine strand + DNA pyrimidine strand (RD), and all RNA (RR). Affinity cleavage reactions were performed on the eight triple helical complexes formed upon binding of the 18-nt D- or R-EDTA•Fe conjugates to each of the four duplex molecules (Figures 1 and 2). To avoid any complication due to differences in oxidative cleavage of DNA and RNA, both strands of DD, DR, RD, and RR were labeled in separate experiments. Each of the eight binding affinities were examined independently in two separate experiments. Only six of eight possible triple helical complexes were formed. At 2 μM concentration of D and R (pH 7.0, 25 °C), oligonucleotide D forms a stable triple helix only with DD and DR duplexes, whereas oligonucleotide R forms a stable complex with all four duplexes DD, DR, RD, and RR. For all cases where the triple helical complex forms, oligonucleotides D and R bind parallel to the purine strand of the Watson-Crick duplexes, DD, DR, RD, and RR.

Quantitative Affinity Cleavage Titration. The association constants for RNA and DNA oligonucleotides-EDTA•Fe D and R (18 nt) binding to 18-bp purine•pyrimidine tracts within each of four 35-bp duplexes, DD, DR, RD, and RR, were measured by quantitative affinity cleavage titration (Figure 2 *Upper*). For this, 5'-^{32}P-end-labeled duplex DNA or RNA and various concentrations of an oligonucleotide-EDTA•Fe D (1 nM - 10 μM) or R (1 nM - 40 μM) were allowed to equilibrate for 24 h at 25 °C in association buffer. Then, the cleavage reactions were initiated by addition of dithiothreitol and incubated for 8 h at 25 °C. The results of a representative experiment performed employing oligonucleotide-EDTA•Fe D targeting the duplex DD are shown in Figure 2 *Lower*.

The amount of product fragments produced during an affinity cleavage experiment is proportional to the fractional occupancy of the duplex target site by the oligonucleotide-EDTA•Fe (11). By measuring the site-specific cleavage produced by bound oligonucleotide-EDTA•Fe as a function of total oligonucleotide concentration, an empirical titration binding isotherm can be constructed and the equilibrium association constant (K_T) can be determined (11). The amounts of radiolabeled DNA in the bands at the target cleavage site and at a reference site were measured from a photostimulable storage phosphor autoradiogram (18). The I_{site} data points were calculated according to Eq. 1 and the ($[O]_{tot}$, I_{site}) data points were fitted using a non-linear least squares method, with K_T and I_{sat} as adjustable parameters (Eq. 2). The mean values of the association constants and the corresponding free energies for D and R binding with DD, DR, RD, and RR were each extracted from three such experiments (Table 1; see Figure 4). The data points obtained were averaged and plotted with average best-fit titration binding isotherms (Figure 3). Triple

helix formation of D + RD and D + RR was not observed up to 40 μM concentration of D. Therefore, only upper limits on these two association constants can be estimated. The relative stabilites of the triple helical complexes are D + DD, R + DD, R + DR, D + DR > R + RD, R + RR » D + RR, D + RD.

Discussion

DNA vs RNA. The differences in the energetics and structures of deoxyribonucleotide and ribonucleotide triple helices undoubtedly are related to the different chemical nature of DNA and RNA. For DNA there is a methyl group at the 5 position of the pyrimidine, thymine. For RNA, the methyl group is absent on uracil. On RNA there is a hydroxyl group at the 2′ position of the ribose sugar that is absent on DNA. One would expect the stacking of a methyl substituent (or lack of) on the adjacent pyrimidine in the bound third strand of the triple helix to be important. It is known from previous work that oligodeoxyribonucleotides containing 2′-deoxyuridine binds more weakly to duplex DNA by triple helix formation than oligodeoxyribonucleotides containing thymidine (19). Hence, we would expect the change of T to U to cause a decrease in affinity, likely due to loss of a stacking interaction. The presence or absence of the 2′-hydroxyl on the sugar that distinguishes RNA from DNA likely determines the conformational preference for A- or B-form with C-3′ endo and C-2′ endo sugar conformations, respectively. RNA duplexes prefer to adopt an A-form helical structure (20). Polymorphic DNA can adopt B- or A-form, and the B-A equilibrium is likely sequence composition dependent (20). Hence the 2′-OH substituents will exert conformational preferences on the triple helical structure(s). X-ray diffraction and NMR studies

of DNA, RNA, and hybrid duplexes and triplexes reveal that sugar conformation can differ in individual strands (21-26).

We found that six stable triplexes are formed, which is consistent with results of Roberts and Crothers (14). However, the order and the scale of free energy values differ (Figure 4) (14). When the Watson-Crick duplex contains RNA in the purine strand, RNA, but not DNA, will bind with reasonable affinity. The six binding affinities observed for this 18-nt sequence studied at pH 7.0 and 25 °C were clustered and ranged from 3.9×10^6 to 5.4×10^5 M^{-1} (Table 1). The corresponding free energies are -9.1 and -7.9 kcal•mol^{-1}, and differ only by 1.2 kcal•mol^{-1}. We estimate that the two possible triplexes which do not form (D + RR and D + RD) must be ≥ 3.6 kcal•mol^{-1} less stable than the R + DD complex. In contrast, Roberts and Crothers (14) measured more than 10 kcal•mol^{-1} variation (corresponding to a 10^8-fold difference in binding affinity) separating the most stable and least stable of the six complexes by van't Hoff analysis of melting curves of six triplexes. We cannot rule out at this time that the differences arise from the different methods of analyses. However, the binding affinities of R or D third strands to double helical nucleic acids are known to be length, sequence composition, pH, and salt dependent (11-13). Therefore, this difference more likely arises from experimental differences in the two studies: length (18 bp vs 12 bp), base composition (15 A•T, 3 G•C vs 4 A•T, 8 G•C), pH (7.0 vs 5.5), cation concentrations (1 mM vs 0 mM spermine), and stability of the target duplex (35-bp duplex vs 12-bp hairpin duplex with 4-nt loop).

Recognition of Double Helical DNA. In this study, the free energies of binding of D and R to double helical DNA are comparable (-9 kcal•mol^{-1}). Oligonucleotides containing D or R will be useful for targeting double-stranded

DNA by triple helix formation. This suggests that *in vivo* targeting of double helical DNA with RNA may be possible. Since the uracil does not contribute as much as thymine to binding, we conclude that the 2'-OH on RNA is compensating in a positive way. In the case studied here R and D bind DD with similar affinities whereas Roberts and Crothers found R formed a more stable complex, R + DD > D + DD (Figure 4).

Recognition of Double Helical DNA-RNA and RNA. The free energies of binding to RNA-DNA hybrids depend on whether the purine tract is RNA or DNA. When the double helix is purineD•pyrimidineR, then R and D bind with comparable affinities (~2 x 10^6 M^{-1}). However, if the hybrid is purineR•pyrimidineD, then R, but not D, binds with similar affinity (~ 6 x 10^5 M^{-1}). Our results differ with those of Roberts and Crothers in which, R + DR was significantly more stable than D + DR. Finally, R, but not D, will bind double helical RNA. The free energy of R binding double helical RNA (R + RR) is ~1.0 kcal•mol^{-1} less favorable than R binding double helical DNA (R + DD) or the DR hybrid (R + DR), but similar to the RD hybrid (R + RD).

Implications. It would appear that there could be several conformational families of triple helices related to the sugar identities of the three strands. Elucidation of the structures of these complexes must await direct studies such as x-ray or high resolution two-dimensional NMR analysis. With regard to the sequence-specific recognition of double helical nucleic acids by triple helix formation, a simple guiding principle is: If the double helix contains DNA in the purine strand, RNA or DNA will bind; if the double helix contains RNA in the purine strand, only RNA will bind.

References

1. Moser, H. E. & Dervan, P. B. (1987) *Science* **238**, 645-650.
2. LeDoan, T., Perrouault, L., Praseuth, D., Habhoub, N., Decout, J. -L., Thuong, N. T., Lhomme, J. & Helene, C. (1987) *Nucleic Acids Res.* **15**, 7749-7760.
3. Maher III, L. J., Wold, B. & Dervan, P. B. (1989) *Science* **245**, 725-730.
4. Strobel, S. A. & Dervan, P. B. (1991) *Nature* **350**, 172-174.
5. Strobel, S. A., Doucette-Stamm, L. A., Riba, L., Housman, D. E. & Dervan, P. B. (1991) *Science* **254**, 1639-1642.
6. Felsenfeld, G., Davies, D. R. & Rich, A. (1957) *J. Am. Chem. Soc.* **79**, 2023-2024.
7. Rajagopal, P. & Feigon, J. (1989) *Biochemistry* **28**, 7859-7870.
8. Cooney, M., Czernuszewicz, G., Postel, E. H., Flint, S. J. & Hogan, M. E. (1988) *Science* **241**, 456-459.
9. Beal, P. A. & Dervan, P. B. (1991) *Science* **251**, 1360-1363.
10. Radhakrishnan, I., de los Santos, C. & Patel, D. J. (1991) *J. Mol. Biol.* **221**, 1403-1418.
11. Singleton, S. F. & Dervan, P. B. (1992) *J. Am. Chem. Soc.* **114**, 6957-6965.
12. Singleton, S. F. & Dervan, P. B. (1992) *Biochemistry* **31**, 10995-11003.
13. Rougee, M., Faucon, B., Mergny, J. L., Barcelo, F., Giovannangeli, C., Garestier, T. & Helene, C. (1992) *Biochemistry* **31**, 9269-9278.
14. Roberts, R. W. & Crothers, D. M. (1992) *Science* **258**, 1463-1466.
15. Milligan, J. F., Groebe, D. R., Witherell, G. W. & Uhlenbeck, O. C. (1987) *Nucleic Acids Res.* **15**, 8783-8798.

16. Sambrook, J., Fritsch, E. F. & Maniatis, T. (1989) *Molecular Cloning*, 2nd Ed., Cold Spring Harbor Laboratory, Cold Spring Harbor, NY.

17. Iverson, B. L. & Dervan, P.B. (1987) *Nucleic Acids Res.* **15**, 7823-7830.

18. Johonston, R. F., Pickett, S. C. & Barker, D. L. (1990) *Electrophoresis* **11**, 355-360.

19. Povsic, T. J. & Dervan, P. B. (1989) *J. Am. Chem. Soc.* **111**, 3059-3061.

20. Saenger, W. (1984) *Principles of Nucleic Acids Structure*, Springer-Verlag, New York.

21. Wang, A. H. -J., Fujii, S., van Boom, J. H., van der Marel, G. A., van Boeckel, S. A. A. & Rich, A. (1982) *Nature* **299**, 601-604.

22. Arnott, S., Bond, P. J., Selsing, E. & Smith, P. J. C. (1976) *Nucleic Acids Res.* **3**, 2459-2470.

23. Chou, S. -H., Flynn, P. & Reid, B. (1989) *Biochemistry* **28**, 2435-2443.

24. Arnott, S., Chandrasekaran, R., Millane, R. P. & Park, H. -S. (1986) *J. Mol. Biol.* **188**, 631-640.

25. Macaya, R. F., Schultze, P. & Feigon, J. (1992) *J. Am. Chem. Soc.* **114**, 781-783.

26. Macaya, R. F., Wang, E., Schultze, P. & Feigon, J. (1992) *J. Mol. Biol.* **225**, 755-773.

Figure 1. Ribbon models of eight triple helical pyrimidine•purine•pyrimidine structures formed by binding of an 18-nt pyrimidine oligonucleotide-EDTA•Fe to the 18-bp target purine sequence within the 35-bp double helix. The DNA and RNA strands are depicted as white and dark ribbons, respectively. The Hoogsteen pyrimidine strand is indicated by the first letter, and the Watson-Crick purine and pyrimidine strands are indicated by the second and third letters, respectively. The conformations of these eight triple helical structures are unknown and, therefore, are uniformly represented here.

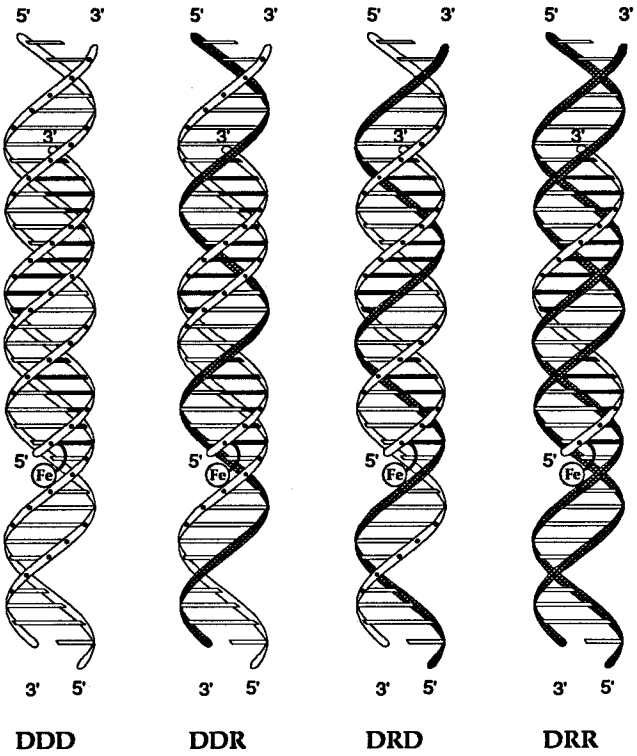
5' 3'
3'
5'
Fe
3' 5'
DDD
DDR
DRD
DRR
RDD
RDR
RRD
RRR

Figure 2. (***Upper***) Sequences of oligodeoxyribonucleotide-EDTA (D), oligoribonucleotide-EDTA (R), and 35-bp duplexes DD, DR, RD, and RR. *T and *u are thymidine-EDTA and uridine-EDTA, respectively. The uppercase letters indicate deoxyribonucleotides (DNA) and the lowercase letters, ribonucleotides (RNA). The box indicates the 18-bp purine target sequence within the 35-bp duplex bound by D or R. (***Lower***) Autoradiogram of a 20% denaturing polyacrylamide gel revealing cleavage products generated by D•Fe in a quantitative affinity cleavage titration experiment performed on the duplex DD labeled at the 5' end of the purine strand with ^{32}P. The white box drawn on the left of autoradiogram indicates the position of the 18-bp target site of the duplex DD. (Lane 1) Products of an A-specific cleavage reaction of DD (17). (Lane 2) Control showing intact ^{32}P-labeled duplex obtained after incubation under the conditions of cleavage reactions in the absence of D•Fe. (Lane 3-19) DNA affinity cleavage products produced by D•Fe at various concentrations: 10.0 μM (Lane 3); 8.0 μM (Lane 4); 4.0 μM (Lane 5); 2.0 μM (Lane 6); 1.0 μM (Lane 7); 800 nM (Lane 8); 400 nM (Lane 9); 200 nM (Lane 10); 100 nM (Lane 11); 80 nM (Lane 12); 40 nM (Lane 13); 20 nM (Lane 14); 10 nM (Lane 15); 8 nM (Lane 16); 4 nM (Lane 17); 2 nM (Lane 18); 1 nM (Lane 19).

5'-*TTTTCTTTTTTCTTTTCT-3' D

5'-*uuuucuuuuuucuuuucu-3' R

5'- GGGCGCAATGGGAAAAGAAAAAAGAAAAGAGCCGCC-3'
3'- CCGCGTTACCCTTTTCTTTTTTCTTTTCTCGGCGGG-5' DD

5'- GGGCGCAATGGGAAAAGAAAAAAGAAAAGAGCCGCC-3'
3'- ccgcguuacccuuuucuuuuuucuuuucucggcggg-5' DR

5'- gggcgcaaugggaaaagaaaaaagaaaagagccgcc-3'
3'- CCGCGTTACCCTTTTCTTTTTTCTTTTCTCGGCGGG-5' RD

5'- gggcgcaaugggaaaagaaaaaagaaaagagccgcc-3'
3'- ccgcguuacccuuuucuuuuuucuuuucucggcggg-5' RR

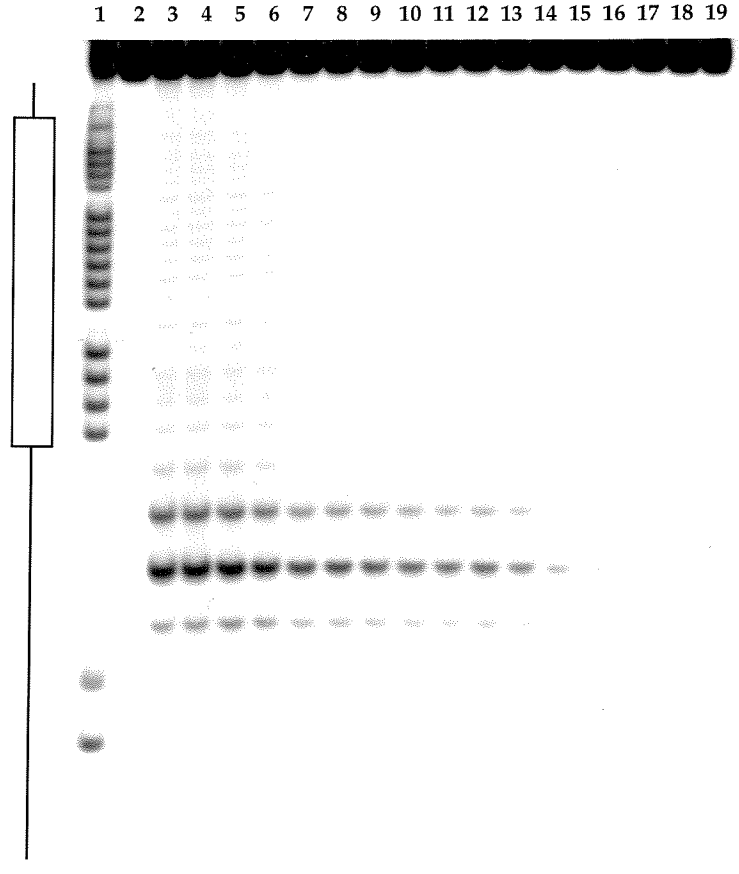

Figure 3. Binding isotherms derived from quantative affinity cleavage titration for six triple heical complexes formed. The $I_{site} \bullet I_{sat}^{-1}$ data represent the average of normalized site-specific cleavage signal intensities from three experiments and binding curves were plotted using the mean values of K_T. (A-F) Binding curves obtained for the duplexes DD to RR labeled at the 5' end of the purine strand with ^{32}P: D + DD (A); D + DR (B); R + DD (C); R + DR (D); R + RD (E); R + RR (F).

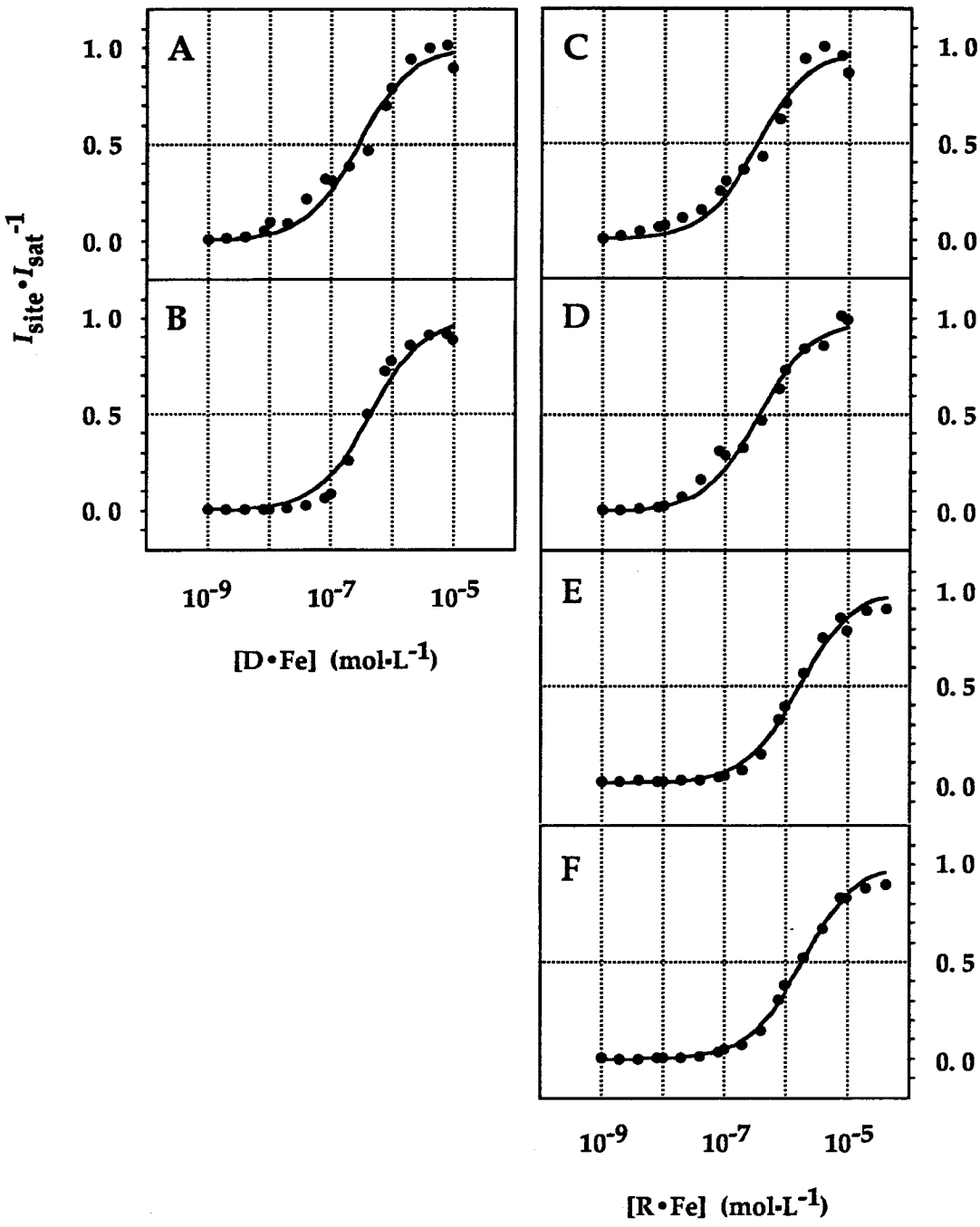
A
B
C
D
E
F
1.0
0.5
0.0
$I_{site} \cdot I_{sat}^{-1}$
10^{-9}
10^{-7}
10^{-5}
[D•Fe] (mol-L^{-1})
[R•Fe] (mol-L^{-1})

Table 1. Equilibrium association constants (K_T, M^{-1}) measured by quantitative affinity cleavage titration at 25 °C and pH 7.0.

Hoogsteen Strand †		Watson-Crick Duplex	Hoogsteen Strand ‡	
D	**R**	**Pu·Py**	**D**	**R**
$3.9 (\pm 0.7) \times 10^6$	$3.3 (\pm 1.3) \times 10^6$	**DD**	$4.2 (\pm 0.6) \times 10^6$	$5.6 (\pm 0.5) \times 10^6$
$2.2 (\pm 0.3) \times 10^6$	$2.9 (\pm 1.1) \times 10^6$	**DR**	$2.0 (\pm 0.6) \times 10^6$	$3.2 (\pm 1.0) \times 10^6$
$<10^4$ *	$6.1 (\pm 1.0) \times 10^5$	**RD**	$<10^4$ *	$7.1 (\pm 1.2) \times 10^5$
$<10^4$ *	$5.4 (\pm 1.0) \times 10^5$	**RR**	$<10^4$ *	$9.2 (\pm 2.2) \times 10^5$

† Hoogsteen strand binding to the duplex labeled at the 5' end of the purine Watson-Crick strand with ^{32}P.

‡ Hoogsteen strand binding to the duplex labeled at the 5' end of the pyrimidine Watson-Crick strand with ^{32}P.

* These estimated values are based on no detectable cleavage of the duplexes RD and RR by D•Fe up to 40 μM.

Figure 4. Comparison of relative stabilites ($\Delta\Delta G^o$, kcal•mol^{-1}) for six triple helical complexes taken from Table 1 (**A**) with values for recent report by Roberts and Crothers (**B**; ref. 14).

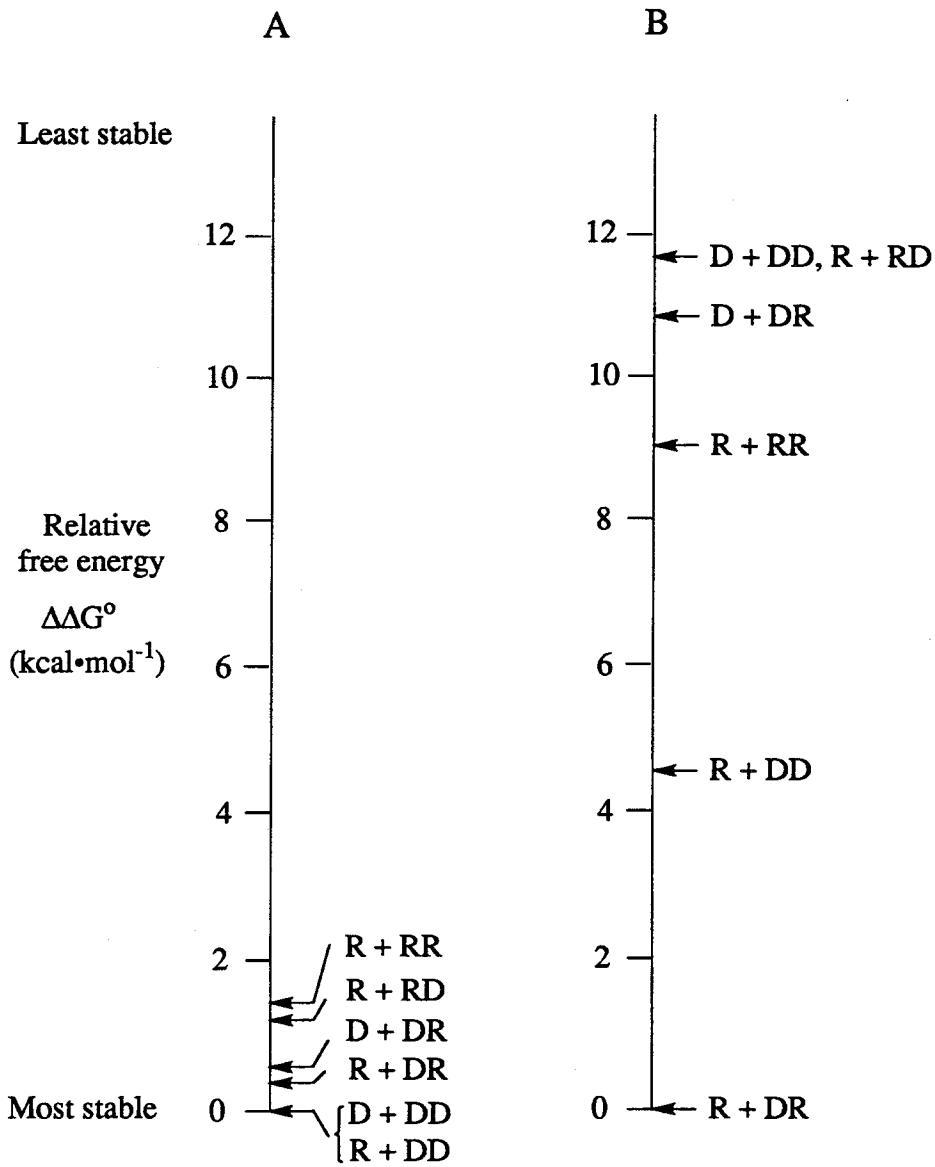
A
B
Least stable
Relative free energy ΔΔG° (kcal•mol-1)
Most stable
12
10
8
6
4
2
0
R + RR
R + RD
D + DR
R + DR
D + DD
R + DD
D + DD, R + RD
D + DR
R + RR
R + DD
R + DR

Figure 5. Data for quantitative affinity cleavage experiments involving DDD and RRR triplexes. The isotherms were measured for different equilibrium and reaction times, respectively.

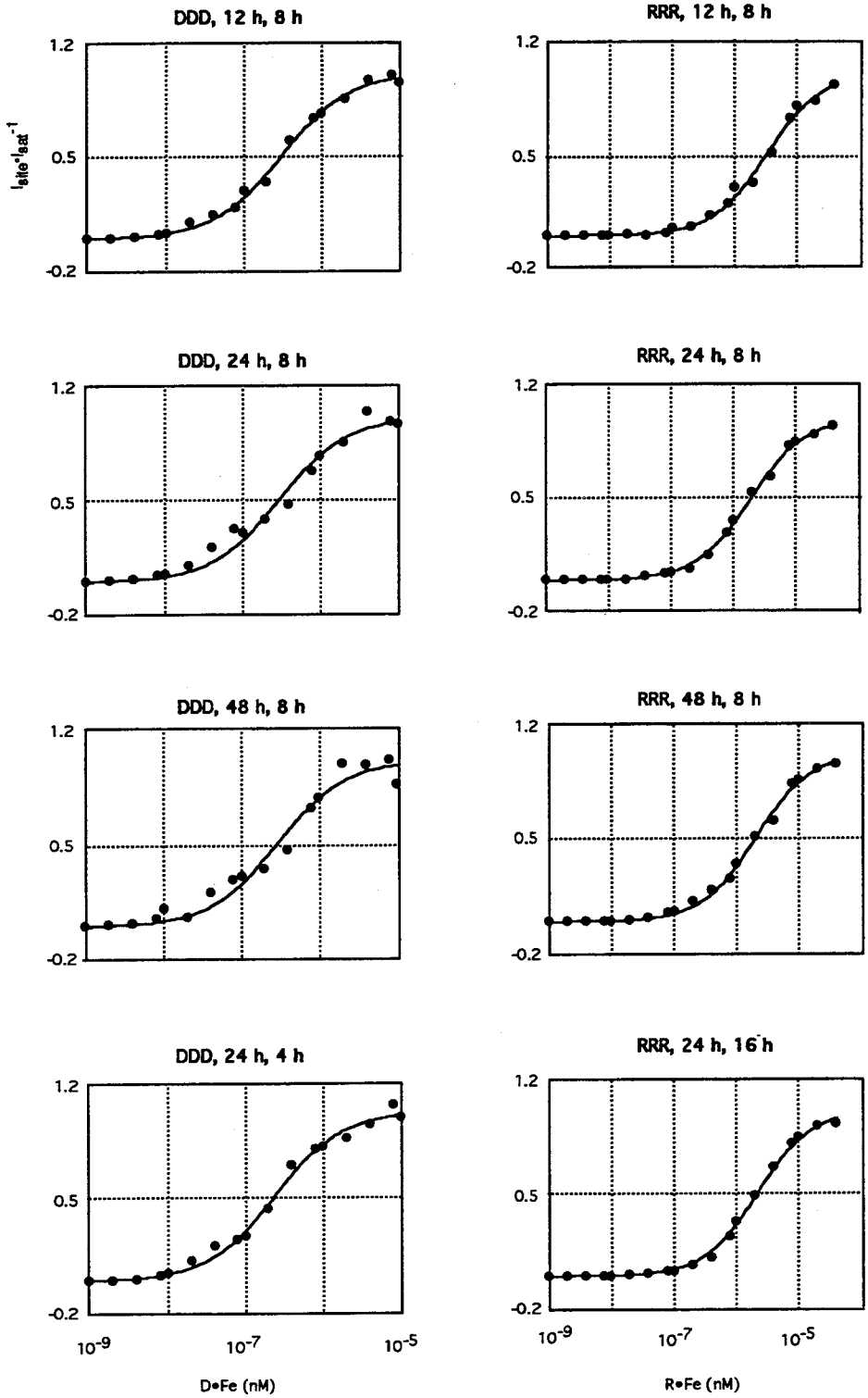
DDD, 12 h, 8 h
RRR, 12 h, 8 h
DDD, 24 h, 8 h
RRR, 24 h, 8 h
DDD, 48 h, 8 h
RRR, 48 h, 8 h
DDD, 24 h, 4 h
RRR, 24 h, 16 h
1.2
0.5
-0.2
$I_{site}^{-1}I_{ext}^{-1}$
10^{-9}
10^{-7}
10^{-5}
D•Fe (nM)
R•Fe (nM)

Table 2. Equilibrium association constant (K_T, M^{-1}) measured by quantitative affinity cleavage titration at 25 °C and pH 7.0*.

DDD, 12h, 8h; $3.3 (\pm 0.6) \times 10^6$	RRR, 12h, 8h; $4.5 (\pm 1.0) \times 10^5$
DDD, 24h, 8h; $3.4 (\pm 0.9) \times 10^6$	RRR, 24h, 8h; $5.5 (\pm 0.9) \times 10^5$
DDD, 48h, 8h; $3.5 (\pm 1.1) \times 10^6$	RRR, 48h, 8h; $5.0 (\pm 0.7) \times 10^5$

DDD, 24h, 8h; $3.4 (\pm 0.9) \times 10^6$	RRR, 24h, 8h; $5.5 (\pm 0.9) \times 10^5$
DDD, 24h, 4h; $4.3 (\pm 0.8) \times 10^6$	RRR, 24h, 16h; $5.3 (\pm 0.7) \times 10^5$

*Hoogsteen strand binding to the duplex labeled at the 5' end of the purine Watson-Crick strand with ^{32}P.

Figure 6. Melting curves of DDD and RRR triplexes performed in a buffer consisting of 50 mM Tris•acetate, pH 7.0, 100 mM NaCl, and 1 mM spermine. All samples were 1 μM in both Watson-Crick duplex and third strand. Melting experiments were performed by heating at 3 °C / 3 min for 10-22 °C and 1 °C / min for 22-80 °C and data were taken every 1.0 °C. UV absorbance at 260 nm was measured on a Hewlett-Packard Model 8452A diode array spectrometer and the absorbance change was scaled to 1.0. The low-temperature transition corresponds to the melting of the triplex, and the high-temperature transition to the duplex.

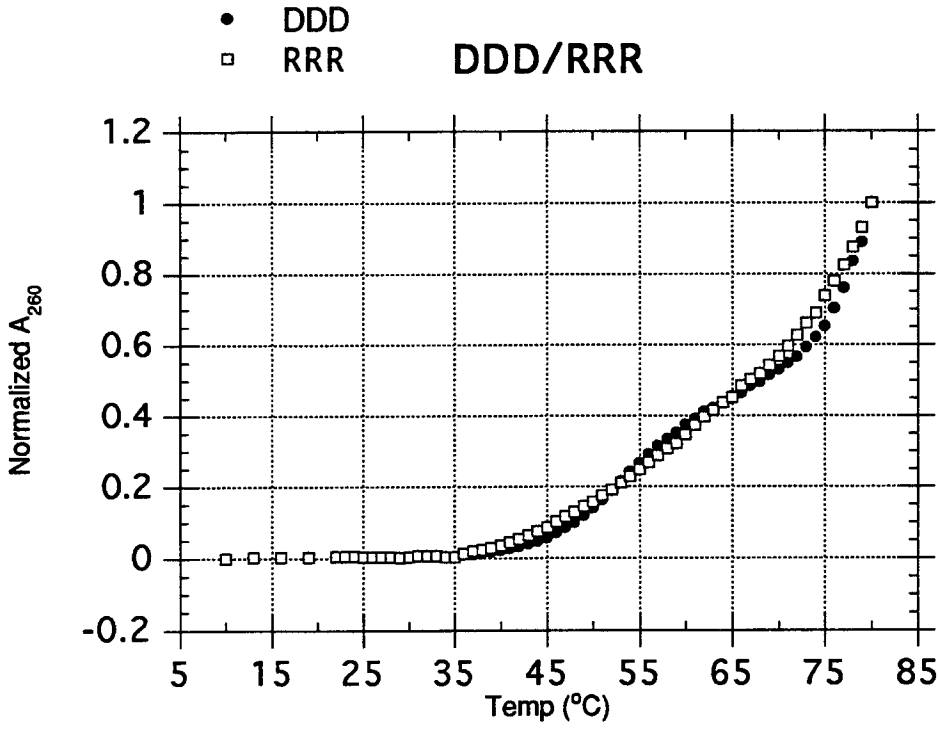
DDD
RRR
DDD/RRR
Normalized A_{260}
1.2
1
0.8
0.6
0.4
0.2
0
-0.2
5
15
25
35
45
55
65
75
85
Temp (°C)

Chapter 2

Different Conformational Families of Pyrimidine•Purine•Pyrimidine Triple Helices Depending on Backbone Composition

Introduction

Two studies of the energetics of triple helix formation by a combination of RNA and DNA strands show different triple helical stabilities depending on backbone composition (1, 2). A pyrimidine RNA strand binds double helical DNA, RNA, and DNA•RNA hybrids, whereas a pyrimidine DNA strand binds duplexes only when the purine strand of the duplex is DNA (1, 2). It would appear that there could be several conformational families of triple helices related to the sugar identities of the three strands. The presence or absence of the 2'-hydroxyl on the sugar that distinguishes RNA from DNA likely determines the conformational preference for A- or B-form duplexes with C-3' endo and C-2' endo sugar conformations, respectively. RNA duplexes prefer to adopt an A-form helical structure, whereas DNA duplexes can adopt B- or A-form (3-5). In DNA•RNA hybrid duplexes, the RNA strand retains an A-like C3'-endo conformation, whereas the DNA strand is not 3'-endo (6-9). With regard to triple helices, all RNA $(U)_n$+$(rA)_n(U)_n$, all DNA $(T)_n$+$(dA)_n(T)_n$, and hybrids $(U)_n$+$(dA)_n(U)_n$ are shown to be all A-form by x-ray fiber diffraction studies (10-12). However, recent structural studies of all DNA triple helices indicate that the triple helix has a B-form conformation with C2'-endo sugar pucker (13-16).

A DNA binding molecule equipped with EDTA•Fe cleaves DNA by oxidation of the deoxyribose backbone via a nonspecific diffusible oxidant, presumably hydroxyl radical, allowing nucleotide positions proximal to the cleaving moiety in the DNA structure to be mapped to nucleotide resolution by high-resolution gel electrophoresis (17-21). EDTA•Fe located in the major groove of right-handed DNA generates an asymmetric cleavage pattern with

maximal cleavage loci shifted to the 5′ side on the opposite strands (19, 21) (Figure 1). The question arises whether the asymmetric shift is sensitive to differences in helical conformations. If so, then affinity cleaving analysis might detect differences in all DNA, all RNA, and hybrid triple helices. Since there is a body of literature on the differences in DNA and RNA double helices, we first tested DNA•DNA, RNA•RNA, and hybrid double helices as a control. Based on these results, we then analyzed the triple helices.

Affinity cleaving using oligoribonucleotide-EDTA (RNA-EDTA) requires a synthetic method for the introduction of EDTA•Fe at unique positions of RNA. We describe here synthesis of RNA-EDTA oligonucleotides and their use to study the conformations of double and triple helical complexes. RNA-EDTA and DNA-EDTA with uridine-EDTA **16** (*U) and thymidine-EDTA **17** (*T), respectively, located at common positions were prepared by the incorporation of the functionalizable uridine **10** and 2′-deoxyuridine **11** derivatives into oligonucleotides followed by a post-automated synthesis modification. First, we examined conformations of DNA, RNA, and DNA•RNA hybrid double helices. The results reveal that for the sequences studied here, the cleavage pattern on the purine strand generated by *U and *T located at the same position on the pyrimidine strand in purine•pyrimidine double helical DD, DR, RD, and RR gradually shifts from 3' to 5', respectively. These findings agree qualitatively with structural data from x-ray analysis, confirming the usefulness of affinity cleaving to investigate differences in helical geometries. The cleavage pattern observed for the pyrimidine strand of the Watson-Crick duplex in triple helices suggests two triple helical conformational families: (i) D+DD, R+DD, D+DR, and R+DR and (ii) R+RD and R+RR. These results

indicate that helical geometries of triple helices are different depending on backbone composition.

Materials and Methods

General. ^{1}H NMR spectra were recorded at 300 MHz on a GE 300 NMR in DMSO-d_6. Chemical shifts are reported in ppm downfield from tetramethylsilane. High-resolution mass spectra (HRMS) were recorded using fast atom bambardment techniques at the Mass Spectrometry Laboratory at the University of California, Riverside. Preparative HPLC was performed on a Hewlett Packard 1050 Series preparative HPLC using a Vydac C18 reverse phase column (1.0 x 25 cm, 5 μm, TP silica). Analytical HPLC was performed on a Hewlett Packard 1090 Series II analytical HPLC using a Vydac C18 reverse phase column (0.46 x 25 cm, 5 μm, HS silica). Flash chromatography was carried out using silica gel 60 (230-400 mesh, Merck). Thin-layer chromatography (TLC) was performed on silica gel 60 F_{254} precoated plates (Merck). All chemicals for the synthesis were purchased from Aldrich unless otherwise specified. Acetonitrile, pyridine, dichloromethane, tetrahydrofuran (THF), and *N,N*-dimethylformamide (DMF) were purchased as anhydrous solvents from Aldrich. Phosphoramidites were purchased from Applied Biosystems (dA, dG, dC, and T) and from BioGenex Laboratories (San Ramon, CA) (rA, rG, rC, and U).

Nucleoside 3. To a solution of 5-iodouridine (5.0 g, 13.5 mmol), *N*-propargyltrifluoroacetamide (5.0 g, 33.3 mmol) (22), and triethylamine (Et_3N, 2.73 g, 27.0 mmol) in DMF (60 mL) were added tetrakis(triphenylphosphine)palladium(0) (1.56 g, 1.35 mmol) and CuI (0.514 g,

2.70 mmol). After stirring in the dark under Ar for 24 h at 25 °C, the mixture was concentrated, suspended in 1:1 CH_2Cl_2:CH_3OH (100 mL), and treated with anion exchange resin (DEAE Sephadex A-25-120, 5 g, ca. 17.5 mequiv, Sigma) for 30 min. The resin was removed by filtration and the mixture was concentrated and purified by flash chromatography using 10% CH_3OH/CH_2Cl_2 to give 3.5 g (65%) of a white solid. TLC (14% CH_3OH/CH_2Cl_2) R_f=0.37; ^1H NMR δ 11.69 (s,1H), 10.09 (t,*J*=5.2Hz,1H), 8.27 (s,1H), 5.75 (d,*J*=5.0Hz,1H), 5.42 (d,*J*=5.4Hz,1H,2'OH), 5.20 (t,*J*=4.9Hz,1H,5'OH), 5.09 (d,*J*=5.2Hz,1H,3'OH), 4.23 (d,*J*=5.4Hz,2H), 4.04 (m,1H), 3.96 (m,1H), 3.85 (m,1H), 3.61 (m,2H); HRMS for $C_{14}H_{15}F_3N_3O_7$ $[MH]^+$, calcd 394.0862, found 394.0869.

Nucleoside 4. Synthesized according to the procedure for nucleoside **3**. Yield=71%; TLC (10% CH_3OH/CH_2Cl_2) R_f=0.32; ^1H NMR δ 11.67 (s,1H), 10.09 (t,*J*=5.5Hz,1H), 8.20 (s,1H), 6.10 (t,*J*=6.6Hz,1H), 5.26 (d,*J*=4.1Hz,1H,3'OH), 5.11 (t,*J*=5.0Hz,1H,5'OH), 4.23 (m,3H), 3.79 (m,1H), 3.60-3.55 (m,2H), 2.12 (m,2H); HRMS for $C_{14}H_{15}F_3N_3O_6$ $[MH]^+$, calcd 378.0912, found 378.0904.

Nucleoside 5. To a solution of **3** (2.7 g, 6.87 mmol) in CH_3OH (100 mL) was added 10% palladium on carbon (300 mg) and the mixture was shaken under H_2 (50 psi) for 10 h. The reaction mixture was filtered through Celite and the filtrate was evaporated to dryness to give 2.6 g (97%) of a white solid. TLC (4% H_2O/CH_3CN) R_f=0.39; ^1H NMR δ 11.34 (s,1H), 9.44 (t,*J*=5.8Hz,1H), 7.75 (s,1H), 5.77 (d,*J*=5.3Hz,1H), 5.37 (d,*J*=5.7Hz,1H,2'OH), 5.09 (m,2H,5'OH+3'OH), 4.04 (m,1H), 3.97 (m,1H), 3.82 (m,1H), 3.59 (m,2H), 3.18 (m,2H), 2.21 (m,2H), 1.65 (m,2H); HRMS for $C_{14}H_{19}F_3N_3O_7$ $[MH]^+$, calcd 398.1175, found 398.1165.

Nucleoside 6. To a solution of **5** (2.5 g, 6.28 mmol) in pyridine (15 mL) at 0 °C was added 4,4'-dimethoxytrityl chloride (DMT•Cl, 2.5 g, 7.37 mmol). After

stirring at 25 °C for 12 h followed by treatment with CH_3OH (15 mL) for 30 min, the reaction mixture was concentrated, treated with 5% $NaHCO_3$ (30 mL) and extracted with CH_2Cl_2 (90 mL). The organic phase was washed once with H_2O (30 mL), dried over $MgSO_4$, concentrated, and purified by flash chromatography using 5% CH_3OH/CH_2Cl_2 to give 3.2 g (73%) of a light brown solid. TLC (8% CH_3OH/CH_2Cl_2) R_f=0.38; ^1H NMR δ 11.41 (s,1H), 9.36 (t,*J*=5.6Hz,1H), 7.43-7.20 (m,10H), 6.89 (d,4H), 5.79 (d,*J*=5.0Hz,1H), 5.47 (d,*J*=5.5Hz,1H,2'OH), 5.17 (d,*J*=5.6Hz,1H,3'OH), 4.17 (m,1H), 4.07 (m,1H), 3.95 (m,1H), 3.73 (s,6H), 3.18 (m,2H), 2.96 (m,2H), 1.86 (m,2H), 1.46 (m,2H); HRMS for $C_{35}H_{36}F_3N_3O_9$ $[M]^+$, calcd 699.2403, found 699.2399.

Nucleoside 7. Synthesized according to the procedure for nucleoside **5**. Yield=96%; TLC (4% H_2O/CH_3CN) R_f=0.47; ^1H NMR δ 11.32 (s,1H), 9.43 (t,*J*=5.2Hz,1H), 7.69 (s,1H), 6.17 (t,*J*=6.9Hz,1H), 5.24 (d,*J*=4.2Hz,1H,3'OH), 5.03 (t,*J*=5.2Hz,1H,5'OH), 4.24 (m,1H), 3.76 (m,1H), 3.56 (m,2H), 3.17 (m,2H), 2.23-2.05 (m,4H), 1.66 (m,2H); HRMS for $C_{14}H_{19}F_3N_3O_6$ $[MH]^+$, calcd 382.1225, found 382.1222.

Nucleoside 8. Synthesized according to the procedure for nucleoside **6**. Yield=65%; TLC (8% CH_3OH/CH_2Cl_2) R_f=0.43; ^1H NMR δ 11.39 (s,1H), 9.36 (t,*J*=5.5Hz,1H), 7.42-7.20 (m,10H), 6.88 (m,4H), 6.20 (t,*J*=6.7Hz,1H), 5.33 (d,*J*=4.6Hz,1H,3'OH), 4.29 (m,1H), 3.87 (m,1H), 3.73 (s,6H), 3.18 (m,2H), 2.97 (m,2H), 2.20 (m,2H), 1.90 (m,2H), 1.47 (m,2H); HRMS for $C_{35}H_{36}F_3N_3O_8$ $[M]^+$, calcd 683.2454, found 683.2457.

Nucleoside 9. To nucleoside **6** (0.20 g, 0.29 mmol) in THF (10 mL) were added pyridine (0.086 mL, 1.06 mmol), silver nitrate (0.058 g, 0.34 mmol), and *t*-butyldimethylsilyl chloride (TBDMS•Cl, 0.056 g, 0.37 mmol, Petrarch Systems). After stirring at 25 °C for 15 h, the solution was filtered into 5% $NaHCO_3$ (10

mL) and extracted with CH_2Cl_2 (30 mL). The extracts were dried, concentrated, and purified by flash chromatography using 25% hexane/ethyl ether to give 0.19 g (79%) of a white solid. TLC (20% Hexane/Ethyl ether) R_f=0.31; ^{1}H NMR δ 11.46 (s,1H), 9.36 (t,*J*=5.5Hz,1H), 7.46-7.22 (m,10H), 6.89 (d,4H), 5.85 (d,*J*=5.5Hz,1H), 5.13 (d,*J*=5.8Hz,1H,3'OH), 4.30 (dd,*J*=4.7Hz,1H), 4.03 (m,2H), 3.74 (s,6H), 3.25 (m,2H), 2.95 (m,2H), 1.81 (m,2H), 1.45 (m,2H), 0.85 (s,9H), 0.08 (s,3H), 0.06 (s,3H); HRMS for $C_{41}H_{50}F_3N_3O_9Si$ $[M]^+$, calcd 813.3268, found 813.3311.

Phosphoramidite 10. To a solution of **9** (0.12 g, 0.15 mmol) in THF (1 mL) were added *N,N*-diisopropylethylamine (DIEA, 0.102 mL, 0.58 mmol) and 2-cyanoethyl *N,N*-diisopropylchlorophosphoramidite (0.030 mL, 0.19 mmol). After stirring for 1 h at 25 °C, the reaction mixture was concentrated and purified by flash chromatography using 30% hexane/1% Et_3N/ethyl ether to give 0.090 g (60%) of the diastereomeric phosphoramidites as a white foam. TLC (20% Hexane/Ethyl ether) R_f=0.35; ^{1}H NMR δ 11.50 (m,1H), 9.36 (m,1H), 7.47-7.24 (m,10H), 6.89 (m,4H), 5.88 (m,1H), 4.48 (m,1H), 4.22-4.14 (m,2H), 3.73 (s,6H), 3.61-3.51 (m,4H), 3.30 (m,2H), 2.94 (m,2H), 2.51 (m,2H), 1.84 (m,2H), 1.46 (m,2H), 1.11 (m,12H), 0.83 (m,9H), 0.50 (m,6H); HRMS for $C_{50}H_{66}F_3N_5O_{10}PSi$ $[M - H]^+$, calcd 1012.4268, found 1012.4276.

Phosphoramidite 11. Synthesized according to the procedure for phosphoramidite **10**. Flash chromatography (60% Hexane/1% Et_3N/Ethyl acetate; Yield=70%; TLC (50% Hexane/Ethyl acetate) R_f=0.29; ^{1}H NMR δ 11.40 (m,1H), 9.36 (m,1H), 7.45-7.21 (m,10H), 6.88 (m,4H), 6.18 (m,1H), 4.53 (m,1H), 4.04 (m,1H), 3.73 (s,6H), 3.64-3.48 (m,4H), 3.28 (m,2H), 2.98 (m,2H), 2.64 (m,2H), 2.35 (m,2H), 1.93 (m,2H), 1.49 (m,2H), 1.12 (m,12H); HRMS for $C_{44}H_{52}F_3N_5O_9P$ $[M - H]^+$, calcd 882.3454, found 882.3488.

EDTA-Triester 13. To a solution of ethylenediaminetetraacetic dianhydride (EDTA-dianhydride, 10.8 g, 42.2 mmol) in DMF (150 mL) were added 2-(trimethylsilyl)ethanol (16.4 g, 138.6 mmol) and 4-dimethylaminopyridine (DMAP, 1.5 g, 12.2 mmol). After stirring at 45 °C for 12 h, 1-(3-dimethylaminopropyl)-3-ethylcarbodiimide hydrochloride (EDCI, 8.85 g, 46.1 mmol) was added. The solution was stirred for 8 h at 25 °C, concentrated, and purified by flash chromatography using 7% CH_3OH/CH_2Cl_2 to yield 5.1 g (20%) of a yellow oil. TLC (10% CH_3OH/CH_2Cl_2) R_f=0.40; ^1H NMR δ 4.09 (t,*J*=8.4Hz,6H), 3.50 (s,6H), 3.32 (s,2H), 2.70 (bs,4H), 0.92 (t,*J*=8.4Hz,6H), 0.02 (s,27H); HRMS for $C_{25}H_{53}N_2O_8Si_3$ $[MH]^+$, calcd 593. 3111, found 593.3082.

Uridine-EDTA 16 (*U). A solution of nucleoside **6** (0.10 g, 0.14 mmol) in ammonia saturated ethanol (10 mL) was stirred at 55 °C for 6 h. After a positive ninhydrin test indicated complete conversion of **6** to a single spot (23), the mixture was concentrated and allowed to react with activated EDTA triethylester **15** (0.095 g, 0.20 mmol) in THF (2 mL) for 2 h (18). The mixture was concentrated and redissolved in 1% trifluoroacetic acid (TFA) in CH_2Cl_2 (10 mL). After stirring for 1 h at 25 °C, the mixture was concentrated and then allowed to react with 0.1 N NaOH (10 mL). After 10 h at 55 °C, the mixture was neutralized with acetic acid, concentrated, loaded on a Sephadex LH-20 column (Pharmacia), and eluted with H_2O. The crude mixture was purified by preparative HPLC. The products were eluted with solvent A (0.1% TFA in H_2O) with a gradient of 3-5% solvent B (0.08% TFA in CH_3CN) over 20 min at a flow rate of 2 mL/min and detection was UV absorption at 260 nm. The fractions containing products were combined and evaporated to dryness to afford 0.045 g (56%) of a white solid. ^1H NMR δ 11.30 (s,1H), 8.13 (t,*J*=5.6Hz,1H), 7.76 (s,1H), 5.77 (d,*J*=5.4Hz,1H), 4.06 (m,1H), 3.98 (m,1H), 3.82

(m,1H), 3.59 (m,2H), 3.45 (s,4H), 3.38 (s,2H), 3.23 (s,2H), 3.09 (m,2H), 2.75 (bs,4H), 2.17 (m,2H), 1.57 (m,2H); HRMS for $C_{22}H_{34}N_5O_{13}$ $[MH]^+$, calcd 576.2153, found 576.2128.

Thymidine-EDTA 17 (*T). Synthesized according to the procedure for *U **16**. Yield=52%; ^1H NMR δ 11.29 (s,1H), 8.13 (t,*J*=5.6Hz,1H), 7.70 (s,1H), 6.17 (t,*J*=6.8Hz,1H), 4.24 (m,1H), 3.76 (m,1H), 3.57 (m,2H), 3.47 (s,4H), 3.42 (s,2H), 3.27 (s,2H), 3.09 (m,2H), 2.77 (bs,4H), 2.21-2.06 (m,4H), 1.56 (m,2H); HRMS for $C_{22}H_{34}N_5O_{12}$ $[MH]^+$, calcd 560.2203, found 560.2193.

RNA-EDTA 20 and DNA-EDTA 23 Synthesis. Oligoribonucleotides and oligodeoxyribonucleotides were synthesized on an Applied Biosystems Model 394 DNA/RNA synthesizer using 2-cyanoethyl phosphoramidite chemistry. Phosphoramidites **10** and **11** (0.15 M solutions in CH_3CN) were incorporated into RNA and DNA, respectively. RNA **18** (1 μmol) containing nucleoside **10** was deprotected by treatment with NH_3 saturated methanol (4 mL) at 25 °C for 24 h and lyophilized. The crude RNA oligonucleotides **19** (0.2 μmol) in THF (50 μL) were treated with 0.3 M activated EDTA-triester **14** in DMF (100 μL). After stirring at 25 °C for 10 min, the reaction was stopped by addition of H_2O (150 μL) and dried. Removal of the silyl protecting groups was carried out in tetrabutylammonium fluoride (TBAF, 300 μL of 1 M solutions in THF) at 25 °C for 24 h. The resulting solution was dried, desalted with a NAP-5 column (Pharmacia) and purified on a 20% polyacrylamide/7 M urea gel. DNA **21** (1 μmol) containing nucleoside **11** was deprotected with NH_4OH (4 mL) at 55 °C and lyophilized. The crude DNA oligonucleotides **22** (0.2 μmol) in 200 mM borate (50 μL, pH 8.9) were treated with 0.3 M activated EDTA-triethylester **15** in DMF (100 μL). After stirring at 25 °C for 10 min, the reaction was stopped by addition of H_2O (150 μL) and dried. Removal of the ethyl protecting groups

was carried out in 0.1 N NaOH (1 mL) at 55 °C for 24 h and neutralized with acetic acid. The resulting mixture was applied to a Sephadex G10-120 column and eluted with H_2O. The crude oligonucleotides were lyophilized and then purified on a 20% polyacrylamide/7 M urea gel. An alternative procedure for the modification of RNA and DNA by either EDTA dianhydride or EDTA monoanhydride was performed as follows (24, 25). The completely deprotected RNA (5 nmol) or DNA (5 nmol) in 0.2 M $NaHCO_3$ (50 μL, pH 8.17) was treated with either EDTA dianhydride (25 μL of 1% w/v DMF solution) or EDTA monoanhydride (5 mg) for 2 h at 25 °C. The reactions were quenched by addition of 100 mM Tris•HCl buffer pH 7.2 (25 μL) and H_2O (150 μL), followed by ethanol precipitation. After purification of the crude oligonucleotide-EDTA on 20% polyacrylamide/7 M urea gels, UV-absorbing bands were excised, crushed, and eluted (0.3 M NaOAc, pH 5.2, 37 °C, 24 h). The resulting solutions were filtered (0.45-μm Centrex filter, Schleicher and Schuell) and desalted (NAP-5 column).

HPLC analysis of RNA-EDTA and DNA-EDTA. The purified oligonucleotide-EDTA (5 nmol) was digested simultaneously with snake venom phosphodiesterase (5 μL, 2 μg/μL, Sigma) and calf intestine alkaline phosphatase (5 μL, 1 unit/μL, Pharmacia) in 50 mM Tris•HCl (pH 8.1), 100 mM $MgCl_2$ at 37 °C for 2 h (50 μL final volume). A filtered aliquot (20 μL) was analyzed by analytical HPLC. The products were eluted with solvent A (250 mM Triethylamine•acetate pH 6.0, 1 mM EDTA) with a gradient of 15-20% solvent B (CH_3OH) over 10 min at a flow rate of 1 mL/min and monitored by UV absorption at 260 nm. Comparison and co-injection with a standard solution containing rC, U, *U, dC, T, and *T established the composition of the

oligonucleotides. The extinction coefficient (260 nm) used for *U and *T was 8,800 $cm^{-1} \bullet M^{-1}$.

Affinity Cleavage Reactions of Double Helical DNA, RNA, and DNA•RNA Hybrids. DNA, DNA-EDTA, and RNA-EDTA oligonucleotides, 36 nt in length, were prepared by chemical synthesis as described above. RNA oligonucleotides, 36 nt in length, were prepared by enzymatic synthesis using T7 RNA polymerase (Pharmacia) and dephosphorylated with calf intestine alkaline phosphatase before labeling (26). DNA and RNA were 5'-end labeled using γ-^{32}P-ATP (≥3000 Ci/mmol, Amersham) and T4 polynucleotide kinase (New England Biolabs) (27). The 5'-^{32}P-end-labeled duplex was prepared by hybridizing labeled strands with their unlabeled complementary strands in 200 mM NaCl, 1 mM EDTA at 37 °C and purified with a 15% nondenaturing polyacrylamide gel. The 5'-end-labeled duplex was extracted with 200 mM NaCl and filtered through a 0.45-μm filter, followed by ethanol precipitation. The cleavage reactions were carried out by adding $Fe(NH_4)_2(SO_4)_2 \bullet 6H_2O$ (10 μM) to the ^{32}P-labeled 35-bp (base pairs) duplex DD, DR, RD, or RR (~20,000 cpm) in 50 mM Tris•acetate, pH 7.0, 100 mM NaCl and then incubating at 25 °C for 2h. Cleavage reactions were initiated by addition of dithiothreitol (4 mM) and allowed to proceed for 4 h at 25 °C. The reactions were stopped by ethanol precipitation and the cleavage products were analyzed by gel electrophoresis.

Affinity Cleavage Reactions of Triple Helical DNA, RNA, and DNA•RNA Hybrids. Labeled 35-bp double helical DNA and RNA oligonucleotides were prepared as described above. The cleavage reactions were carried out by combining a mixture of oligonucleotide-EDTA D or R (2 μM) and $Fe(NH_4)_2(SO_4)_2 \bullet 6H_2O$ (2.2 μM) with the ^{32}P-labeled 35-bp duplex DD, DR,

RD, or RR (~20,000 cpm) in association buffer (50 mM Tris•acetate, pH 7.0, 100 mM NaCl, 1 mM spermine, and 200 μM bp calf thymus DNA (Pharmacia)) and then incubating at 25 °C for 2h. Cleavage reactions were initiated by addition of dithiothreitol (4 mM) and allowed to proceed for 4 h at 25 °C. The reactions were stopped by ethanol precipitation and the cleavage products were analyzed by gel electrophoresis.

Affinity Cleavage Analysis. Histograms of the cleavage data were derived by densitometry of the autoradiogram. The cleavage intensity at a particular nucleotide was normalized using the cleavage intensity at the nucleotide cleaved the most efficiently in each strand. Arrow heights indicate the extent of cleavage at the indicated base.

Results and Discussion

Synthesis of RNA-EDTA and DNA-EDTA

Design. For the chemical synthesis of RNA equipped with EDTA, we desired a practical method that would be compatible with RNA chemical synthesis and deprotection conditions. When standard base protecting groups are used, deprotection of DNA oligonucleotides requires NH_4OH treatment. In contrast, deprotection of RNA oligonucleotides which contain the 2'-TBDMS group is carried out by treatment with ammonia saturated methanol/ethanol and TBAF treatment (28). In the case of DNA-EDTA, the ethyl ester was chosen to protect the EDTA carboxylic acids (20). The three esters of the tethered EDTA are hydrolyzed by 0.1 N NaOH rather than NH_4OH to circumvent aminolysis of the EDTA ethyl esters. Under these conditions, all base and phosphate protecting groups are removed and oligonucleotides are cleaved from the support. However, the same deprotection scheme cannot be used for the

synthesis of RNA-EDTA because the 2'-TBDMS protecting group is labile to these basic conditions (29). NaOH treatment for the deprotection of chemically synthesized RNA leads to hydrolysis of phosphodiester linkages.

On the basis of all these considerations, the post-automated synthesis modification of RNA oligonucleotides containing a primary amine linked to the 5 position of uridine by EDTA derivatives such as EDTA protected with the 2-(trimethylsilyl)ethyl ester, EDTA dianhydride, and EDTA monoanhydride was developed. The post-automated synthesis modification was made possible by the use of a modified uridine phosphoramidite **10** in the synthesis of RNA oligonucleotides. The primary amino group linked to the 5 position of uridine-alkylamine **10** is revealed for modification by treatment with ammonia/methanol. Activated EDTA esters can be employed to modify RNA oligonucleotides before TBAF treatment and 2-(trimethylsilyl)ethyl esters can be deprotected by TBAF treatment. Alternatively, fully deprotected oligoribonucleotides with nucleoside **10** can be modified by either EDTA dianhydride or EDTA monoanhydride.

Synthesis of phosphoramidites 10 and 11. A scheme for the synthesis of phosphoramidites **10** and **11** is shown in Figure 2. 5-Iodouridine **1** and 5-iodo-2'-deoxyuridine **2** were converted to **3** and **4** respectively, using a palladium-catalyzed coupling reaction with *N*-propargyltrifluoroacetamide (30). Hydrogenation of **3** and **4** afforded **5** and **7**, respectively. The 5'-hydroxyl group of **5** and **7** was protected as the DMT ether to give **6** and **8**. Subsequent reaction of **6** with TBDMS•Cl afforded **9** (31). Activation of **9** and **8** with 2-cyanoethyl *N,N*-diisopropylchlorophosphoramidite afforded phosphoramidites **10** and **11**, respectively.

The EDTA-triester **13** was prepared from EDTA dianhyride in a one-pot reaction in 20% yield (Figure 3). The EDTA-triethylester was synthesized by copper-mediated monohydrolysis of the tetraethyl ester of EDTA (18).

Synthesis and Purification of Oligonucleotide-EDTA. Oligonucleotides **18** and **21** were synthesized by automated methods using 2-cyanoethyl phosphoramidite chemistry (32). The phosphoramidites **10** and **11** were incorporated into RNA and DNA with 90-95% coupling efficiency. Deprotection of oligoribonucleotides **18** with anhydrous saturated methanolic ammonia at 25 °C affected the concomitant cleavage of oligonucleotides from the support and removal of the amino and phosphate protecting groups, leaving the 2'-O-silyl ethers intact (Figure 5). The functionalizable oligoribonucleotides **19** with 2'-TBDMS groups were modified using the activated EDTA-triester **14**. Silyl groups on the 2' position and EDTA were removed by treatment with TBAF. The crude RNA-EDTA **20** was desalted with Sephadex-G-25. Base labile protecting groups of oligodeoxynucleotides **21** were removed by treatment with 30% NH_4OH (Figure 6). Oligodeoxynucleotides **22** with alkylamino-linker were reacted with the activated EDTA-triethylester **15**, followed by deprotection with 0.1 N NaOH. RNA-EDTA **20** and DNA-EDTA **23** were purified on a 20% denaturing polyacrylamide gel. A 40-nt RNA modified with EDTA can be resolved from an unmodified one on a 20% gel of 0.8 mm thickness.

Base Composition Analysis of RNA-EDTA and DNA-EDTA. Enzymatic digestion of oligonucleotide-EDTA was carried out to confirm the integrity of *U, **16** and *T, **17** (Figure 7). Purified RNA-EDTA and DNA-EDTA were treated with snake venom phosphodiesterase and calf intestine alkaline phosphatase to give the corresponding nucleoside monomers. The enzymatic

digestion products of oligonucleotide-EDTA were analyzed by reverse phase HPLC. Analysis of 5'-*$UU_3CU_6CU_4CU$-3' revealed *U, U, and rC nucleosides. Similarly, 5'-*$TT_3CT_6CT_4CT$-3' afforded *T, T, and dC nucleosides. These results confirm the presence of U* and T* and suggest that nucleosides **10** and **11** can be utilized in automated oligonucleotide synthesis and post-automated synthesis modification without complications.

Analysis of the Double Helix by Affinity Cleaving

The structure of each of four 35-bp duplexes, DD, DR, RD, and RR, was characterized by affinity cleaving (Figure 8). For this, *U and *T modified with EDTA at the 5 position were incorporated into the same position of the 36-nt pyrimidine strand in the Watson-Crick duplex. 10 μM concentration of $Fe(NH_4)_2(SO_4)_2 \cdot 6H_2O$ was mixed with 5'-end-labeled duplex containing *U and *T in buffer (50 mM Tris•acetate, pH 7.0, 100 mM NaCl, 25 °C) and dithiothreitol was added to initiate cleavage. Histograms revealing the positions and extent of cleavage are shown in Figure 9. The cleavage patterns are nearly identical in the pyrimidine strands, whereas the position of maximal cleavage observed on opposite purine strands is shifted to the 5' direction in the order: DD, DR, RD, and RR. These results are consistent with structural data from x-ray studies. The cleavage efficiency at a nucleotide position is related to its distance in space from the *T/*U. This distance is determined by two parameters: the axial rise per nucleotide residue (h) and the twist angle (t) of the helix. Both h and t change when going from B-form to A-form duplexes and the predicted changes are consistent with the observed changes seen in the cleavage pattern. For example, maximal cleavage on the purine strand occurs four and six nucleotides to the 5′ side of *T and *U in double helical DD and RR, respectively. Upon going from B-form to A-form duplexes, the more distant

nucleotide position in A-form RNA is brought closer in space to EDTA•Fe relative to the same position in B-form DNA due to the change in h and t (h=3.38 Å, t=36° for B-form DNA (3); h=2.81 Å, t=32.7° for A-form RNA (4)) (Figure 10). This leads to the different cleavage patterns seen between B-form DNA and A-form RNA duplexes. These findings confirm that affinity cleaving analysis is a sensitive method for detecting differences in helical conformations. The cleavage patterns of the two hybrids fall in between double helical DD and RR. Similar results were obtained from a gel mobility study of purine•pyrimidine double helices (DNA>hybrids>RNA) (1). These results indicate that it is unlikely that all hybrid helices adopt an A-form double helical structure (h=3.03-3.46 Å, t=32.7° or 36° for poly(rA)•poly(T) (6); h=3.06 Å, t=32.7° for poly(dA)•poly(U) (7)).

Analysis of the Triple Helix by Affinity Cleaving

Oligonucleotides RNA- and DNA-EDTA•Fe (D and R) (18 nt in length) were allowed to bind to 18 bp purine•pyrimidine tracts within each of four 35-bp duplexes, DD, DR, RD, and RR (Figure 11). For this, 5'-end-labeled duplex and 2 μM concentration of an oligonucleotide-EDTA•Fe D or R were mixed in association buffer. Affinity cleavage reactions were performed on six triple helical complexes comprised of combinations of DNA and RNA. Oligonucleotide D forms a stable triple helix only with DD and DR whereas oligonucleotide R forms a stable complex with all DD, DR, RD, and RR (Figure 12). For all cases, oligonucleotides D and R bind parallel to the purine strand of the Watson-Crick duplexes. An asymmetric cleavage pattern with maximal cleavage shifted to the 5′ side of U* or T* on the opposite strands was observed, indicating that oligonucleotides D and R are located in the major groove of the Watson-Crick duplexes. Comparison of histograms reveals that the similar

cleavage pattern is observed for all purine strands of the Waston-Crick duplex in the six triple helices, whereas the cleavage pattern on the pyrimidine strands of the Waston-Crick duplex appears different between two triple helical groups: (i) D+DD, R+DD, D+DR, and R+DR and (ii) R+RD and R+RR. R+RD and R+RR give additional cleavage at sites closer to the 5' end of the pyrimidine strand. In Figure 13, the cleavage patterns for D+DD and R+RR triple helical complexes are mapped to B-form DNA and A-form RNA double helices, respectively. The cleavage sites cover four and six nucleotides, with the most distal cleavage five and eight nucleotides to the 5′ side of *T and *U on the pyrimidine strand in D+DD and R+RR triple helices, respectively. All these sites are proximal to EDTA•Fe located on the third strand in the major groove of the Watson-Crick B-form DNA and A-form RNA. The proximity of these cleavage sites to EDTA•Fe in space correlates with the high and low twist angle and axial rise per residue in B-form DNA and A-form RNA, respectively. Based on these results, it would appear that the Watson-Crick DNA duplex in the D+DD triple helix adopts a different helical conformation compared to the RNA duplex in the R+RR triple helix. The DNA or RNA identity of the purine strand of the Watson-Crick duplex seems to be a determinant of the triple helix conformation. Elucidation of parameters such as helical twist, axial rise per residue, sugar pucker, X-displacement, and base-pair inclination that distinguish one triple helical family from the other must now await multidimensional NMR and x-ray experiments (33).

In summary, a chemical method for the sequence-specific incorporation of EDTA•Fe at unique sites of RNA has been presented. This methodology includes the synthesis of phosphoramidites of uridine modified with a protected amine at the 5 position, compatible with automated solid-phase RNA

synthesis and subsequent modification by activated EDTA derivatives. Chemical synthesis may have advantages relative to the enzymatic synthesis for the preparation of RNA oligonucleotides equipped with nucleic acid cleaving function. Using RNA polymerase, it was not possible to incorporate a functionalizable nucleoside into RNA at a single site unless a site-specific novel base pairing scheme distinguishable from Watson-Crick A-T(U) and G-C base pairing is used (34, 35). All these complications can be avoided by relatively convenient chemical synthesis of RNA with uridine-alkylamine **10** and post-automated synthesis modification. The method developed here allows the preparation of RNA bearing the derivatizable uridine at a single and specific site. The size of oligonucleotides that can be derivatized with EDTA is limited by resolution of sequences differing only by an EDTA moiety on a strand separating gel.

The availability of RNA-EDTA extends the affinity cleaving methods to the study of structures of duplex DNA, RNA, and DNA•RNA hybrids and triple helix formation of all possible triple helical complexes. Different cleavage patterns in six triple helices were observed depending on backbone composition, indicating that at least two conformational families exist. Confirmation of this must now await multidimensional NMR and x-ray experiments which should reveal the structure underpinning these families.

References

1. Roberts, R. W. & Crothers, D. M. (1992) *Science* **258**, 1463-1466.
2. Han, H. & Dervan, P. B. (1993) *Proc. Natl. Acad. Sci. U.S.A.* **90**, 3806-3810.
3. Saenger, W. (1984) *Principles of Nucleic Acids Structure*, Springer-Verlag, New York.
4. Dock-Bregeon, A. C., Chevrier, B., Podjarny, A., Johnson, J., de Bear, J. S., Gough, G. R., Gilham, P. T. & Moras, D. (1989) *J. Mol. Biol.* **209**, 459-474.
5. Chou, S. -H., Flynn, P. & Reid, B. (1989) *Biochemistry* **28**, 2422-2435.
6. Zimmerman, S. B. & Pheiffer, B. H. (1981) *Proc. Natl. Acad. Sci. U.S.A.* **78**, 78-82.
7. Arnott, S., Chandrasekaran, R., Millane, R. P. & Park, H. -S. (1986) *J. Mol. Biol.* **188**, 631-640.
8. Chou, S. -H., Flynn, P. & Reid, B. (1989) *Biochemistry* **28**, 2435-2443.
9. Salazar, M., Fedoroff, O. Y., Miller, J. M., Ribeiro, S. & Reid, B. R. (1993) *Biochemistry* **32**, 4207-4215.
10. Arnott, S. & Bond, P. J. (1973) *Nature New Biol.* **244**, 99-101.
11. Arnott, S. & Selsing, E. (1974) *J. Mol. Biol.* **88**, 509-521.
12. Arnott, S., Bond, P. J., Selsing, E. & Smith, P. J. C. (1976) *Nucleic Acids Res.* **3**, 2459-2470.
13. Macaya, R. F., Schultze, P. & Feigon, J. (1992) *J. Am. Chem. Soc.* **114**, 781-783.
14. Macaya, R. F., Wang, E., Schultze, P., Sklenar, V. & Feigon, J. (1992) *J. Mol. Biol.* **225**, 755-773.
15. Howard, F. B., Todd Miles, H., Liu, K., Frazier, J., Raghunathan, G. & Sasisekharan, V. (1992) *Biochemistry* **31**, 10671-10677.

16. Ouali, M., Letellier, R., Adnet, F., Liquier, J., Sun, J. -S., Lavery, R. & Taillandier, E. (1993) *Biochemistry* **32**, 2098-2103.

17. Hertzberg, R. P. & Dervan, P. B. (1984) *Biochemistry* **23**, 3934-3945.

18. Taylor, J. S., Schultz, P. G. & Dervan, P. B. (1984) *Tetrahedron* **40**, 457-465.

19. Sluka, J. P., Griffin, J. H., Mack, D. P. & Dervan, P. B. (1990) *J. Am. Chem. Soc.* **112**, 6369-6374.

20. Dreyer, G. B. & Dervan, P. B. (1985) *Proc. Natl. Acad. Sci. U.S.A.* **82**, 968-972.

21. Moser, H. E. & Dervan, P. B. (1987) *Science* **238**, 645-650.

22. Pailer, M. & Huebsch, W. J. (1966) *Monatsh. Chem.* **97**, 1541-1553.

23. Gordon, A. J. & Ford, R. A. (1972) *The Chemist's Companion: A Handbook of Practical Data, Techniques, and References*, John Wiley & Sons, New York.

24. Lin, S. -B., Blake, K. R., Miller, P. S. & Ts'o, P. O. P. (1989) *Biochemistry* **28**, 1054-1061.

25. Ebright, Y. W., Chen, Y., Pendergrast, P. S. & Ebright, R. H. (1992) *Biochemistry* **31**, 10664-10670.

26. Milligan, J. F., Groebe, D. R., Witherell, G. W. & Uhlenbeck, O. C. (1987) *Nucleic Acids Res.* **15**, 8783-8798.

27. Sambrook, J., Fritsch, E. F. & Maniatis, T. (1989) *Molecular Cloning: A Laboratory Manual 2nd Ed.*, Cold Spring Harbor Laboratory, Cold Spring Harbor.

28. Wu, T., Ogilvie, K. K. & Pon, R. T. (1989) *Nucleic Acids Res.* **17**, 3501-3517.

29. Ogilvie, K. K. (1973) *Can. J. Chem.* **51**, 3799-3807.

30. Hobbs, F. W., Jr. (1989) *J. Org. Chem.* **54**, 3420-3422.

31. Hakimelahi, G. H., Proba, Z. A. & Ogilvie, K. K. (1982) *Can. J. Chem.* **60**, 1106-1113.

32. Gait, M. J. (1984) *Oligonucleotide Synthesis: A Practical Approach,* IRL Press, Washington DC.

33. Sekharudu, C. Y., Yathindra, N. & Sundaralingam, M. (1993) *J. Biomol. Struc. Dyn.* **11**, 225-244.

34. Chen, C. -H. B., Gorin, M. B. & Sigman, D. S. (1993) *Proc. Natl. Acad. Sci. U.S.A.* **90**, 4206-4210.

35. Tor, Y. & Dervan, P. B. (1993) *J. Am. Chem. Soc.* **115**, 4461-4467.

36. Iverson, B. L. & Dervan, P. B. (1987) *Nucleic Acids Res.* **15**, 7823-7830.

37. Donis-Keller, H. (1980) *Nucleic Acids Res.* **8**, 3133-3142.

38. Maxam, A. M. & Gilbert, W. (1980) *Methods Enzymol.* **65**, 499-560.

Figure 1. Cleavage patterns produced by a diffusible oxidant generated by EDTA•Fe localized in the major groove of right-handed DNA. The edges of the bases are shown as open bars for the minor groove and crosshatched for the major groove, respectively. The filled circles show points of cleavage along the phosphodiester deoxyribose backbone.

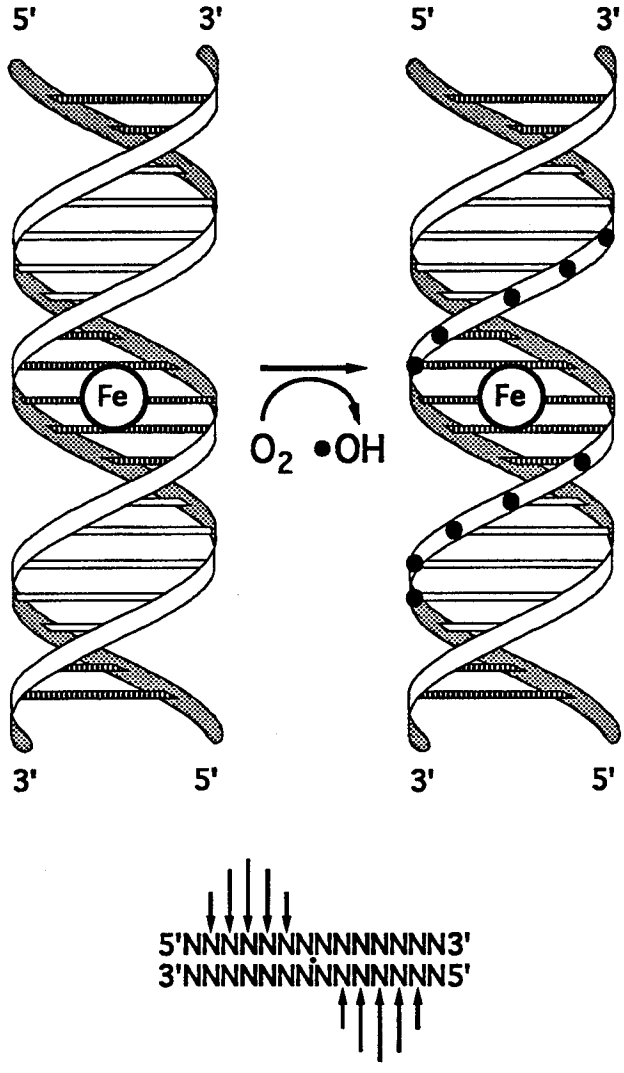
5'
3'
Fe
O_2 •OH
5'
3'
Fe
3'
5'
3'
5'
5'NNNNNNNNNNNNN3'
3'NNNNNNNNNNNNN5'

Figure 2. Scheme for the synthesis of phosphoramidites **10** and **11**. Reaction conditions: (a) Et_3N, $[(C_6H_5)_3P]_4Pd$, CuI, DMF; (b) Pd/C, MeOH; (c) DMT•Cl, pyridine; (d) TBDMS•Cl, $AgNO_3$, pyridine; (e) $[(CH_3)_2CH]_2NP(Cl)OCH_2CH_2CN$, DIEA, THF.

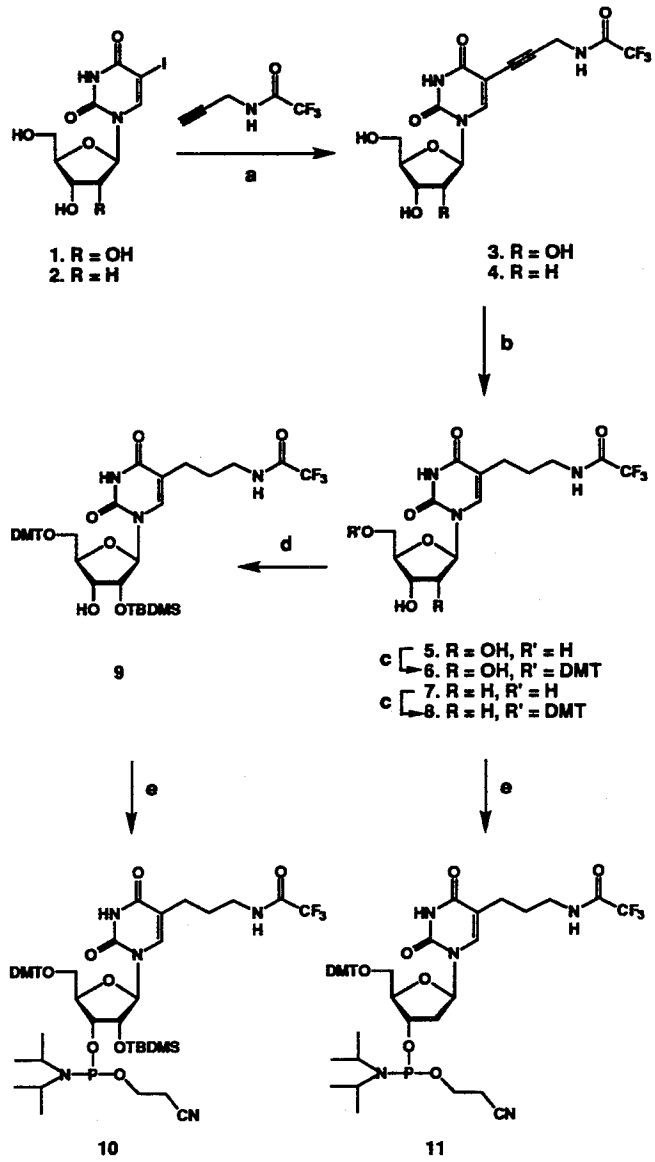
1. R = OH
2. R = H
a
3. R = OH
4. R = H
b
d
9
c
5. R = OH, R' = H
6. R = OH, R' = DMT
c
7. R = H, R' = H
8. R = H, R' = DMT
e
e
10
11

Figure 3. (***Upper***) Scheme for the synthesis of EDTA tri-(trimethylsilyl)ethyl ester **13.** Reaction conditions: (a) 3 equiv of 2-(trimethylsilyl)ethanol, DMAP, DMF; (b) 1 equiv of EDCI. (***Lower***) EDTA-triester **14** and **15** activated by 1.1 equiv of *N,N'*-Dicyclohexylcarbodiimide, 1.1 equiv of *N*-hydroxysuccinimide, THF.

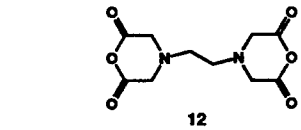

12

a, b

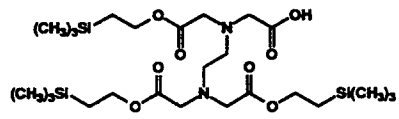

13

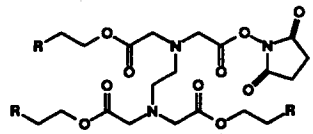

14. R = $Si(CH_3)_3$
15. R = H

Figure 4. Scheme for the synthesis of *U **16** and *T **17**. Reaction conditions: (a) NH_3/ethanol; (b) activated EDTA$(Et)_3$; (c) TFA; (d) 0.1 N NaOH; (e) acetic acid.

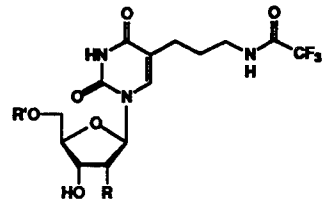

6. R = OH, R' = DMT
8. R = H, R' = DMT

a - e

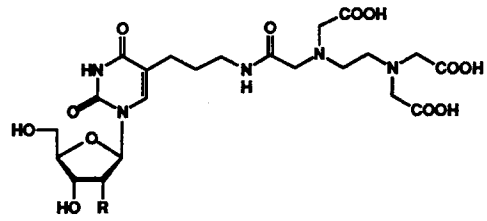

16. R = OH
17. R = H

Figure 5. General synthetic scheme for RNA-EDTA. Phenoxyacetyl groups are designated by Pac and benzoyl groups by Bz.

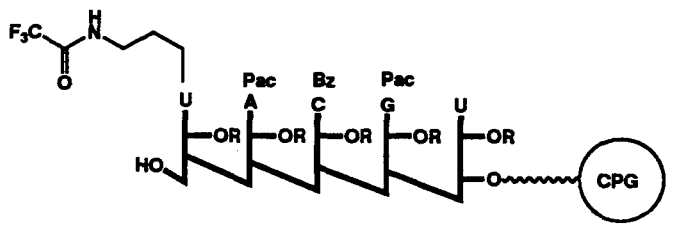

18. R = TBDMS

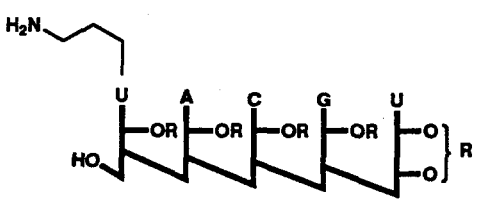

19. R = TBDMS

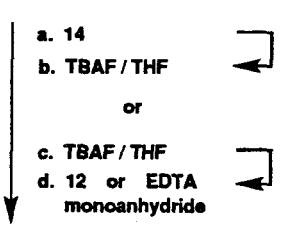

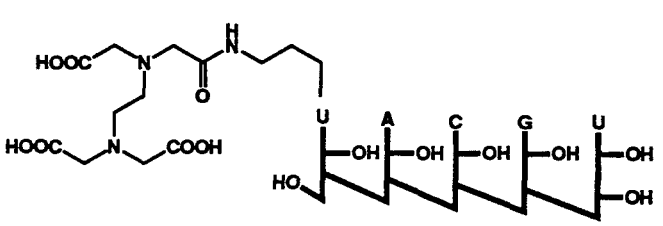

20

Figure 6. General synthetic scheme for DNA-EDTA. Isobutyl groups are designated by iBu.

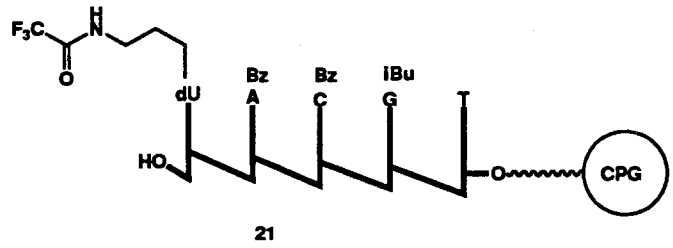
F3C
H
N
O
dU
Bz
A
Bz
C
iBu
G
T
HO
O
CPG

21

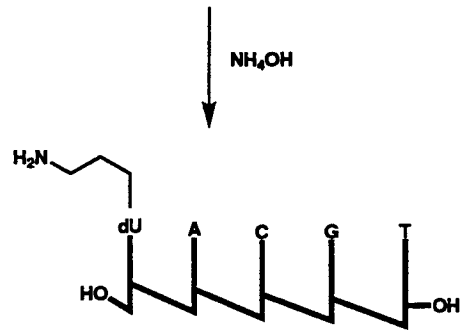
NH4OH
H2N
dU
A
C
G
T
HO
OH

22

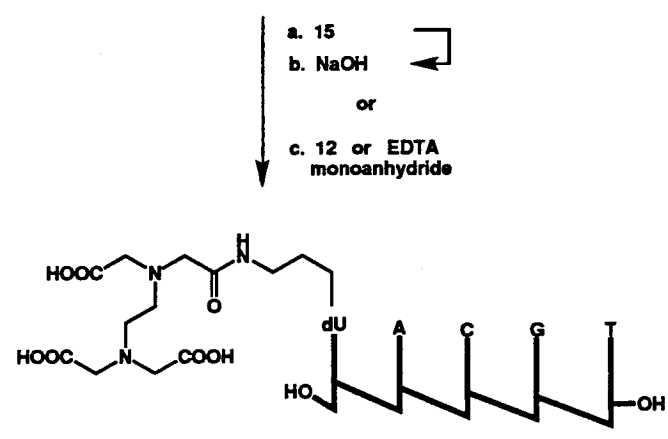
a. 15
b. NaOH
or
c. 12 or EDTA
monoanhydride
HOOC
N
H
N
O
HOOC
N
COOH
dU
A
C
G
T
HO
OH

23

Figure 7. HPLC analysis of the enzymatic digestion of RNA-EDTA, 5′-*$UU_3CU_6CU_4CU$-3′ (trace b) and DNA-EDTA, 5′-*$TT_3CT_6CT_4CT$-3′ (trace d) compared to the chromatogram of authentic nucleosides (trace a, c).

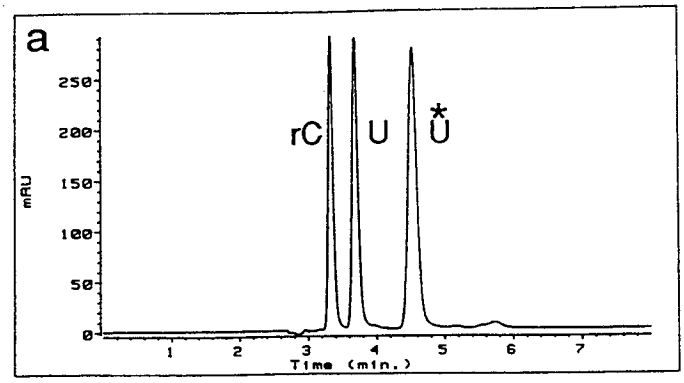
a
rC
U
*U
mAU
Time (min.)

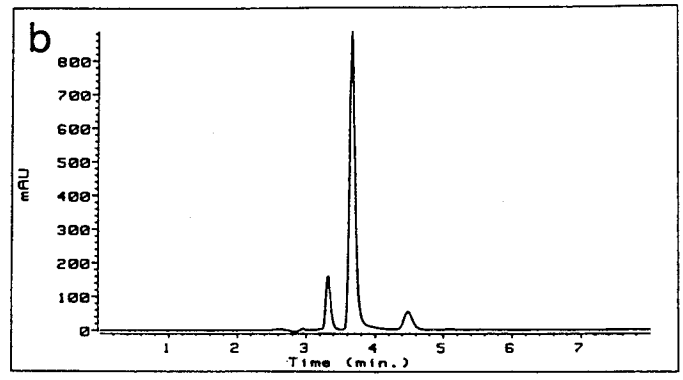
b
mAU
Time (min.)

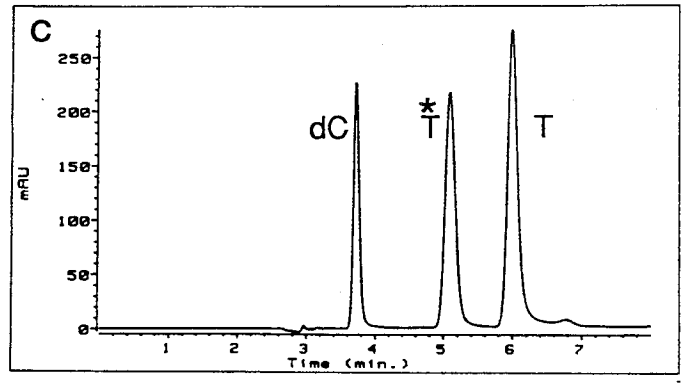
c
dC
*T
T
mAU
Time (min.)

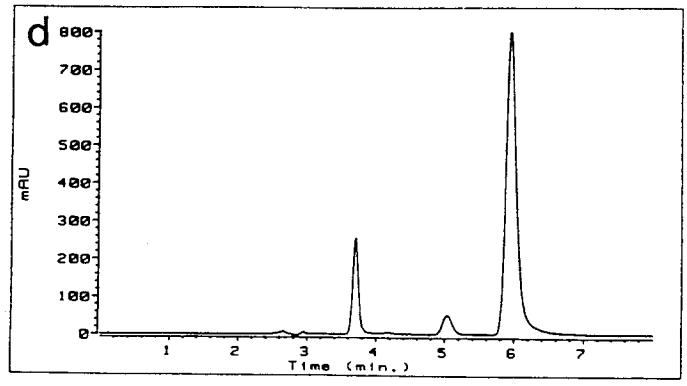
d
mAU
Time (min.)

Figure 8. (***Upper***) Sequences of DNA-EDTA (**3**), RNA-EDTA (**4**), and 35-bp duplexes DD (**1** + **3**), DR (**1** + **4**), RD (**2** + **3**), and RR (**2** + **4**). The uppercase letters indicate DNA and the lowercase letters, RNA. (***Lower***) Autoradiogram of a 20% denaturing polyacrylamide gel showing affinity cleavage reactions. (Lane 2, 4, 6, 8, 12, 14, 16, 18) Control showing intact 5′ labeled 35-bp duplex standard obtained after treatment according to the cleavage reactions in the absence of Fe. (Lane 3, 5, 7, 9, 13, 15, 17, 19) Affinity cleavage products produced in the presence of Fe. (Lane 1) A-specific chemical sequencing of (5′-^{32}P PuD)(PyD) (36). (Lane 10, 20) A+U enzymatic sequencing (Phy M) of (5′-^{32}P PuR) and (5′-^{32}P PyR), respectively (37). (Lane 11) T-specific chemical sequencing ($KMnO_4$) of (5′-^{32}P PyD) (38). Watson and Crick strands are indicated by (Pu) and (Py), where D indicates DNA and R, RNA.

1 5'- GGGCGCAATGGGAAAAGAAAAAAGAAAAGAGCCGCC - 3' D

2 5'- gggcgcaaugggaaaagaaaaaagaaaagagccgcc - 3' R

3 5'- GGGCGGCTCTTTTCTTTTTTCTTTTCCCATTGCGCC - 3' D

4 5'- gggcggcucuuuucuuuuuucuuuucccauugcgcc - 3' R

A 5'- GGGCGCAATGGGAAAAGAAAAAAGAAAAGAGCCGCC - 3' DD
3'- CCGCGTTACCCTTTTCTTTTTTCTTTTCTCGGCGGG - 5'

B 5'- GGGCGCAATGGGAAAAGAAAAAAGAAAAGAGCCGCC - 3' DR
3'- ccgcguuacccuuuucuuuuuucuuuucucggcggg - 5'

C 5'- gggcgcaaugggaaaagaaaaaagaaaagagccgcc - 3' RD
3'- CCGCGTTACCCTTTTCTTTTTTCTTTTCTCGGCGGG - 5'

D 5'- gggcgcaaugggaaaagaaaaaagaaaagagccgcc - 3' RR
3'- ccgcguuacccuuuucuuuuuucuuuucucggcggg - 5'

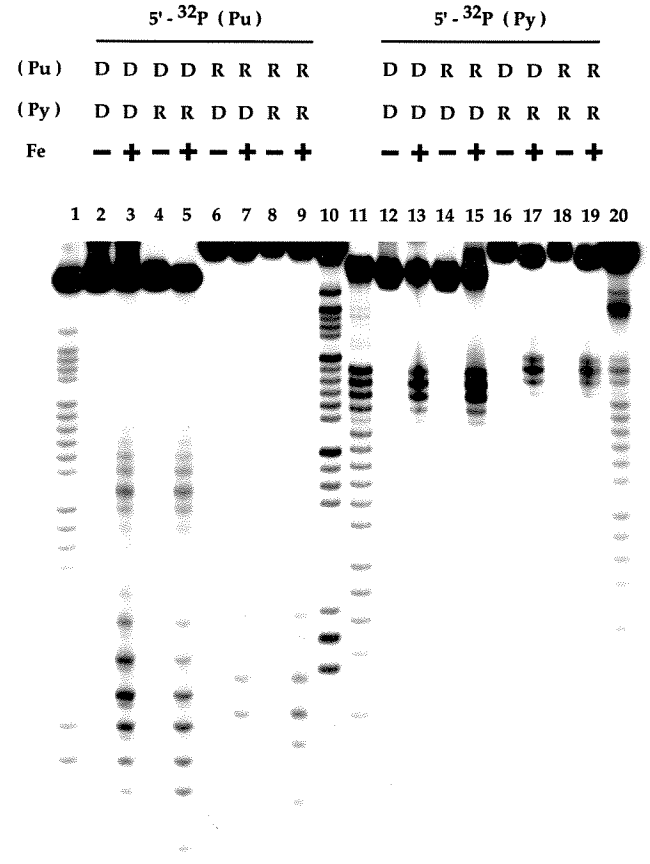

Figure 9. Histograms of the cleavage data derived from the autoradiogram in Figure 8.

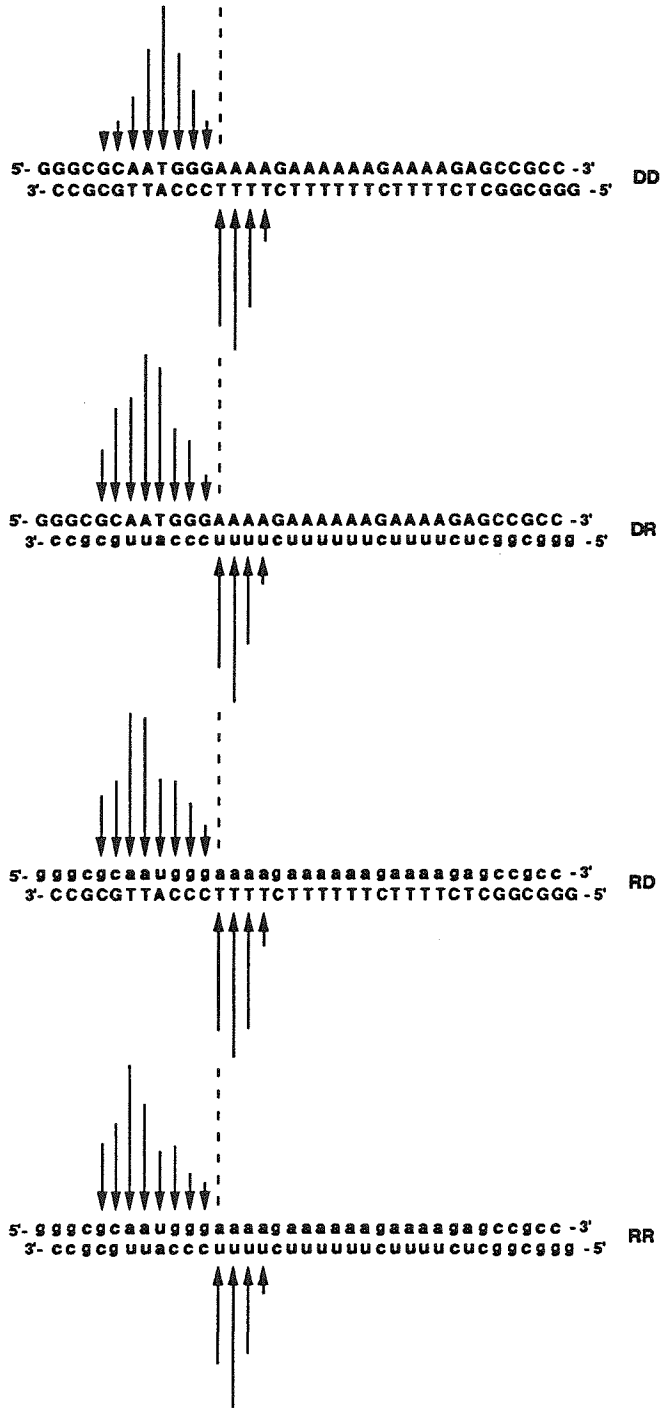
5'- GGGCGCAATGGGAAAAGAAAAAAGAAAAGAGCCGCC -3'
3'- CCGCGTTACCCTTTTCTTTTTTCTTTTCTCGGCGGG -5'
DD
5'- GGGCGCAATGGGAAAAGAAAAAAGAAAAGAGCCGCC -3'
3'- ccgcguuacccuuuucuuuuuucuuuucucggcggg -5'
DR
5'- gggcgcaaugggaaaagaaaaaagaaaagagccgcc -3'
3'- CCGCGTTACCCTTTTCTTTTTTCTTTTCTCGGCGGG -5'
RD
5'- gggcgcaaugggaaaagaaaaaagaaaagagccgcc -3'
3'- ccgcguuacccuuuucuuuuuucuuuucucggcggg -5'
RR

Figure 10. Schematic representation of B-form DNA (left) and A-form RNA (right) of the sequences (GCAA(T/U)GGGAAA) obtained by using the Biopolymer module of Insight II (version 2.2.0) from Biosym Technologies. The purine strand is shown in red and the pyrimidine strand in blue. The sugars of the maximal cleavage sites on the purine and pyrimidine strand are shown in yellow and the thymidine and uridine bases on the pyrimidine strand where *T and *U are placed are shown in white.

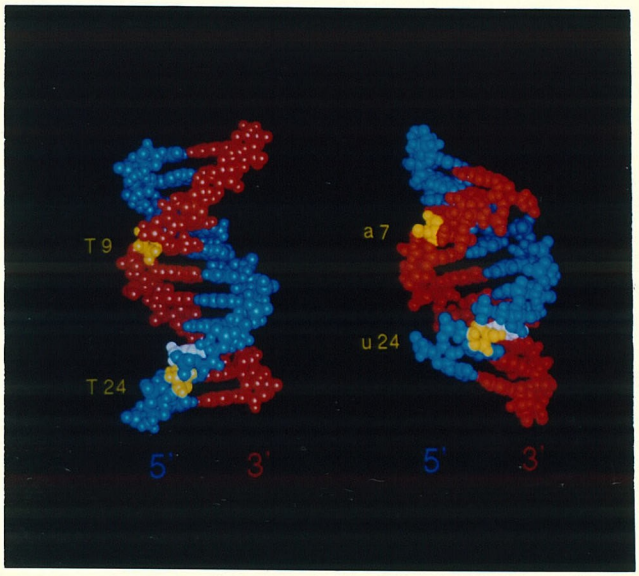
T 9
T 24
5'
3'
a 7
u 24
5'
3'

Figure 11. (*Upper*) Sequences of DNA-EDTA (D), RNA-EDTA (R), and 35-bp duplexes DD, DR, RD, and RR. The uppercase letters indicate DNA and the lowercase letters, RNA. The box indicates the 18-bp purine target sequence within the 35-bp duplex bound by D or R. (*Lower*) Autoradiogram of a 20% denaturing polyacrylamide gel showing affinity cleavage reactions. (Lane 2, 5, 8, 11, 16, 19, 22, 25) Control showing intact 5′ labeled 35-bp duplex standard obtained after treatment according to the cleavage reactions in the absence of oligonucleotide-EDTA•Fe. (Lane 3, 4, 6, 7, 9, 10, 12, 13, 17, 18, 20, 21, 23, 24, 26, 27) Affinity cleavage products produced in the presence of oligonucleotide-EDTA•Fe. (Lane 1) A-specific chemical sequencing of (5′-^{32}P PuD)(PyD). (Lane 14, 28) A+U enzymatic sequencing of (5′-^{32}P PuR) and (5′-^{32}P PyR), respectively. (Lane 15) T-specific chemical sequencing of (5′-^{32}P PyD). Hoogsteen strands are indicated by Py•Fe and Watson and Crick strands are indicated by (Pu) and (Py), where D indicates DNA and R, RNA.

5'- *TTTTCTTTTTTCTTTTCT - 3' D

5'- *uuuucuuuuuucuuuucu - 3' R

5'- GGGCGCAATGGGAAAAGAAAAAAGAAAAGAGCCGCC - 3' DD
3'- CCGCGTTACCCTTTTCTTTTTTCTTTTCTCGGCGGG - 5'

5'- GGGCGCAATGGGAAAAGAAAAAAGAAAAGAGCCGCC - 3' DR
3'- ccgcguuacccuuuucuuuuuucuuuucucggcggg - 5'

5'- gggcgcaauggggaaaagaaaaaagaaaagagccgcc - 3' RD
3'- CCGCGTTACCCTTTTCTTTTTTCTTTTCTCGGCGGG - 5'

5'- gggcgcaauggggaaaagaaaaaagaaaagagccgcc - 3' RR
3'- ccgcguuacccuuuucuuuuuucuuuucucggcggg - 5'

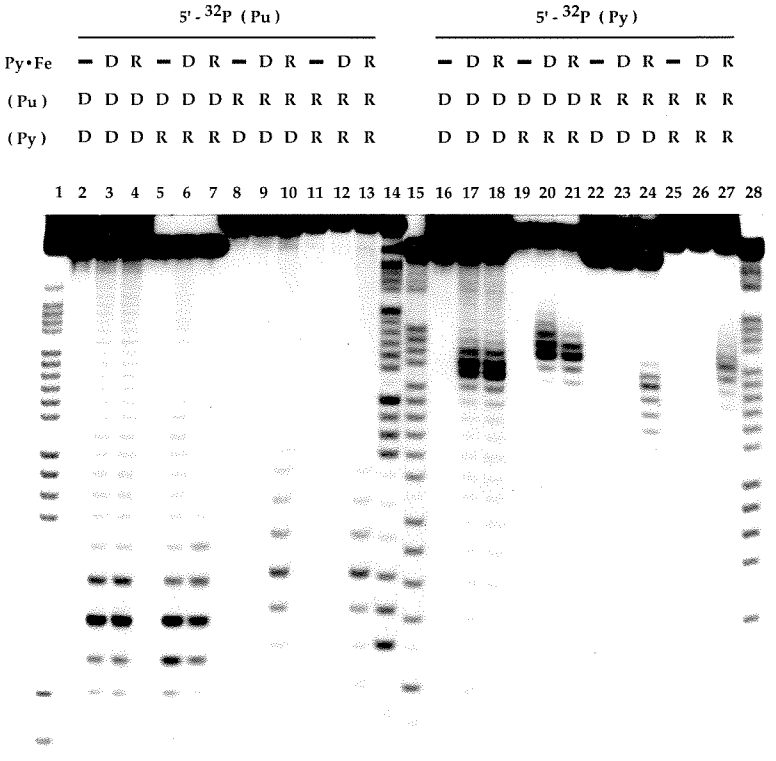

Figure 12. Histograms of the cleavage data derived from the autoradiogram in Figure 11.

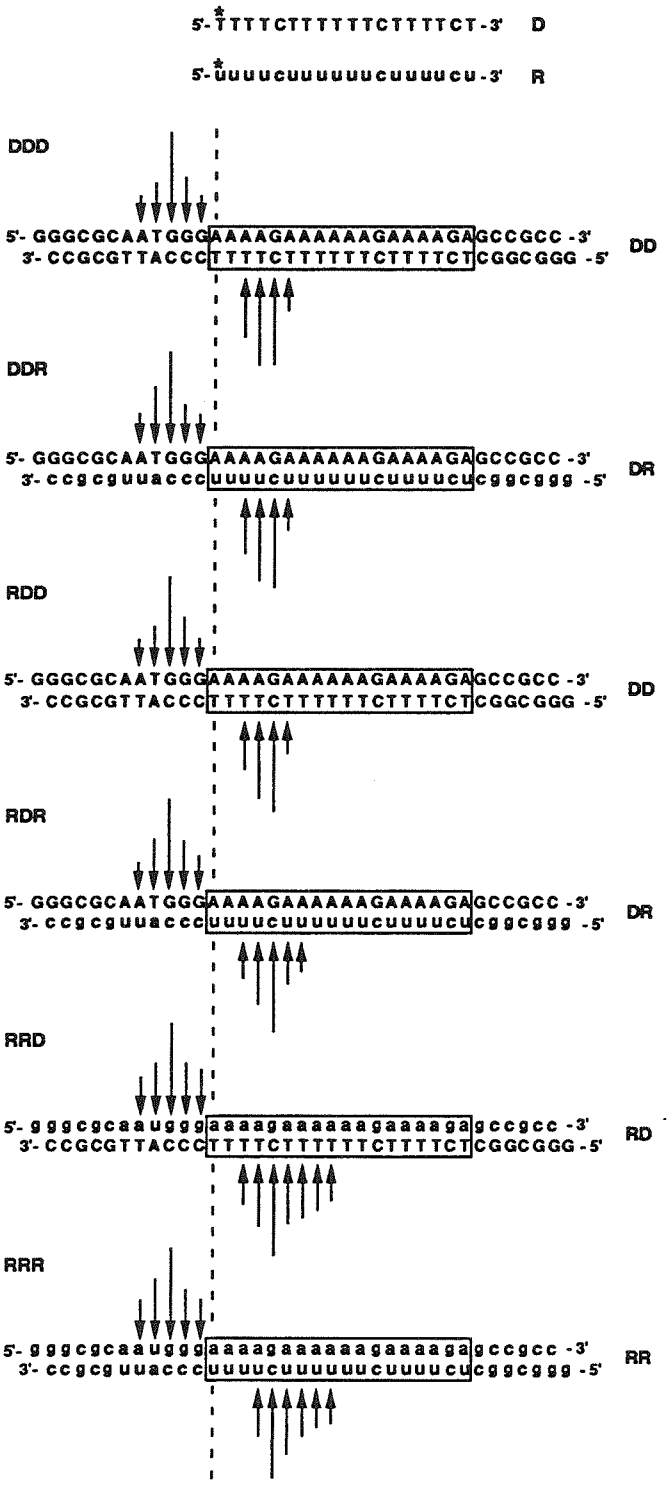
5'-*TTTTCTTTTTTCTTTTCT-3' D
5'-*uuuucuuuuuucuuuucu-3' R
DDD
5'- GGGCGCAATGGGAAAAGAAAAAAGAAAAGAGCCGCC -3'
3'- CCGCGTTACCCTTTTCTTTTTTCTTTTCTCGGCGGG -5'
DD
DDR
5'- GGGCGCAATGGGAAAAGAAAAAAGAAAAGAGCCGCC -3'
3'- ccgcguuacccuuuucuuuuuucuuuucucggcggg -5'
DR
RDD
5'- GGGCGCAATGGGAAAAGAAAAAAGAAAAGAGCCGCC -3'
3'- CCGCGTTACCCTTTTCTTTTTTCTTTTCTCGGCGGG -5'
DD
RDR
5'- GGGCGCAATGGGAAAAGAAAAAAGAAAAGAGCCGCC -3'
3'- ccgcguuacccuuuucuuuuuucuuuucucggcggg -5'
DR
RRD
5'- gggcgcaaugggaaaagaaaaaagaaaagagccgcc -3'
3'- CCGCGTTACCCTTTTCTTTTTTCTTTTCTCGGCGGG -5'
RD
RRR
5'- gggcgcaaugggaaaagaaaaaagaaaagagccgcc -3'
3'- ccgcguuacccuuuucuuuuuucuuuucucggcggg -5'
RR

Figure 13. Models of the structures of base triplets built on B-form DNA (left) and A-form RNA (right) of the sequences (CAA(T/U)GGGAAAAGAAAAAA) obtained as described in Figure 10. The purine strand is shown in red and the pyrimidine strand in blue. The sugars of the cleavage sites on the Watson-Crick purine and pyrimidine strands are shown in yellow. The thymidine and uridine bases on the third strand where *T and *U are placed to form *T•AT and *U•AU base triplets are shown in white.

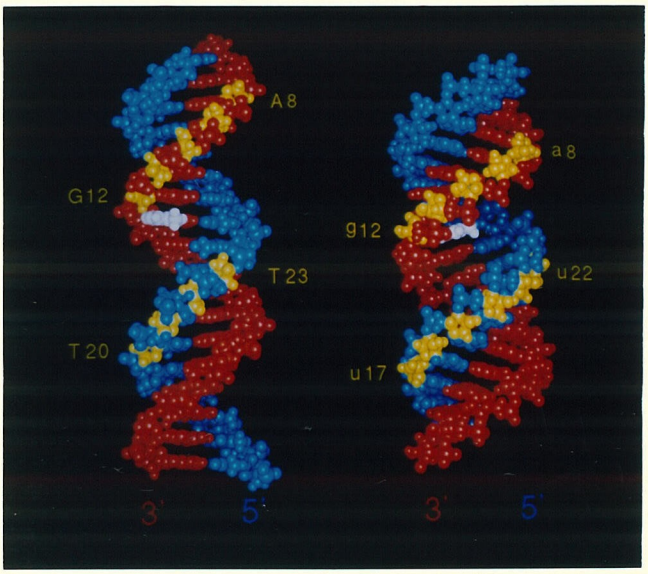
A8
G12
T23
T20
3'
5'
a8
g12
u22
u17
3'
5'

Chapter 3

Visualization of RNA Tertiary Structure by RNA-EDTA•Fe(II) Autocleavage. Analysis of tRNA(*U47)^{Phe}•Fe(II)

Introduction

RNA molecules require specifically folded tertiary structures for their biological and chemical functions (1, 2). Although RNA secondary structures can be determined by chemical and enzymatic modification reagents and comparative sequence analysis, significantly less is known about the tertiary structure of RNAs. At present, the tertiary structures of only some small RNAs have been determined by high-resolution x-ray crystallographic and NMR analysis (3-13). In the absence of such high-resolution studies, there is a need for new methods for analyzing the folded structure of RNA in solution.

Attachment of EDTA•Fe(II) to small molecules, proteins, and oligonucleotides has proven useful for studying the structures of such molecules in complex with nucleic acids (14-22). Upon addition of a reducing agent such as dithiothreitol or sodium ascorbate, the EDTA•Fe(II) moiety generates a nonspecific diffusible oxidant, most likely hydroxyl radical. Cleavage at several nucleotide positions proximal in space to the unique location of the bound EDTA•Fe(II) affords DNA or RNA fragments of different size and amount. Hence structural information regarding the nucleotides neighboring the discretely bound ligand-EDTA•Fe(II) can be determined by electrophoretic separation of nucleic acid cleavage products on a high-resolution polyacrylamide gel. The size and amount of cleaved fragments relate to the distance in the three-dimensional structure.

The question arises whether self-cleavage of a folded RNA structure with EDTA•Fe(II) at a unique base position would be useful for analyzing nearest neighbors by cleavage pattern analysis. Yeast $tRNA^{Phe}$ is an attractive candidate for initial studies because its three-dimensional structure is well-

characterized by x-ray crystallography and the solution structure of the fully unmodified yeast $tRNA^{Phe}$ has been shown to be similar to that of the native yeast $tRNA^{Phe}$ (3, 23-25). The correlation of autocleavage data with those from the crystal structure of the native tRNA would establish the potential of autocleavage for analyzing tertiary structures of RNAs. tRNA-EDTA suitable for intramolecular autocleavage studies was constructed by the chemical incorporation of *U into the 3'-half fragment of tRNA at position U47 followed by enzymatic ligation to the 5'-half tRNA using T4 DNA ligase (Figure 1) (22, 26). Lead specific cleavage of $tRNA(*U47)^{Phe}$ indicates that the folded structure is not disrupted by the presence of EDTA at the *U47 position (Table 1; see Figure 2) (9, 27). The autocleavage pattern of $tRNA(*U47)^{Phe}$•Fe(II) correlates reasonably well with the high-resolution x-ray crystal structure, leading to the conclusion that autocleavage may be applicable for studies of tertiary structures of RNAs (Figure 4).

Materials and Methods

General. Adenosine 5'-triphosphate and DNase I were purchased from Pharmacia and T4 polynucleotide kinase and T4 RNA ligase were obtained from New England Biolabs. T4 DNA ligase was purchased from United States Biochemical. [γ-^{32}P]ATP (~6000 Ci/mmol; 1 Ci = 37 GBq) and [5'-^{32}P]pCp (~3000 Ci/mmol) were obtained from Amersham and New England Nuclear, respectively. Phosphoramidites were purchased from Applied Biosystems (dA, dG, dC, and T) and from BioGenex Laboratories (San Ramon, CA) (rA, rG, rC, and U).

tRNA and tRNA(*U47)^{Phe} Preparation. Oligonucleotides were synthesized by standard automated solid-support chemistry using an Applied Biosystems model 394 DNA/RNA synthesizer. RNA oligonucleotides with EDTA at a single uridine position were prepared as described (22). RNA was 5′-end labeled using T4 polynucleotide kinase and [γ-^{32}P]ATP (28). RNA was 3′-end labeled using T4 RNA ligase and [5′-^{32}P]pCp (29). Prior to the ligation with T4 DNA ligase, 3′-half RNA was phosphorylated at the 5′ end with T4 polynucleotide kinase and ATP (28). The 5′-^{32}P-end-labeled tRNA was prepared by ligation of 5′-^{32}P-labeled 5′-half tRNA (1-36) to 3′-half tRNA (37-76) using a 50 base DNA template (10-59) complementary to the 3′ end of 5′-half tRNA (27 nt) and the 5′ end of 3′-half tRNA (23 nt) (Figure 1) (26). The 3′-^{32}P-end-labeled tRNA was prepared by using 5′-half tRNA and 3′-^{32}P-labeled 3′-half tRNA. 5'-half tRNA (50 pmol) and 3'-half tRNA (50 pmol) were added to the DNA template (50 pmol) in 20 μL of hybridization buffer (10 mM Tris•HCl, pH 7.6, 10 mM KCl), heated to 90 °C for 1 min and cooled to room temperature over 1 h. Following hybridization, 2.5 μL of 10X ligase buffer (660 mM Tris•HCl, pH 7.6, 660 μM ATP, 66 mM $MgCl_2$, 100 mM DTT) and 2.5 μL of 10 units/μL T4 DNA ligase were added. After a 6 h incubation at 16 °C, the reaction was treated with 1 μL of 10 units/μL DNase I for 30 min at 37 °C. Samples were ethanol precipitated, purified by electrophoresis on a 20% polyacrylamide/7 M urea gel (0.8 mm thickness), and eluted in 250 μL elution buffer (0.3 M sodium acetate) at room temperature. Eluted RNAs were ethanol precipitated, dried, and stored at -20 °C until use.

Cleavage Reactions. All tRNAs were renatured by heating to 70 °C for 1 min in 10 mM Tris•HCl, pH 7.0 and slow cooling to room temperature prior to use. A typical 50-μL reaction mixture contained 2 μM tRNA (~200,000 cpm), 20 mM

Tris•HCl, pH 7.0, 10 mM $MgCl_2$, and 20 mM NaCl. The lead cleavage reaction was carried out by addition of $Pb(OAc)_2$ (200 μM) at 25 °C and at appropriate intervals 5-μL aliquots were removed, added to 5 μL of stop buffer (7 M urea/50 mM EDTA/dyes), and analyzed on a 15% polyacrylamide/7 M urea gel (27). Autocleavage reactions for tRNA(*U47)^{Phe} were performed by incubation of tRNA(*U47)^{Phe} with $Fe(NH_4)_2(SO_4)_2 \cdot 6H_2O$ (1 μM) for 2 h at 25 °C followed by addition of dithiothreitol (4 mM). After 8 h at 25 °C, the cleavage reactions were analyzed by loading 20,000 cpm of the sample on a 20% polyacrylamide/7 M urea wedge gel (W x L = 31.0 x 38.5 cm, 0.4 mm at top and 1.2 mm at bottom). The amount of product fragments was quantitated by PhosphorImager analysis (Molecular Dynamics) (30).

Results and Discussion

Site for the Incorporation of *U. Examination of the high resolution x-ray crystal structure of yeast tRNA^{Phe} and of mutant studies suggests that nucleotide position U47 of tRNA is a reasonable choice for EDTA•Fe(II) attachment (3-6, 27, 31-33). The presence of a modified base, 3-(3-amino-3-carboxypropyl)uridine, located in the loop, occurs naturally at U47 of *Escherichia coli* tRNA^{Phe} (34).

tRNA-EDTA Preparation. 5'-half tRNA, 36 nt in length, and 3'-half tRNA, 40 nt in length, were synthesized by automated methods using 2-cyanoethyl phosphoramidite chemistry (35). 3'-half tRNA with *U at the U47 position was prepared by the incorporation of phosphoramidites of the functionalizable uridine-amine into oligoribonucleotides followed by subsequent modification with activated EDTA derivatives as described (Figure 1) (22). RNA

oligonucleotides containing *U with the attached EDTA moiety displayed a reduced electrophoretic mobility and could be purified on a 20% denaturing gel of 0.8 mm thickness (22). A 5-10% yield of purified RNA-EDTA was obtained on a 1 μmol scale oligonucleotide synthesis. A DNA template with 50 bases complementary to 5′-half and 3′-half tRNA was used to juxtapose the ligation substrates. Full length tRNAs, 76 nt in length, were constructed by ligation of 5′-half tRNA to 3′-half tRNA using T4 DNA ligase (Figure 1) (26). The yield after ligation was approximately 10-15% for both tRNA and tRNA-EDTA.

Lead Cleavage Assay. The lead cleavage reaction was carried out to examine the correct folding of tRNA(*U47)^{Phe}. Analysis of the Pb(II) cleavage rates of the yeast tRNA^{Phe} mutants shows that the rate of cleavage is sensitive to the proper tertiary structure (27). The major lead specific cleavage sites of tRNA(*U47)^{Phe} in 20 mM Tris•HCl, pH 7.0, 10 mM $MgCl_2$, 20 mM NaCl, 2 μM tRNA, and 200 μM $Pb(OAc)_2$ were located between U17 and G18 in the D loop (Figure 2 *Upper*). Under the conditions used here, tRNA(*U47)^{Phe} exhibits a cleavage rate similar to that of unmodified tRNA^{Phe} whose rate is two times slower than that of native yeast tRNA^{Phe} (Table 1; see Figure 2). This is consistent with previous results (27). The site and rate of lead cleavage observed for tRNA(*U47)^{Phe} indicate that the presence of EDTA at position U47 does not significantly alter the folding of tRNA, confirming that tRNA(*U47)^{Phe} can adopt a conformation similar to that of the native folded tRNAs.

Autocleavage. The sites of autocleavage in tRNA-EDTA•Fe(II) with *U at position U47 were determined by using 5′- or 3′-^{32}P-end-labeled tRNA(*U47)^{Phe}•Fe(II) (Figure 3). Autocleavage was performed under conditions similar to those used for Pb(II) cleavage. The labeled

tRNA(*U47)^{Phe} was renatured, equilibrated with Mg^{2+} for 20 min, and treated with Fe(II). After 2 h at room temperature, autocleavage reactions were initiated by addition of dithiothreitol and incubated for 8 h at 25 °C. Cleavage sites between nucleotides 1 to 40 were mapped with 5'-end-labeled tRNA(*U47)^{Phe} and those between 41 to 76 with 3'-end-labeled tRNA(*U47)^{Phe}. Comparison of autocleavage products from tRNA(*U47)^{Phe} in the absence and presence of Fe(II) reveals cleavage sites and efficiencies (Figure 3, lanes 5, 12; lanes 6, 13). Very low levels of nonspecific cleavage were observed when unmodified tRNA^{Phe} was subjected to cleavage with EDTA•Fe(II), propane-EDTA•Fe(II), and Fe(II) at final concentrations of 1 μM, demonstrating that the observed autocleavage was generated by EDTA•Fe(II) tethered to tRNA at *U47 (Figure 3, lanes 2-4; lanes 9-11).

Six regions of specific cleavage were identified: nucleotides 7-9, 14-21, 22-27, 44-51, 56-61, and 66-68 (Figure 4A). Strongest cleavage was observed at nucleotides 44-51 which are adjacent to *U47, corresponding to 5% of the intact tRNA(*U47)^{Phe}. The sites of autocleavage are represented by circles on the secondary structure diagram (Figure 4B). Five regions with weaker cleavage were mapped on the tertiary structure of tRNA^{Phe} (Figure 4C) (6). The five medium cleavage sites centered at positions U8, G18, G26, G57, and A67 are estimated to be within 11-24 Å from the 5-carbon position of *U47 in the tertiary structure. An intensity ratio (θ), defined as autocleavage at the given nucleotide to the average autocleavage in the region 44-51, was compared with the distance (d) measured between the 5-carbon of *U47 and the 4'-carbons of the nucleotides. For positions U8 and A67, which are at 11 and 14 Å from *U47, the cleavage intensity (θ) is 0.3 and 0.4, respectively. For G18, G26, and G57, which are at 24 Å, θ is 0.4. This reveals that the cleavage intensity is insensitive

to fine tuning distances in the 11-24 Å range. This is likely due to the fact that not every ribose at fixed distance has identical reactivity or that the tethered EDTA•Fe(II) moiety may have preferred positions to "rut" on the folded molecule. The lack of autocleavage ($\theta \leq 0.04$) at the acceptor stem and 3′ end (d = 38 Å for A73) and the anticodon stem and loop (d = 50 Å for G34) is also consistent with the three-dimensional structure, since these regions are distant from *U47.

Implications and Limitations. Although there is overall agreement between the autocleavage data and the crystal structure for the tRNA study here, there are limitations which may be relevant to the general applicability of autocleavage for studying tertiary structures of large RNA molecules. The cleavage data correlate with three-dimensional distance only in broad categories: adjacent to *U (strong cleavage), proximal to *U in the range 11-24 Å (medium cleavage), and distal to *U in the range >40 Å (very weak cleavage). For large RNA structures, this low resolution information may be sufficient to distinguish between different hypothetical models. In addition, this approach may be useful for studying tRNA-ribosome interactions as well as tertiary structures of larger RNAs.

References

1. Cech, T. R. (1990) *Annu. Rev. Biochem.* **59**, 543-568.
2. Draper, D. E. (1992) *Acc. Chem. Res.* **25**, 201-207.
3. Kim, S. H., Quigley, G. J., Suddath, F. L., McPherson, A., Sneden, D., Kim, J. J., Weinzierl, J. & Rich, A. (1973) *Science* **179**, 285-288.
4. Kim, S. H., Sussman, J. L., Suddath, F. L., Quigley, G. J., McPherson, A., Wang, A. H. J., Seeman, N. C. & Rich, A. (1974) *Proc. Natl. Acad. Sci. U.S.A.* **71**, 4970-4974.
5. Robertus, J. D., Ladner, J. E., Finch, J. T., Rhodes, D., Brown, R. S., Clark, B. F. C. & Klug, A. (1974) *Nature* **250**, 546-551.
6. Quigley, G. J. & Rich, A. (1976) *Science* **194**, 796-806.
7. Holbrook, S. R., Sussman, J. L., Warrant, R. W., Church, G. M. & Kim, S. H. (1977) *Nucleic Acids Res.* **4**, 2811-2820.
8. Jack, A., Ladner, J. E., Rhodes, D., Brown, R. S. & Klug, A. (1977) *J. Mol. Biol.* **111**, 315-328.
9. Brown, R. S., Dewan, J. C. & Klug, A. (1985) *Biochemistry* **24**, 4785-4801.
10. Westhof, E., Dumas, P. & Moras, D. (1985) *J. Mol. Biol.* **184**, 119-145.
11. Rould, M. A., Perona, J. J., Soll, D. & Steitz, T. A. (1989) *Science* **246**, 1135-1142.
12. Holbrook, S. R., Cheong, C., Tinoco, I., Jr. & Kim, S. H. (1991) *Nature* **353**, 579-581.
13. Nikonowicz, E. P. & Pardi, A. (1992) *Nature (London)* **355**, 184-186.
14. Dervan, P. B. (1986) *Science* **232**, 464-471.
15. Taylor, J. S., Schultz, P. G. & Dervan, P. B. (1984) *Tetrahedron* **40**, 457-465.

16. Sluka, J. P., Griffin, J. H., Mack, D. P. & Dervan, P. B. (1990) *J. Am. Chem. Soc.* **112**, 6369-6374.

17. Dreyer, G. B. & Dervan, P. B. (1985) *Proc. Natl. Acad. Sci. U.S.A.* **82**, 968-972.

18. Moser, H. E. & Dervan, P. B. (1987) *Science* **238**, 645-650.

19. Wang, J. -F. & Cech, T. R. (1992) *Science* **256**, 526-529.

20. Jayasena, S. D. & Johnston, B. H. (1992) *Proc. Natl. Acad. Sci. U.S.A.* **89**, 3526-3530.

21. Han, H. & Dervan, P. B. (1993) *Proc. Natl. Acad. Sci. U.S.A.* **90**, 3806-3810.

22. Han, H. & Dervan, P. B. (1994) *Nucleic Acids Res.*, submitted.

23. Hall, K. B., Sampson, J. R., Uhlenbeck, O. C. & Redfield, A. G. (1989) *Biochemistry* **28**, 5794-5801.

24. Latham, J. A. & Cech, T. R. (1989) *Science* **245**, 276-282.

25. Huttenhofer, A. & Noller, H. F. (1992) *Proc. Natl. Acad. Sci. U.S.A.* **89**, 7851-7855.

26. Moore, M. J. & Sharp, P. A. (1992) *Science* **256**, 992-997.

27. Behlen, L. S., Sampson, J. R., DiRenzo, A. B. & Uhlenbeck, O. C. (1990) *Biochemistry* **29**, 2515-2523.

28. Sambrook, J., Fritsch, E. F. & Maniatis, T. (1989) *Molecular Cloning: A Laboratory Manual* (Cold Spring Harbor Lab., Plainview, NY), 2nd Ed.

29. England, T. E. & Uhlenbeck, O. C. (1978) *Nature (London)* **275**, 560-561.

30. Johnston, R. F., Pickett, S. C. & Barker, D. L. (1990) *Electrophoresis* **11**, 355-360.

31. Sampson, J. R. & Uhlenbeck, O. C. (1988) *Proc. Natl. Acad. Sci. U.S.A.* **85**, 1033-1037.

32. Sampson, J. R., DiRenzo, A. B., Behlen, L. S. & Uhlenbeck, O. C. (1989) *Science* **243**, 1363-1366.

33. Pan, T., Gutell, R. R. & Uhlenbeck, O. C. (1991) *Science* **254**, 1361-1364.

34. Ofengand, J., Denman, R., Nurse, K., Liebman, A., Malarek, D., Focella, A. & Zenchoff, G. (1988) *Methods Enzymol.* **164**, 372-397.

35. Gait, M. J. (1984) *Oligonucleotide Synthesis: A Practical Approach* (IRL Press, Washington DC).

36. Peattie, D. A. (1979) *Proc. Natl. Acad. Sci. U.S.A.* **76**, 1760-1764.

Figure 1. (*Upper Left*) Uridine-amine (U^{NH_2}) and uridine-EDTA (*U). (*Upper Right*) Scheme for the synthesis of 3′-^{32}P-labeled 3′-half tRNA. (*Lower*) Sequences of oligonucleotides, 5′-half, 3′-half, and DNA template used to construct 3′-^{32}P-labeled tRNA-EDTA by ligation with T4 DNA ligase. *U indicates uridine-EDTA that is incorporated at U47. A 3'-hydroxyl and a 5'-phosphate are shown in the ligation junction at which phosphodiester bond formation is catalyzed by T4 DNA ligase.

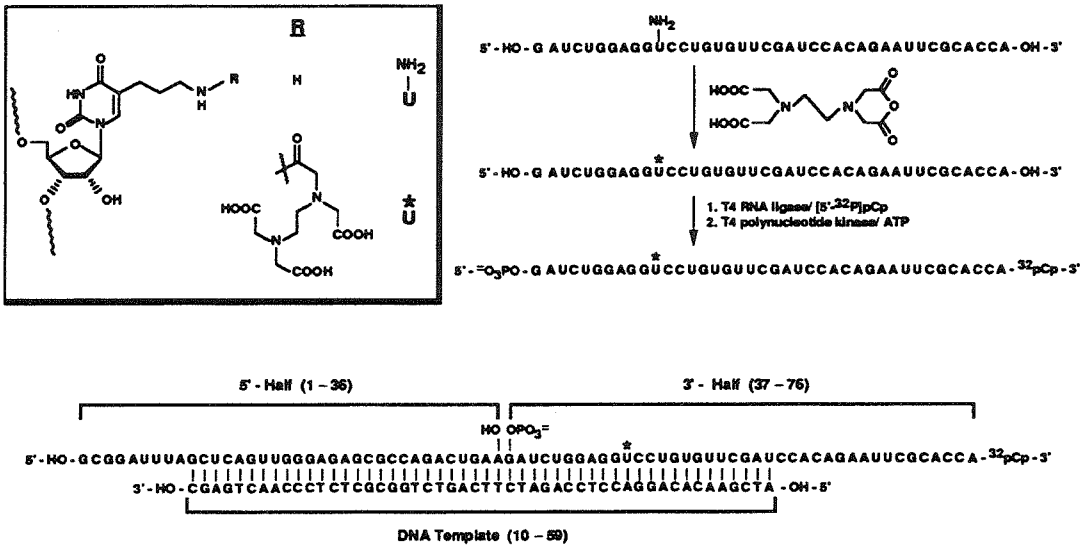
R
H
NH2
U
U*
OH
HOOC
COOH
COOH
5'-HO-G AUCUGGAGGUCCUGUGUUCGAUCCACAGAAUUCGCACCA-OH-3'
HOOC
HOOC
1. T4 RNA ligase/ [5'-32P]pCp
2. T4 polynucleotide kinase/ ATP
5'-=O3PO-G AUCUGGAGGUCCUGUGUUCGAUCCACAGAAUUCGCACCA-32pCp-3'

5'-Half (1-36)
3'-Half (37-76)
HO OPO3=
5'-HO-GCGGAUUUAGCUCAGUUGGGAGAGCGCCAGACUGAAGAUCUGGAGGUCCUGUGUUCGAUCCACAGAAUUCGCACCA-32pCp-3'
3'-HO-CGAGTCAACCCTCTCGCGGTCTGACTTCTAGACCTCCAGGACACAAGCTA-OH-5'
DNA Template (10-59)

Figure 2. (*Upper*) Autoradiogram of a 15% denaturing polyacrylamide gel showing lead cleavage reactions of a 3'-^{32}P-labeled tRNA(*U47)^{Phe}. (Lanes 1-6) Cleavage products produced from tRNA(*U47)^{Phe}, which were allowed to react for 0, 1, 2, 5, 8, and 12 min, respectively. (Lane 7) A-specific chemical sequencing (36). (*Lower*) Cleavage kinetics of native yeast tRNA^{Phe} (▪), unmodified tRNA^{Phe} (●), and tRNA(*U47)^{Phe} (o).

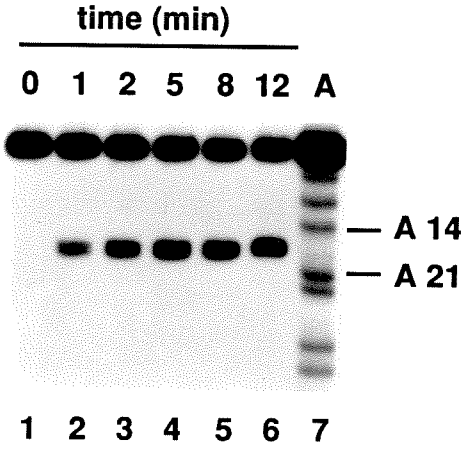
time (min)
0 1 2 5 8 12 A
A 14
A 21
1 2 3 4 5 6 7

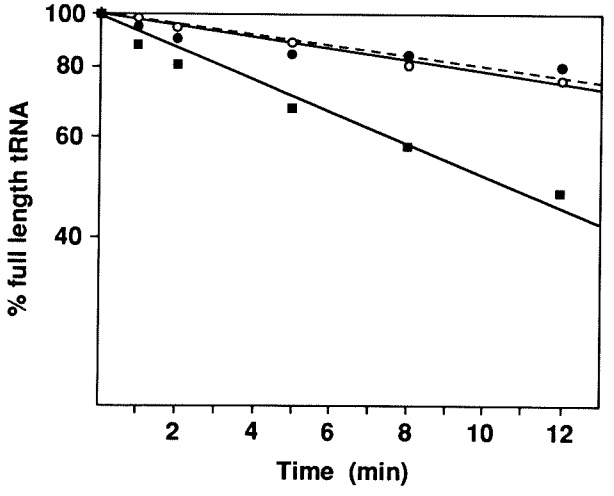
100
80
60
40
% full length tRNA
2 4 6 8 10 12
Time (min)

Table 1. Rate of lead cleavage for tRNA

	k_{obs} (s^{-1} x 10^4)	rel k_{obs}
Yeast $tRNA^{Phe}$	7.9 (± 1.2)	1
Unmodified $tRNA^{Phe}$ §	3.5 (± 0.4)	0.44
$tRNA(*U47)^{Phe}$	3.4 (± 0.5)	0.43

§Unmodified $tRNA^{Phe}$ was prepared by ligation of the synthetic 5'-half tRNA to the synthetic 3'-half tRNA containing uridine at position 47 using T4 DNA ligase.

Figure 3. Autoradiogram of a 20% denaturing polyacrylamide wedge gel showing affinity cleavage reactions of unmodified $tRNA^{Phe}$ and $tRNA(*U47)^{Phe}$ labeled with ^{32}P at the 5' end (lanes 1-7) and at the 3' end (lanes 8-14). (Lanes 1-6, 8-13) Cleavage products of unmodified $tRNA^{Phe}$ (lanes 1-4, 8-11) and $tRNA(*U47)^{Phe}$ (lanes 5-6, 12-13) obtained after incubation under the conditions of autocleavage reactions in the absence of Fe(II) (lanes 1, 5, 8, 12) and the presence of EDTA•Fe(II) (lanes 2, 9), propane-EDTA•Fe(II) (lanes 3, 10), and Fe(II) (lanes 4, 6, 11, 13). (Lanes 7, 14) A-specific chemical sequencing (36).

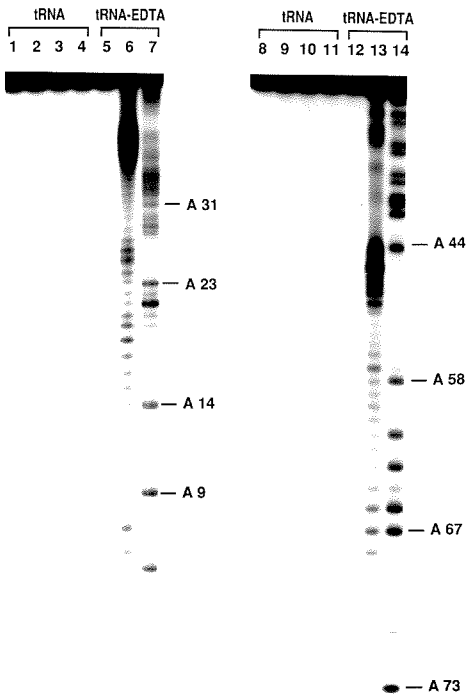
tRNA
tRNA-EDTA
1 2 3 4 5 6 7
A 31
A 23
A 14
A 9
tRNA
tRNA-EDTA
8 9 10 11 12 13 14
A 44
A 58
A 67
A 73

Figure 4. (A) Histogram of the cleavage data derived from autoradiogram in Figure 3. The heights of the bars represent the relative cleavage intensities at the indicated bases. Six cleavage regions, 7-9, 14-21, 22-27, 44-51, 56-61, and 66-68, were mapped on the secondary and tertiary structures shown below. (B) tRNA(*U47)^{Phe} autocleavage sites mapped on the secondary structure of tRNA^{Phe}. The position of *U47 is indicated by the filled circle. (C) tRNA(*U47)^{Phe} autocleavage sites mapped on a ribbon diagram of the tertiary structure adapted from the crystal structure of yeast tRNA^{Phe} (6). Filled circles indicate points of cleavage along the phosphodiester backbone with size corresponding to relative cleavage intensity. The position of *U47 is indicated by the filled circle with Fe.

A

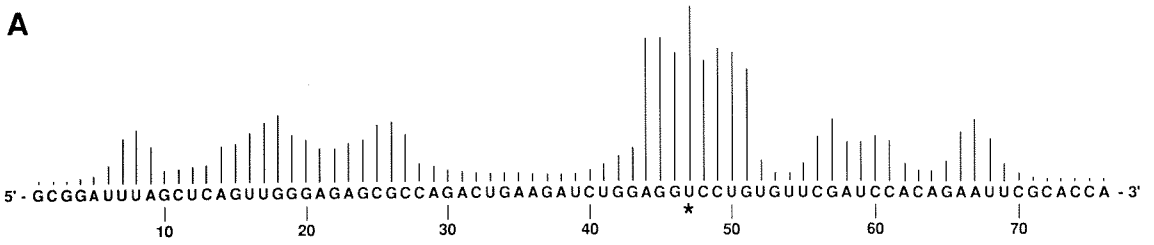
5' - GCGGAUUUAGCUCAGUUGGGAGAGCGCCAGACUGAAGAUCUGGAGGUCCUGUGUUCGAUCCACAGAAUUCGCACCA - 3'
10
20
30
40
50
60
70

B

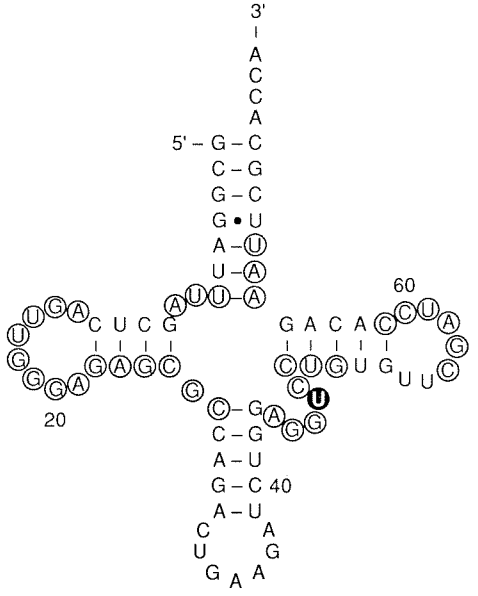
3'
5'
20
40
60

C

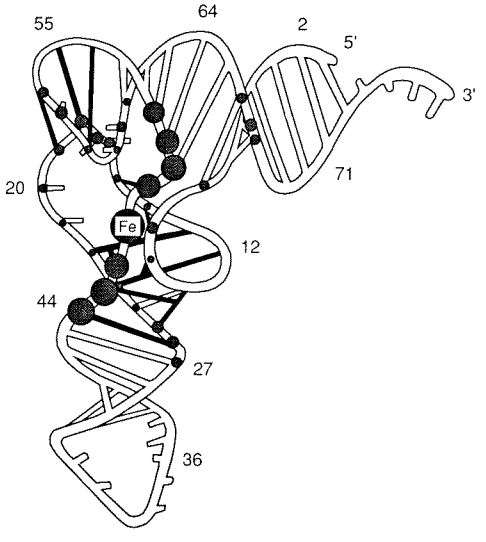
55
64
2
5'
3'
71
20
Fe
12
44
27
36

Chapter 4

Mapping Regions in Eukaryotic Ribosomes That Are Accessible to Methidiumpropyl-EDTA•Fe(II) and EDTA•Fe(II)

Introduction

Ribosomes, ubiquitous ribonucleoproteins, require specifically folded RNA tertiary structures to carry out the essential process of protein biosynthesis in the cell. The ribosomal RNAs (rRNAs) in ribosomes interact directly with messenger RNA, transfer RNA, factors, and various ribosome-directed antibiotics and are involved in codon-anticodon interaction, the peptidyltransferase region, and subunit association (1-10). Low resolution three-dimensional models of 16S rRNA in the *Escherichia coli* small ribosomal subunit have been derived from methods such as chemical and enzymatic probing, comparative sequence analysis, biophysical approaches, and site-specific mutagenesis (11-13). In contrast to prokaryotic (especially *E. coli*) ribosomes, far less is known about rRNA conformations of eukaryotic ribosomes.

MPE•Fe(II), which consists of EDTA•Fe(II) tethered to the intercalator methidium, has proven useful for studying interactions between DNA binding molecules and DNAs as well as structures of RNAs (14-21). Upon addition of dithiothreitol or sodium ascorbate plus hydrogen peroxide, the EDTA•Fe(II) moiety cleaves DNA and RNA by oxidation of the backbone via a nonspecific diffusible oxidant, most likely hydroxyl radical. Analysis of the cleavage products on a high-resolution denaturing polyacrylamide gel allows nucleotide positions accessible to the cleaving moiety to be mapped to nucleotide resolution.

Here, we report the use of MPE•Fe(II) in conjuction with primer extension for studies of 18S and 28S rRNA structures in eukaryotic ribosomes. EDTA•Fe(II), a solvent-base untethered reagent, was used for comparison (22-

26). Intact ribosomes from *D. melanogaster* were used since *D. melanogaster* is a eukaryote which is well-characterized biochemically and genetically. The results reveal that cleavage occurs in a limited number of accessible regions of 18S and 28S rRNAs. The 18S and 28S rRNA regions that are susceptible to cleavage by MPE•Fe(II) and EDTA•Fe(II) are located within regions defined previously as "expansion segments". Accessibility to the cleaving agents indicates that these expansion segment regions are probably exposed on the surface of the intact eukaryotic ribosomes. The presence of certain surface-exposed rRNA sequences in eukaryotic ribosomes capable of actively translating *in vitro* has interesting implications for the spatial arrangement of rRNAs in ribosomes.

Materials and Methods

Preparation of the Embryo Lysate. The embryo lysate was prepared essentially as described by Scott et al. (27). Two grams of freshly collected *D. melanogaster* embryos (0-20 h) were dechorionated in 100 mL of a 1:1 mixture of 95% ethanol and chlorox (2% sodium hypochlorite) for one min on ice. Embryos were then washed thoroughly with ice-cold phosphate buffered saline (50 mM KH_2PO_4, pH 7.5, 100 mM NaCl) and pelleted at 1,000 x g for 4 min at 0 °C. The pellet was resuspended in 2 mL of 10 mM Hepes, pH 7.6 and homogenized by 10-20 strokes of a loose-fitting Dounce homogenizer on ice. The homogenate was centrifuged at 40,000 x g for 20 min at 0 °C. After centrifugation, the clear supernatant was removed and immediately used for reactions with chemical reagents.

MPE•Fe(II) and EDTA•Fe(II) Reactions with Ribosomes in Lysates. A reaction mixture containing 100 μL lysate, 15 μL of the appropriate 10X concentration of preformed MPE•Fe(II) or EDTA•Fe(II) and 25 μL H_2O was preincubated for 5 min at 25 °C. The cleavage reaction was initiated by addition of 5 μL each of freshly prepared 30X sodium ascorbate and 30X H_2O_2 solutions. The reaction was incubated for 30 min at 25 °C and stopped by adding 850 μL of denaturing buffer (4 M guanidinium thiocyanate, 25 mM sodium citrate, pH 7.0, 0.5% sarcosyl). The RNA was purified according to the procedure of Chomczynski and Sacchi (28). The reaction mixture was transferred to a 15 mL polypropylene tube and kept on ice at all times unless otherwise indicated. Sequentially, 0.1 mL of 2 M sodium acetate, pH 4.0, 1 mL of water saturated phenol, and 0.2 mL of chloroform-isoamyl alcohol mixture (49:1) were added to the tube. The final suspension was mixed thoroughly, cooled on ice for 15 min, and centrifuged at 10,000 x g for 20 min at 4 °C. After centrifugation, the aqueous phase was transferred to a prechilled tube and mixed with 2.5 vol of cold 95% ethanol plus 1/3 vol of 10 M NH_4OAc. The RNA was precipitated for 2 h at -70 °C and pelleted by centrifugation at 10,000 x g for 20 min at 4 °C. The RNA pellet was dissolved in 0.3 mL of denaturing buffer and transferred to a 1.5 mL eppendorf tube. The RNA was precipitated by addition of 900 μL of 95% cold ethanol and 100 μL of 10 M NH_4OAc. After centrifugation at 16,000 x g for 30 min at 4 °C, the RNA pellet was washed with 1 mL 70% ethanol, dried in a Savant Speed Vac concentrator, and resuspended at 1 μg/μL in water.

Preparation of 5'-end Labeled Primers. The DNA oligonucleotides were synthesized on a 1 μmol scale using β-cyanoethyl phosphoramidite chemistry on an Applied Biosystems Model 308B DNA synthesizer. The oligonucleotides

were removed from the support and deprotected by treatment with concentrated NH_4OH at 55 °C for 24 h. After completion of the reaction, the crude oligonucleotides were lyophilized and purified by gel electrophoresis on a denaturing 20% polyacrylamide gel (40 x 20 x 0.2 cm, 1:20 cross linked, 7.5 M urea, 1X TBE buffer (100 mM Tris•borate, pH 8.3, 2 mM EDTA)) at 550 V for 24 h. The major UV-absorbing bands were excised from the gel and crushed, and the oligonucleotides were eluted from the gel into 4 mL of 200 mM NaCl, 1 mM EDTA at 37 °C for 24 h. The gel material was removed from the eluted oligonucleotides by filtration through a cellulose acetate filter (0.45 μm pore size) and the resulting filtrate was dialyzed against doubly distilled water for 72 h. Oligonucleotide concentrations were determined by UV-absorbance at 260 nm. The oligonucleotides were labeled at their 5′ ends by reaction with T4 polynucleotide kinase (New England Biolabs) and [γ-^{32}P]ATP (Amersham) as described (15 μL final volume) (29). The labeled DNA was precipitated from 200 μL of 1:3 0.3 M sodium acetate, pH 5.2/95% ethanol, rinsed with 1 mL 70% ethanol, dried, and dissolved in H_2O. Specific radioactivity was measured with a Beckman LS3801 scintillation counter.

Primer Extension. Primer extension was performed as described (30, 31). 3 μL of 5′-end labeled primers (~500,000 cpm) and 1 μL of 1 μg/μL RNA were dissolved in 1 μL of 5X hybridization buffer (250 mM K•Hepes, pH 7.0, 500 mM KCl). The reaction mixture was heated to 90 °C and then slowly cooled to 50 °C. The extension mixture was prepared by addition of 2 μL of 10X entension buffer (500 mM Tris•HCl, pH 8.3, 250 mM KCl, 100 mM $MgCl_2$), 4 μL of 2.5 mM dNTP (2.5 mM each dATP, dCTP, dGTP, and TTP), 0.5 μL of 80 mM DTT, 8 μL H_2O, and 0.5 μL AMV reverse transcriptase (~20 units/μL, Life Sciences) to 5 μL of the cooled RNA/primer hybrid mixture. Dideoxy

sequencing reactions contained 2 μL of 2.5 mM dNTP and 2 μL of the appropriate 0.25 mM ddNTP instead of 4 μL of 2.5 mM dNTP (32). Extension of the primer was allowed to proceed for 30 min at 43 °C and terminated by addition of 100 μL of 0.3 M sodium acetate, pH 5.2 and 300 μL of 95% ethanol. The sample was cooled on ice for 1 h and the cDNA transcripts were pelleted by centrifugation at 16,000 x g for 20 min. The pellets were washed with 1 mL 70% ethanol, dried under vaccum, and resuspended in 10 μL of loading buffer (80% formamide, 1X TBE, 0.02% bromophenol blue, 0.02% xylene cyanol). Upon heat denaturation at 90 °C for 2 min followed by quick cooling, 100,000 cpm of the sample was loaded onto a wedge gel (W x L = 31.0 cm x 38.5 cm, 0.4 mm at top and 1.2 mm at bottom, 8% polyacrylamide (1:20 Bis), 1X TBE, 7.5 M urea). Electrophoresis was at 1,200 V for 4 to 5 h until the bromophenol blue eluted from the bottom of the gel. The gel was transferred to Whatman 3MM paper and dried on a Bio-Rad Model 483 slab gel drier for 2 h at 80 °C. Kodak X-Omat AR film was exposed to the dried gel without an intensifying screen for 10-20 h at room temperature. Autoradiograms were scanned on a LKB UltroScan XL laser densitometer operating at 633 nm. Peak heights for each of cleavage band were corrected by subtracting backgrounds from corresponding control lane bands and equated to the relative cleavage efficiencies at that site. These values are relative and cannot be compared with the values of the other gels.

Results and Discussion

Cleavage Reactions and Primer Extension. The scheme for cleavage of *D. melanogaster* ribosomes with MPE•Fe(II) or EDTA•Fe(II) is shown in Figure 1.

D. melanogaster embryos were dechorionated and lysed on ice to afford the lysate. An *in vitro* translation experiment showed that the lysate was competant to convert polyuridylic acid into polyphenylalanine, indicating that ribosomes in the lysate were intact (unpublished data). The lysate was incubated with preformed MPE•Fe(II) or EDTA•Fe(II) for 5 min at room temperature, and the cleavage reaction was initiated with sodium ascorbate and hydrogen peroxide. After 30 min, total RNA was isolated using the guanidinium thiocyanate procedure (28). Identification of the cleavage sites was performed by primer extension as described (30, 31). The cleavage sites can be identified for distances of about 100-150 nucleotides from the priming position. A set of 15 and 37 DNA oligonucleotide primers have been used, covering the length from 1 to 1970 along the 18S rRNA (1995 nts in length, 1-1995) and from 1 to 3893 along the 28S rRNA (3925 nts in length, 1-1813 for 28Sα and 1859-3970 for 28Sβ), respectively (Figure 2) (33, 34). The 5′-^{32}P-end-labeled primers were hybridized with the rRNA and extended with reverse transcriptase in the presence of the four deoxynucleoside triphosphates. The transcripts were analyzed by electrophoresis on an 8% denaturing polyacrylamide gel. All primers used for this study could be extended with reverse transcriptase in the presence of rRNA templates, confirming good selection of primers. Site-specific cleavage of the rRNA gave rise to bands corresponding to the length of DNA from the 5′ end of the primer to the nucleotide immediately preceding the 3′ side of the cleavage site. Cleavage sites were identified by comparison with dideoxy sequencing lanes run on the same gel. Artifact bands in the control lane, presumably arising from strong secondary structures in the RNA template or from nicks caused by the instabilty of template RNA compared to DNA, were distinguished from sites of MPE•Fe(II) or EDTA•Fe(II) attack by their

occurrence in transcripts using the unreacted control RNA. The region between 1279 and 1221 of 18S rRNA could not be examined because the hypermodified nucleotide 3-[3-amino-3-carboxypropyl]-1-methyl pseudouridine (amψ) at position 1279 halts reverse transcription of rRNA one nucleotide before amψ when 18S primer 10 (address 1330-1350) was used (35). The stop at the base 1858 of 28S rRNA was seen because mature 28S rRNA in *D. melanogaster* consists of two fragments, 28Sα (1-1813) and 28Sβ (1859-3970) (33). The extreme 3′ end of 18S, 28Sα, and 28Sβ could not be examined by primer extension (1950-1995 in 18S rRNA, 1758-1813 in 28Sα rRNA, and 3894-3970 in 28Sβ rRNA).

Cleavage Sites and Expansion Segments in 18S and 28S rRNAs. Autoradiograms from MPE•Fe(II) and EDTA•Fe(II) cleaving experiments are shown in Figure 3. The relative efficiency of cleavage at a site by MPE•Fe(II) was calculated densitometrically by subtracting the cleavage generated by 250 μM Fe(II) (lane 4) from that generated by 50 μM MPE•Fe(II) (50 μM MPE/250 μM Fe(II), a 1 to 5 molar ratio of MPE to Fe(II)) (lane 5). The relative efficiency of cleavage sites by EDTA•Fe(II) was calculated by subtracting the background control (lane 9) from cleavage generated by 2.5 mM EDTA•Fe(II) (2.5 mM EDTA/2.5 mM Fe(II), a 1 to 1 molar ratio of EDTA to Fe(II)) (lane 10). Histograms of MPE•Fe(II) and EDTA•Fe(II) cleavage sites are shown in Figure 4 (33, 34). Only a limited number of sites in 18S and 28S rRNAs are cleaved by 50 μM MPE•Fe(II) and 2.5 mM EDTA•Fe(II) [323 nts (16%) and 229 nts (11%) in 18S rRNA and 431 nts (11%) and 422 nts (11%) in 28S rRNA by MPE•Fe(II) and EDTA•Fe(II), respectively]. Cleavage by MPE•Fe(II) occurs at a lower concentration than cleavage by EDTA•Fe(II) (50 μM vs. 2.5 mM). In addition, MPE•Fe(II) induced cleavage at more sites than did EDTA•Fe(II) (16% vs. 11% in 18S rRNA and 11% vs.11% in 28S rRNA). At a higher concentration of

MPE•Fe(II) (500 μM), cleavage was more efficient, but no additional cleavage sites were observed (unpublished data).

The cleavage sites were mapped on the proposed secondary structure (Figures 5 and 6) (36-38). The cleavage sites are clustered in a few distinct regions of secondary structure (V2-4 and V6-7 in 18S rRNA and D1-3, D6, D7b, stem 44, D8-10, D12 in 28S rRNA). Most of the cleavage sites of 18S and 28S rRNA by MPE•Fe(II) and EDTA•Fe(II) at the concentrations used here are located within the expansion segments, rRNA elements with highly variable (V) or divergent (D) sizes and sequences; and not all expansion segments are cleaved (39-41). Since MPE•Fe(II) and EDTA•Fe(II) require backbone accessibility for cleavage to occur, sites at which cleavage occurs are exposed on the surface of ribosomes. Cleavage is notably lacking in core segments, rRNA elements with highly conserved secondary structures, although the regions, 2014-2017/2026-2028/2048-2050 and 2823-2829/2893-2898, in 28S rRNA are subject to cleavage by MPE•Fe(II). Lack of cleavage by MPE•Fe(II) and EDTA•Fe(II) is due to inaccessibility on the surface of fully assembled ribosomes caused by protection of rRNA with proteins, by involvement of rRNA in tertiary interactions with other portions of the rRNA, or by location of rRNA in interior regions of ribosomes.

A comparison of MPE-Fe(II) cleavage sites with those induced by EDTA•Fe(II) shows that most of the cleavage sites in 18S and 28S rRNAs are generated by both MPE•Fe(II) and EDTA•Fe(II) (Figures 4 and 5). However, several cleavage sites are generated exclusively by one of the reagents. For example, the V3 regions of 18S rRNA that are subject to cleavage by MPE•Fe(II) show almost no cleavage by EDTA•Fe(II). Therefore, this region of rRNA is somehow protected from cleavage by EDTA•Fe(II), but is still able to bind to

MPE•Fe(II). This region might be a binding site for loosely bound proteins, which can be displaced by MPE•Fe(II) or exposed by induced conformational changes in rRNA upon binding of MPE•Fe(II) to other rRNA sites.

With a few exceptions, most of cleavage sites of 18S and 28S rRNAs by MPE•Fe(II) occur in double stranded stem regions and at junctions between stems and loops [e.g., see V2 (207-263), V3 (484-519), and V7 (1881-1915) in 18S rRNA and D1 (127-152), D6 (1567-1592), and core segments (2010-2060 and 2823-2898) in 28S rRNA (Figure 5)]. This is in general agreement with an intercalative binding mode for MPE•Fe(II). A similar result was observed for a 345 nt fragment of *E. coli* 16S rRNA (20). This suggests that the cleavage pattern by MPE•Fe(II) could be used to distinguish different secondary structures of equivalent energy. Two possible secondary structural models which cannot be distinguished on energetic criteria have been proposed for the 830-946 region of the 18S rRNA expansion segment V4 by Hancock et al. (36) (Figures 7A and 7B). The alternative potential secondary structure for this region was proposed by De Rijk et al. (42) (Figure 7C). Superposition of our cleavage data on these structures of the 830-946 region reveals that the cleavage sites on structure A are located in stems and at stem-loop junctions, while in structure B the sites are located in several unstructured regions. Thus, this region should be represented by structure A, as shown in Figure 7A (36). The model C also seems to fit the experimental cleavage data for the 830-946 region (Figure 7C) (42).

The presence of certain surface-exposed rRNA sequences in expansion segments might be important evidence for morphological structures of eukaryotic ribosomes. Eukaryotic small subunits contain structural features termed eukaryotic lobes and archaebacterial bills at the bottom and on the head

of the subunit, respectively (43, 44). Eukaryotic lobes of small ribosomal subunits are composed primarily of rRNA and thought to be about 300 nucleotide long (45). Three-dimensional models of *E. coli* small ribosomal subunits predict that the eukaryotic lobes and archaebacterial bills consist of expansion segments of eukaryotic 18S rRNA (11, 13). Based on the model, expansion segments V2, V4, and V7 in *D. melanogaster* 18S rRNA are related to eukaryotic lobes and V6 constitutes archaebacterial bills. In addition, these expansion segments are accommodated into the compact structure of the *E. coli* small ribosomal subunit by being exposed on the ribosome surface. Indeed, these expansion segments were cleaved by MPE•Fe(II) and EDTA•Fe(II) (206 MPE•Fe(II) and 157 EDTA•Fe(II) cleavage sites for V2, V4, and V7; 81 MPE•Fe(II) and 72 EDTA•Fe(II) cleavage sites for V6). These results provide experimental evidence that eukaryotic lobes as well as archaebacterial bills are composed primarily of accessible rRNA and suggest which sequences are contained within them. Eukaryotic lobes are also present at the bottom of the eukaryotic large ribosomal subunit and exposed on the surface (43, 44). It is possible that sequences in expansion segments accessible to these cleaving reagents in 28S rRNA might be involved in the eukaryotic lobe structure of the large subunit.

A genetic tag has been inserted within eukaryotic 26S rRNAs for analysis of eukaryotic ribosomal mutations. 18 and 119 base pair tags that were inserted within the first expansion segment of domain I of *Saccharomyces cerevisiae* 26S rRNA and the D12 segments of rRNA of *Tetrahymena thermophila* 26S rRNA, respectively, were not deleterious to the cells, suggesting that the biosynthesis and function of ribosomes are not affected by such insertions (46, 47). These sites correspond to the D1 and D12 expansion segments of *D. melanogaster*

where MPE•Fe(II) cleavage sites were observed (Figure 5). These results suggest that MPE•Fe(II) and EDTA•Fe(II) cleavage sites could provide information about the other sites within rRNA that are good candidates for the insertion of a genetic tag. The insertion of a tag within MPE•Fe(II) and EDTA•Fe(II) cleavage sites would not interfere with the proper processing, assembly, and functioning of ribosomes.

Cleavage patterns on expansion segments can be used for designing oligonucleotides of potential value for eukaryotic ribosomal RNA-based cell staining, immune electron microscopic studies, and the preparation of heavy-metal derivatives of ribosomes for the phase evaluation of crystallographic studies (48-54). Because of the abundance of rRNA in cells and the high sequence variability of the expansion segments among species, phylogenetic, species-specific, fluorescently labeled oligonucleotides complementary to putative single-stranded region of surface-exposed rRNA in expansion segments might be useful to distinguish between intact eukaryotic cells and to measure the ribosome content of different cell types (48). These probes should hybridize with rRNA in expansion segments of intact ribosomes since cleavage sites are presumably exposed on the surface of eukaryotic ribosomes so that the delivery of probes is thought to be less hindered. The availability of specific rRNA sequences on the surface of eukaryotic ribosomes allows these regions to be mapped on the three-dimensional structure of ribosomes by using the technology of DNA-hybridization electron microscopy (49, 50). Surface-exposed single-stranded rRNA in expansion segments can be a first target site for introduction of a heavy-atom compound to ribosomes using DNA oligonucleotides (51, 52).

Conclusions

In conclusion, the method we used offers a simple way to determine the detailed structure of ribosomal RNA within ribosomes. A combination of MPE•Fe(II) and EDTA•Fe(II) can be used to identify, to nucleotide resolution, regions of rRNAs that are accessible on the surface of the eukaryotic ribosomes in an actively translating *in vitro* system. Generation of a nonspecific diffusible oxidant by MPE•Fe(II) and EDTA•Fe(II) is not inhibited by redox-inactive metal ions present in the cell-free *in vitro* system. The application of this technique to intact ribosomes from other eukaryotic species will provide information about the conservation of ribosomal RNA packaging within ribosomes and be useful for studies of the evolutionary origins and phylogenetic investigations of expansion segments from different species of eukaryotes. In addition, information about the cleavage sites can be useful in the aspect of designing experiments required to study eukaryotic ribosomes.

References

1. Dahlberg, A. E. (1989) *Cell* **57**, 525-529.
2. Shine, J. & Dalgarno, L. (1974) *Proc. Natl. Acad. Sci. U.S.A.* **71**, 1342-1346.
3. Ofengand, J., Ciesiolka, J., Denman, R. & Nurse, K. (1986) in *Structure, Function and Genetics of Ribosomes* (Hardesty, B. & Kramer, G., Eds.) pp 473-494, Springer-Verlag, New York.
4. Moazed, D. & Noller, H. F. (1986) *Cell (Cambridge, Mass.)* **47**, 985-994.
5. Moazed, D. & Noller, H. F. (1989) *Cell (Cambridge, Mass.)* **57**, 585-597.
6. Moazed, D. & Noller, H. F. (1989) *Nature* **342**, 142-148.
7. Barta, A., Steiner, G., Brosius, J., Noller, H. F. & Kuechler, E. (1984) *Proc. Natl. Acad. Sci. U.S.A.* **81**, 3607-3611.
8. Moazed, D., Robertson, J. M. & Noller, H. F. (1988) *Nature* **334**, 362-364.
9. Moazed, D. & Noller, H. F. (1987) *Nature* **327**, 389-394.
10. Noller, H. F., Hoffarth, V. & Zimniak, L. (1992) *Science* **256**, 1416-1419.
11. Stern, S., Weiser, B. & Noller, H. F. (1988) *J. Mol. Biol.* **204**, 447-481.
12. Stern, S., Powers, T., Changchien, L. -M. & Noller, H. F. (1989) *Science* **244**, 783-790.
13. Brimacombe, R., Atmadja, J., Stiege, W. & Schuler, D. (1988) *J. Mol. Biol.* **199**, 115-136.
14. Hertzberg, R. P. & Dervan, P. B. (1982) *J. Am. Chem. Soc.* **104**, 313-315.
15. Van Dyke, M. W., Hertzberg, R. P. & Dervan, P. B. (1982) *Proc. Natl. Acad. Sci. U.S.A.* **79**, 5470-5474.
16. Hertzberg, R. P. & Dervan, P. B. (1984) *Biochemistry* **23**, 3934-3945.
17. Dervan, P. B. (1986) *Science* **232**, 464-471.

35. Youvan, D. C. & Hearst, J. E. (1981) *Nucleic Acids Res.* **9**, 1723-1741.

36. Hancock, J. M., Tautz, D. & Dover, G. A. (1988) *Mol. Biol. Evol.* **5**, 393-414.

37. Gutell, R. R. (1993) *Nucleic Acids Res.* **21**, 3051-3054.

38. Gutell, R. R., Gray, M. W. & Schnare, M. N. (1993) *Nucleic Acids Res.* **21**, 3055-3074.

39. Clark, C. G., Tague, B. W., Ware, V. C. & Gerbi, S. A. (1984) *Nucleic Acids Res.* **12**, 6197-6220.

40. Stebbins-Boaz, B. & Gerbi, S. A. (1991) *J. Mol. Biol.* **217**, 93-112.

41. Gerbi, S. A. (1994) in *Ribosomal RNA: Structure, Evolution, Processing and Function in Protein Synthesis* (Zimmermann, R. A. & Dahlberg, A. E., Eds.) CRC-Telford, in press.

42. De Rijk, P., Neefs, J. -M., Van de Peer, Y. & De Wachter, R. (1992) *Nucleic Acids Res.* **20**, 2075-2089.

43. Henderson, E., Oakes, M., Clark, M. W., Lake, J. A., Matheson, A. T. & Zillig, W. (1984) *Science* **225**, 510-512.

44. Oakes, M., Henderson, E., Scheinman, A., Clark, M. & Lake, J. A. (1986) in *Structure, Function and Genetics of Ribosomes* (Hardesty, B. & Kramer, G., Eds.) pp 47-67, Springer-Verlag, New York.

45. Kuhlbrandt, W. & Unwin, P. N. T. (1982) *J. Mol. Biol.* **156**, 431-448.

46. Musters, W., Venema, J., Van der Linden, G., Van Heerikhuizen, H., Klootwijk, J. & Planta, R. J. (1989) *Mol. Cell. Biol.* **9**, 551-559.

47. Sweeney, R. & Yao, M. -C (1989) *EMBO J.* **8**, 933-938.

48. DeLong, E. F., Wickham, G. S. & Pace, N. R. (1989) *Science* **243**, 1360-1363.

49. Oakes, M. I. & Lake, J. A. (1990) *J. Mol. Biol.* **211**, 897-906.

50. Oakes, M. I., Kahan, L. & Lake, J. A. (1990) *J. Mol. Biol.* **211**, 907-918.

51. Weinstein, S., Jahn, W., Hansen, H., Wittmann, H. G. & Yonath, A. (1989) *J. Biol. Chem.* **264**, 19138-19142.

52. Yonath, A. & Wittmann, H. G. (1989) *Trends Biochem. Sci.* **14**, 329-335.

53. Lasater, L. S., Olson, H. M., Cann, P. A. & Glitz, D. G. (1988) *Biochemistry* **27**, 4687-4695.

54. Hill, W. E., Weller, J., Gluick, T., Merryman, C., Marconi, R. T., Tassanakajohn, A. & Tapprich, W. E. (1990) in *The Ribosome: Structure, Function and Evolution* (Hill, W. E., Dahlberg, A., Garrett, R. A., Moore, P. B., Schlessinger, D. & Warner, J. R., Eds.) pp 253-261, American Society for Microbiology, Washington, DC

Figure 1. (A) MPE•Fe(II) and EDTA•Fe(II). (B) Scheme for cleavage of ribosomes by MPE•Fe(II).

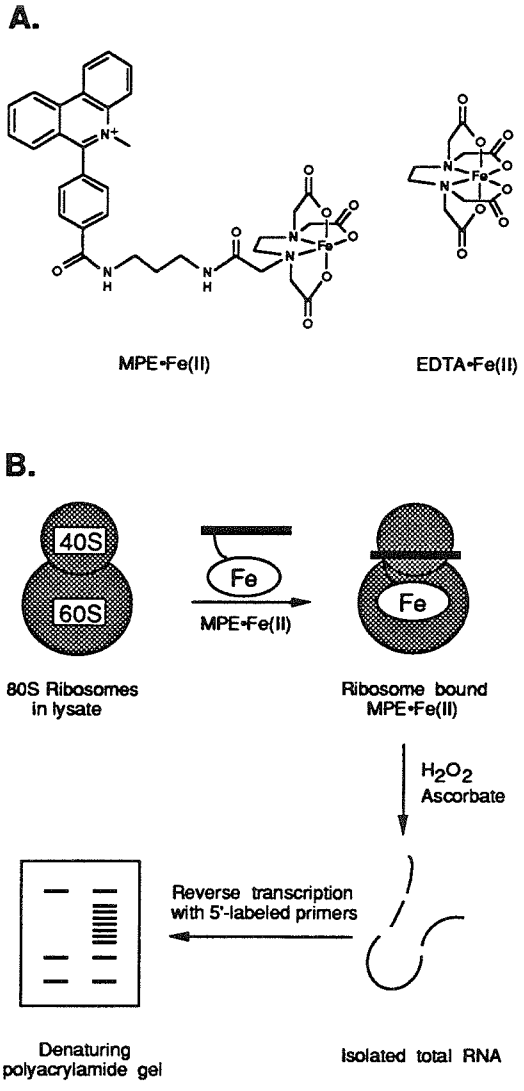
A.
MPE•Fe(II)
EDTA•Fe(II)
B.
40S
60S
Fe
MPE•Fe(II)
80S Ribosomes in lysate
Ribosome bound MPE•Fe(II)
H_2O_2
Ascorbate
Reverse transcription with 5'-labeled primers
Denaturing polyacrylamide gel
Isolated total RNA

Figure 2. DNA primers used for primer extension of *D. melanogaster* (A) 18S and (B) 28S rRNAs. The sequence is numbered according to Tautz et al. (33). Additional 25 nucleotides of 28S rRNA absent in Tautz et al. (33) are counted (34).

A. Primers for 18S rRNA

1	281 – 300	5' – AGATCTGTCGTCGGTACAAG – 3'
2	430 – 450	5' – TGGGTAATTTACGCGCCTGCT – 3'
3	541 – 561	5' – CCCTCCAATTGGTCCTTGTTA – 3'
4	730 – 750	5' – ACAAGTATTTAATCACATATA – 3'
5	841 – 861	5' – AAGCCTGCTTTAAGCACTCTA – 3'
6	881 – 900	5' – TTATTTCATTATCCCATGCA – 3'
7	971 – 991	5' – CACCTCTCGCGTCGTAATACT – 3'
8	1030 – 1050	5' – TGAAAACATCTTTGGCAAATG – 3'
9	1221 – 1245	5' – TGCCCTTCCGTCAATTCCTTTAAGT – 3'
10	1330 – 1350	5' – CATAGATTCGAGAAAGAGCTA – 3'
11	1530 – 1550	5' – GACAAACCAACAGGTACGGCT – 3'
12	1601 – 1621	5' – CCTGTTATTGCTCAATCTCAT – 3'
13	1781 – 1800	5' – ATGCGAGTTAATGACTCACA – 3'
14	1909 – 1929	5' – AGTTCGGTCAACTTTTGCGAA – 3'
15	1950 – 1970	5' – ACGGAAACCTTGTTACGACTT – 3'

B. Primers for 28S rRNA

1	117 – 137	5' – AGACAAAGTGACTTAGTGCTG – 3'
2	189 – 209	5' – AAGGACTTAAATCGTTAATTT – 3'
3	344 – 364	5' – ACTATCGGTCTCATGGTTATA – 3'
4	444 – 464	5' – CGGATATTCAGGTTCATCGGG – 3'
5	542 – 562	5' – ATATGCTAATAGATTACAATG – 3'
6	644 – 664	5' – AATCTATCAGCACTTTATCAA – 3'
7	752 – 772	5' – CTGAATCTTTCGCATTGTTAA – 3'
8	875 – 895	5' – AAATAGCTAAAAAACTAATCC – 3'
9	975 – 995	5' – CATATATGCTCAAGGTACGTT – 3'
10	1087 – 1107	5' – CTATACTCAATTCTGACAATC – 3'
11	1187 – 1207	5' – CCAGATAAGATTATTTTATAT – 3'
12	1287 – 1307	5' – CCTTGATCTTCATATCAAGAA – 3'
13	1414 – 1434	5' – AAGCAACCAACGCCTTTCATG – 3'
14	1546 – 1566	5' – ATCTACTTTAGCGGTAATGTA – 3'
15	1609 – 1629	5' – GCATACCATTGTACCTTCCTA – 3'
16	1758 – 1778	5' – TTAGGACCGACTAACTCGTGA – 3'
17	1950 – 1970	5' – CTTCTTTATGGTCGTTCCTGT – 3'
18	2056 – 2076	5' – ATATGTCATGCTCTTCTAGCC – 3'
19	2167 – 2187	5' – AGACTCTTCACCTTGGAGACC – 3'
20	2281 – 2301	5' – ATGTTATTGTTTCCCAATCAA – 3'
21	2359 – 2379	5' – CGTAACTAAACTATCCGGGGA – 3'
22	2409 – 2429	5' – CCCAAATAGTATTCTTAAAAA – 3'
23	2468 – 2488	5' – AGTTCTGAATTGATTGTTAAT – 3'
24	2548 – 2568	5' – AATCACATTGTGTCAACACCC – 3'
25	2678 – 2698	5' – TAATCCATTCATGCGCGTCAC – 3'
26	2783 – 2803	5' – TTAGAGTCAAGCTCAAAAGGG – 3'
27	2853 – 2873	5' – GACGATACCAAACCGAGGTCT – 3'
28	2982 – 3002	5' – ATCAAGAAGCTTGCATCAAAA – 3'
29	3076 – 3096	5' – GGAGTTATACCAAATTTTCAA – 3'
30	3139 – 3159	5' – GTACCGCCCCAGTCAAACTCC – 3'
31	3289 – 3309	5' – TTTAAACCAAAAGGATCGATA – 3'
32	3408 – 3428	5' – TCACAATGATAGGAAGAGCCG – 3'
33	3518 – 3538	5' – CAACAACGTTTTGTCATTAGT – 3'
34	3629 – 3649	5' – GTTCAGGCATAATCCAACGGA – 3'
35	3717 – 3737	5' – TTATAAACTTTAAATGGTTTA – 3'
36	3840 – 3860	5' – TGTCATTGTATTAAATAATGC – 3'
37	3894 – 3914	5' – CCACTTACAACACCTTGCCTG – 3'

Figure 3. Autoradiograms of 8% denaturing polyacrylamide gels used to analyze the 5′-^{32}P-end labeled DNA transcribed from *D. melanogaster* 18S (upper) and 28S rRNA (lower) by primer extension using reverse transcriptase. (Lanes 1-5, 8-10) DNA transcript products of reverse transcription of rRNAs prepared from ribosomes treated with various reagents: no reagent (lanes 1 and 8); H_2O_2 and sodium ascorbate (lanes 2 and 9); 50 μM MPE for 5 min, followed by 10 mM H_2O_2 and sodium ascorbate for 20 min (lane 3); 250 μM Fe(II) for 5 min, followed by 10 mM H_2O_2 and sodium ascorbate for 20 min (lane 4); 50 μM MPE•Fe(II) (50 μM MPE/250 μM Fe(II)), followed by 10 mM H_2O_2 and sodium ascorbate for 20 min (lane 5); 2.5 mM EDTA•Fe(II) (2.5 mM EDTA/2.5 mM Fe(II)), followed by H_2O_2 and sodium ascorbate for 20 min (lane 10). (Lanes 6, 7, 11, and 12) Dideoxy sequencing in the presence of ddT (lanes 6 and 11) or ddC (7 and 12) (32).

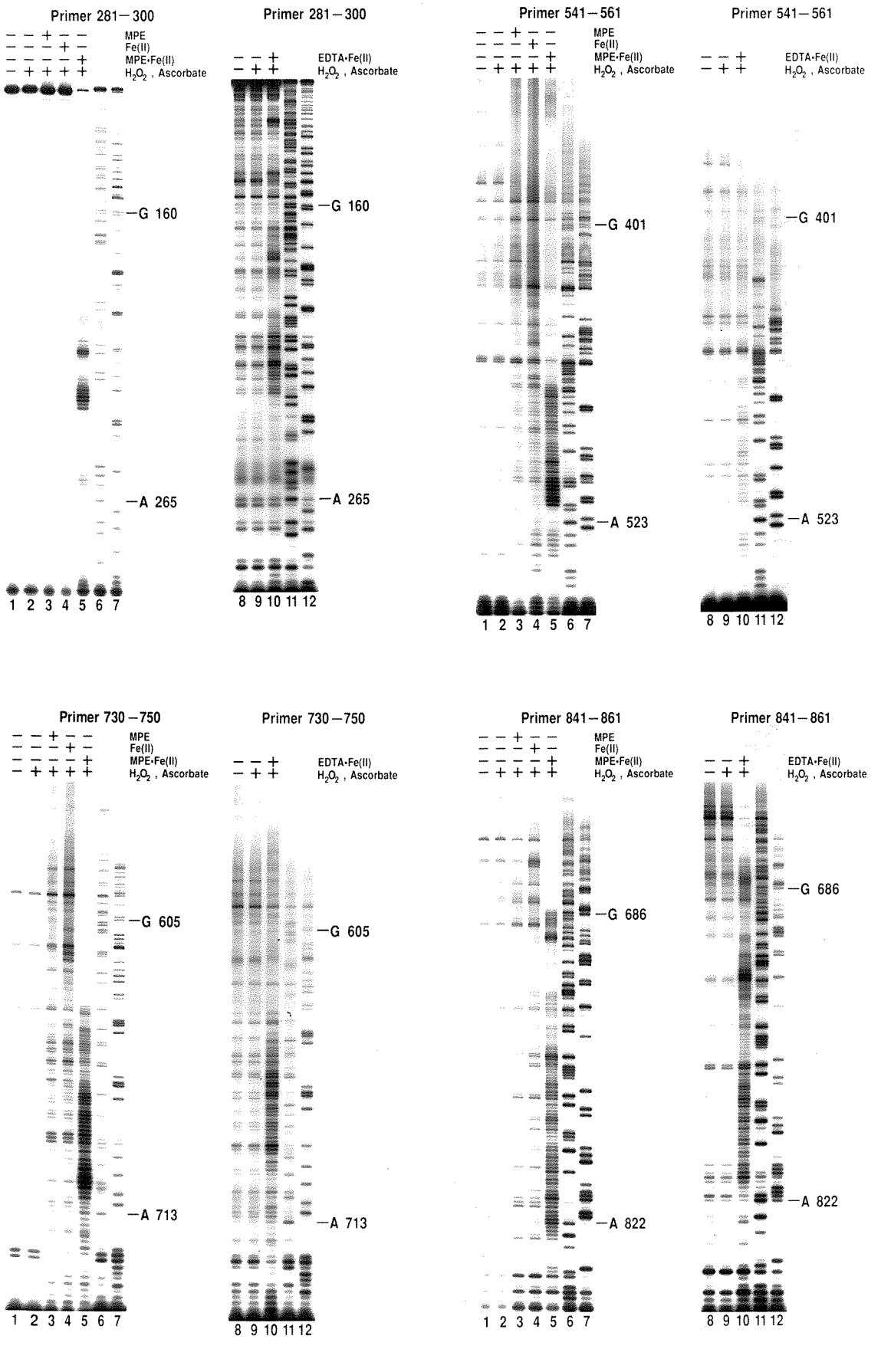
Primer 281—300
MPE
Fe(II)
MPE·Fe(II)
H2O2 , Ascorbate
G 160
A 265
1 2 3 4 5 6 7
Primer 281—300
EDTA·Fe(II)
H2O2 , Ascorbate
G 160
A 265
8 9 10 11 12
Primer 541—561
MPE
Fe(II)
MPE·Fe(II)
H2O2 , Ascorbate
G 401
A 523
1 2 3 4 5 6 7
Primer 541—561
EDTA·Fe(II)
H2O2 , Ascorbate
G 401
A 523
8 9 10 11 12
Primer 730—750
MPE
Fe(II)
MPE·Fe(II)
H2O2 , Ascorbate
G 605
A 713
1 2 3 4 5 6 7
Primer 730—750
EDTA·Fe(II)
H2O2 , Ascorbate
G 605
A 713
8 9 10 11 12
Primer 841—861
MPE
Fe(II)
MPE·Fe(II)
H2O2 , Ascorbate
G 686
A 822
1 2 3 4 5 6 7
Primer 841—861
EDTA·Fe(II)
H2O2 , Ascorbate
G 686
A 822
8 9 10 11 12

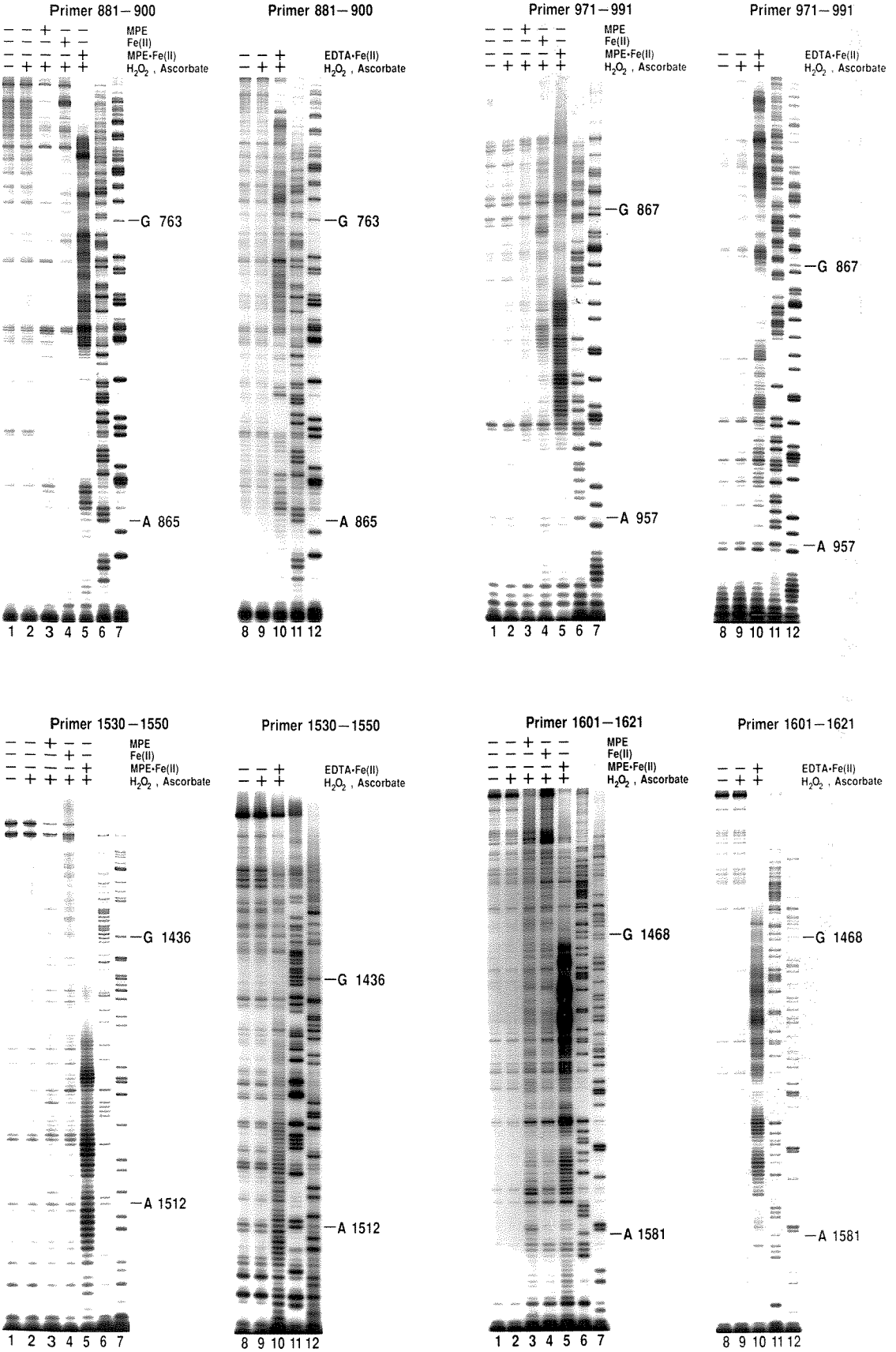
Primer 881–900
MPE
Fe(II)
MPE·Fe(II)
H2O2 , Ascorbate
G 763
A 865
1 2 3 4 5 6 7
Primer 881–900
EDTA·Fe(II)
H2O2 , Ascorbate
G 763
A 865
8 9 10 11 12
Primer 971–991
MPE
Fe(II)
MPE·Fe(II)
H2O2 , Ascorbate
G 867
A 957
1 2 3 4 5 6 7
Primer 971–991
EDTA·Fe(II)
H2O2 , Ascorbate
G 867
A 957
8 9 10 11 12
Primer 1530–1550
MPE
Fe(II)
MPE·Fe(II)
H2O2 , Ascorbate
G 1436
A 1512
1 2 3 4 5 6 7
Primer 1530–1550
EDTA·Fe(II)
H2O2 , Ascorbate
G 1436
A 1512
8 9 10 11 12
Primer 1601–1621
MPE
Fe(II)
MPE·Fe(II)
H2O2 , Ascorbate
G 1468
A 1581
1 2 3 4 5 6 7
Primer 1601–1621
EDTA·Fe(II)
H2O2 , Ascorbate
G 1468
A 1581
8 9 10 11 12

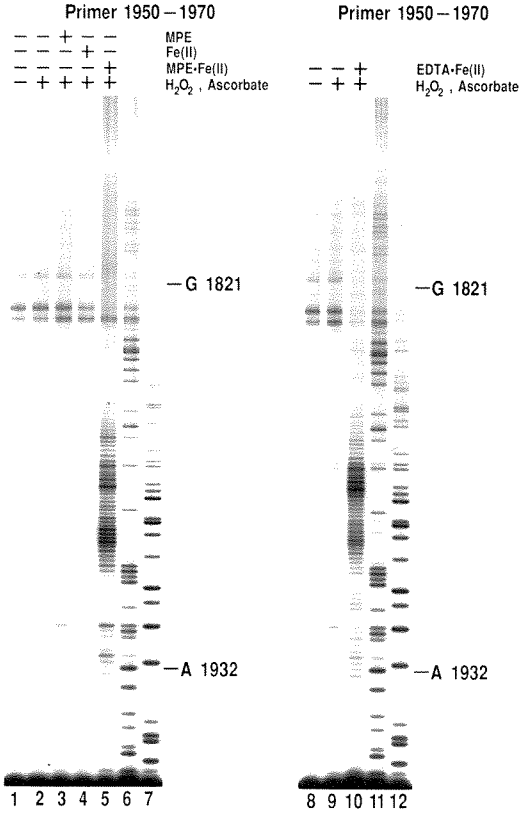
Primer 1950 – 1970
– – + – –
– – – + –
– – – – +
– + + + +
MPE
Fe(II)
MPE·Fe(II)
H2O2 , Ascorbate
– G 1821
– A 1932
1 2 3 4 5 6 7
Primer 1950 – 1970
– – +
– + +
EDTA·Fe(II)
H2O2 , Ascorbate
– G 1821
– A 1932
8 9 10 11 12

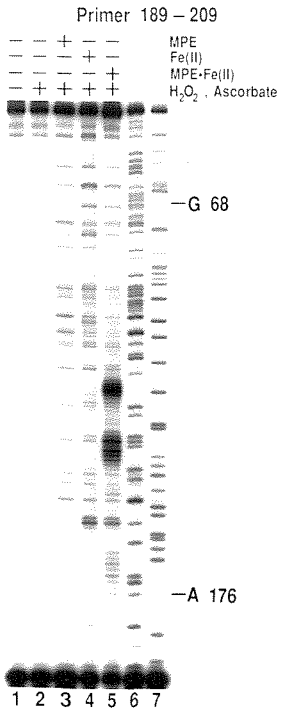
Primer 189 – 209
MPE
Fe(II)
MPE•Fe(II)
H_2O_2 , Ascorbate
G 68
A 176
1 2 3 4 5 6 7

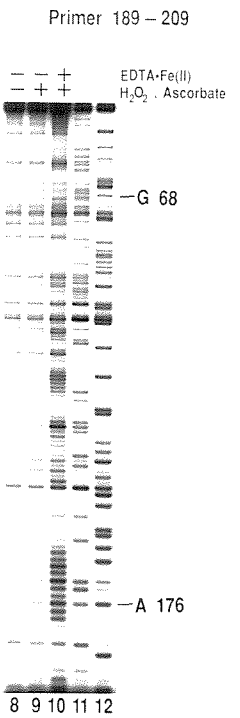
Primer 189 – 209
EDTA•Fe(II)
H_2O_2 , Ascorbate
G 68
A 176
8 9 10 11 12

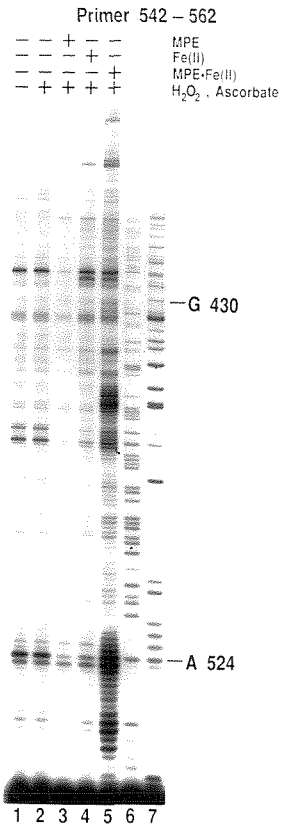
Primer 542 – 562
MPE
Fe(II)
MPE•Fe(II)
H_2O_2 , Ascorbate
G 430
A 524
1 2 3 4 5 6 7

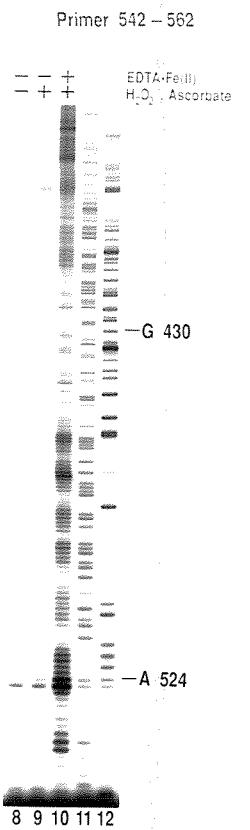
Primer 542 – 562
EDTA•Fe(II)
H_2O_2 , Ascorbate
G 430
A 524
8 9 10 11 12

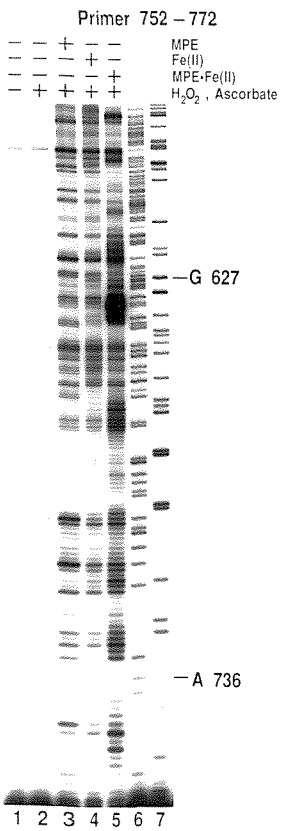
Primer 752 – 772
MPE
Fe(II)
MPE•Fe(II)
H_2O_2 , Ascorbate
G 627
A 736
1 2 3 4 5 6 7

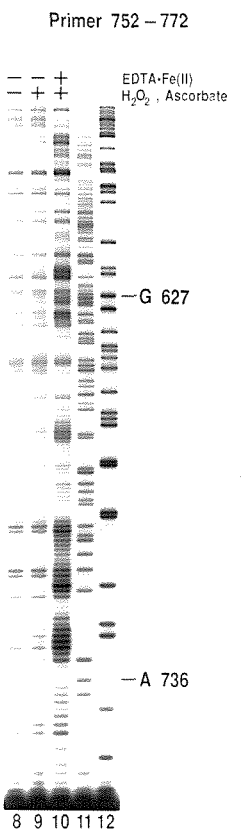
Primer 752 – 772
EDTA•Fe(II)
H_2O_2 , Ascorbate
G 627
A 736
8 9 10 11 12

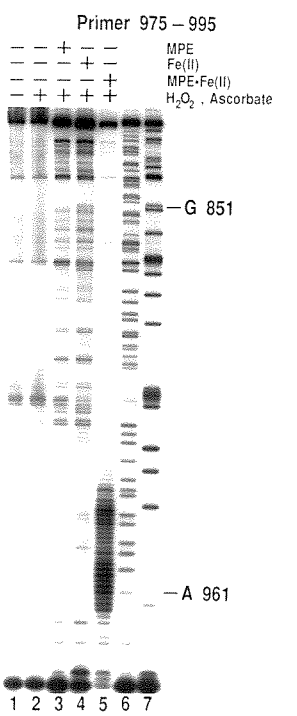
Primer 975 – 995
MPE
Fe(II)
MPE•Fe(II)
H_2O_2 , Ascorbate
G 851
A 961
1 2 3 4 5 6 7

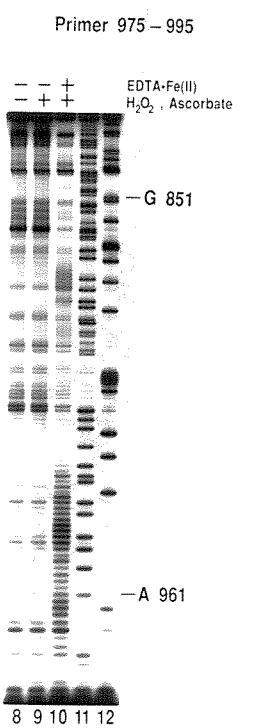
Primer 975 – 995
EDTA•Fe(II)
H_2O_2 , Ascorbate
G 851
A 961
8 9 10 11 12

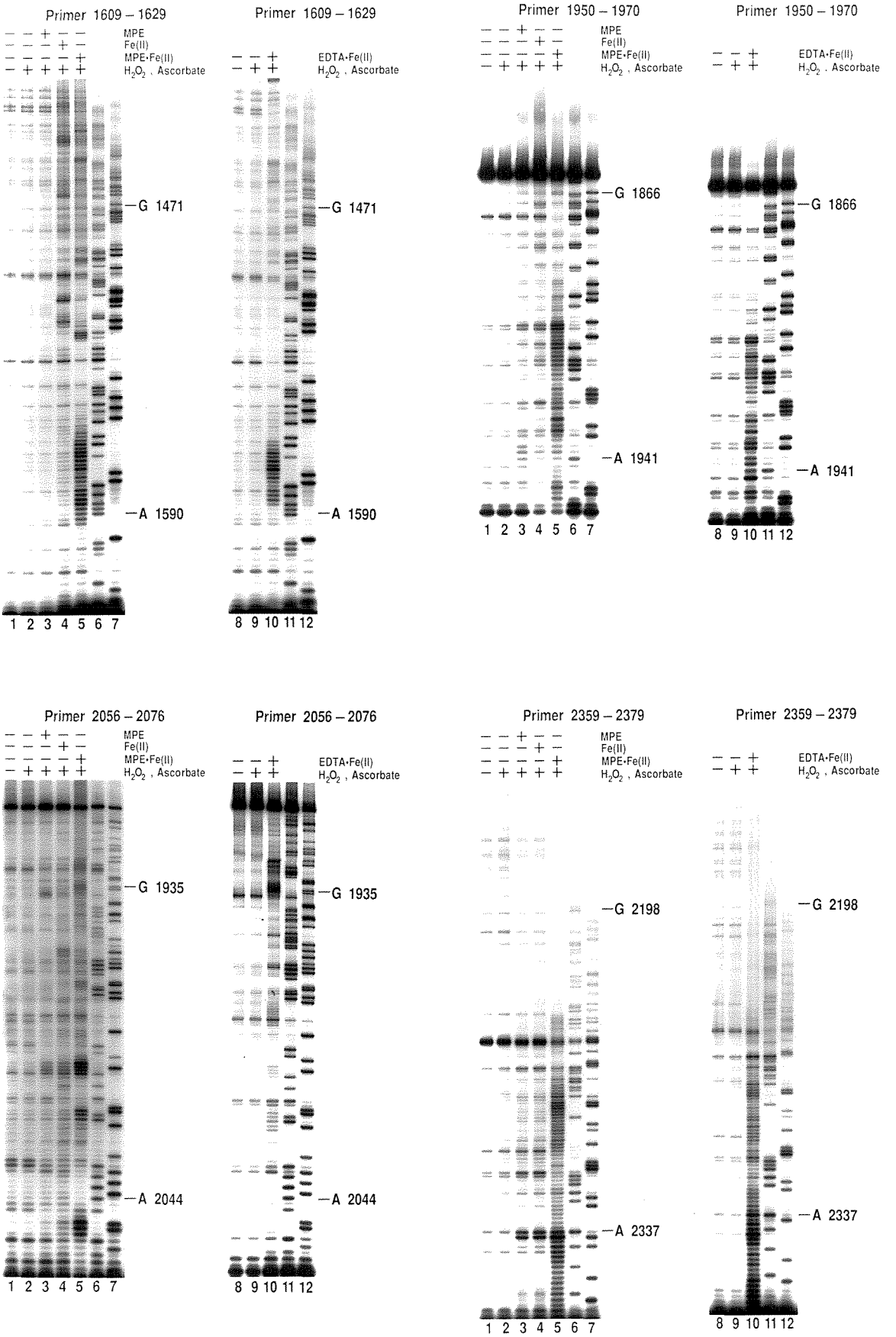
Primer 1609 – 1629
MPE
Fe(II)
MPE·Fe(II)
H2O2 , Ascorbate
G 1471
A 1590
1 2 3 4 5 6 7
Primer 1609 – 1629
EDTA·Fe(II)
H2O2 , Ascorbate
G 1471
A 1590
8 9 10 11 12
Primer 1950 – 1970
MPE
Fe(II)
MPE·Fe(II)
H2O2 , Ascorbate
G 1866
A 1941
1 2 3 4 5 6 7
Primer 1950 – 1970
EDTA·Fe(II)
H2O2 , Ascorbate
G 1866
A 1941
8 9 10 11 12
Primer 2056 – 2076
MPE
Fe(II)
MPE·Fe(II)
H2O2 , Ascorbate
G 1935
A 2044
1 2 3 4 5 6 7
Primer 2056 – 2076
EDTA·Fe(II)
H2O2 , Ascorbate
G 1935
A 2044
8 9 10 11 12
Primer 2359 – 2379
MPE
Fe(II)
MPE·Fe(II)
H2O2 , Ascorbate
G 2198
A 2337
1 2 3 4 5 6 7
Primer 2359 – 2379
EDTA·Fe(II)
H2O2 , Ascorbate
G 2198
A 2337
8 9 10 11 12

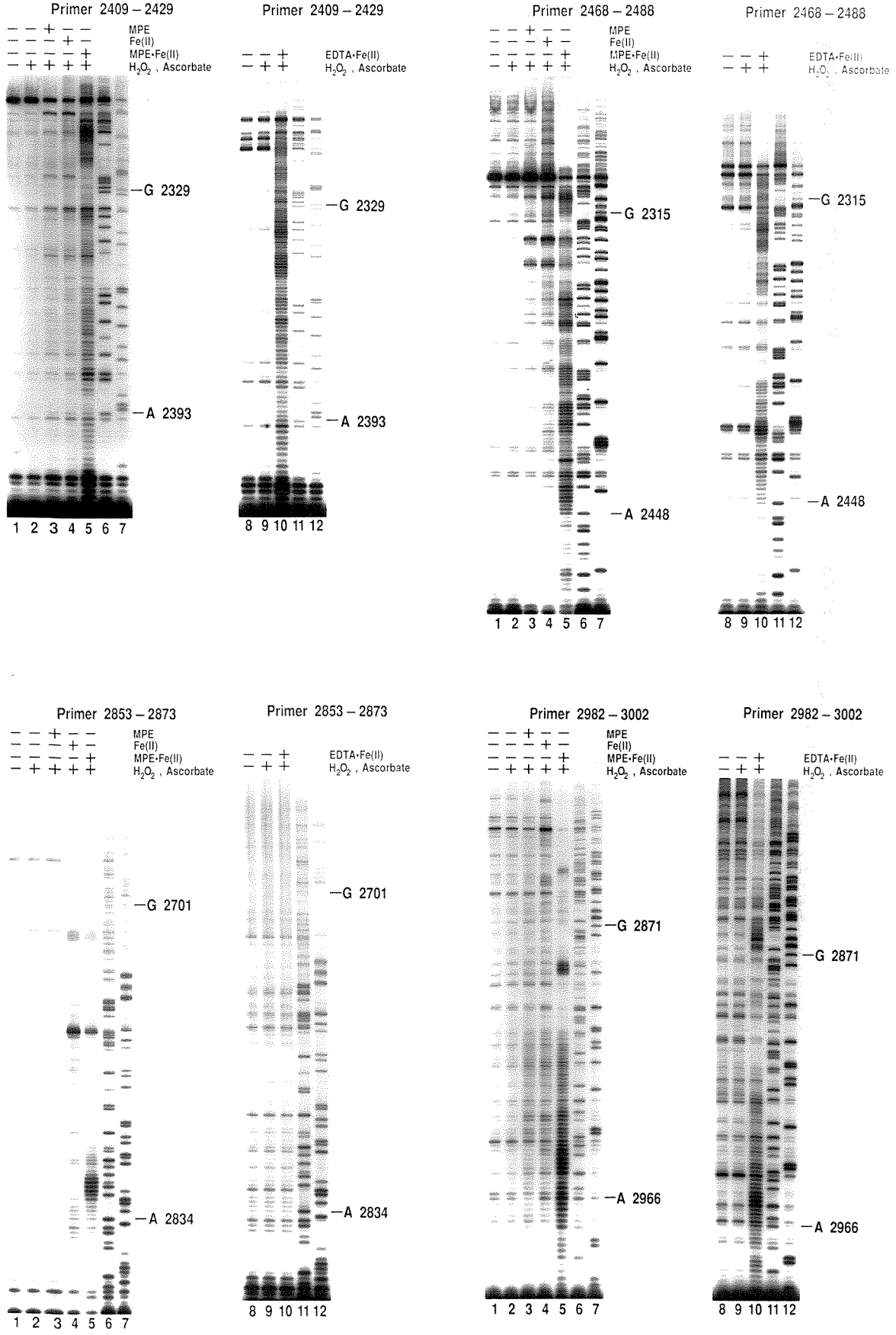
Primer 2409 – 2429
MPE
Fe(II)
MPE·Fe(II)
H2O2 , Ascorbate
G 2329
A 2393
1 2 3 4 5 6 7
Primer 2409 – 2429
EDTA·Fe(II)
H2O2 , Ascorbate
G 2329
A 2393
8 9 10 11 12
Primer 2468 – 2488
MPE
Fe(II)
MPE·Fe(II)
H2O2 , Ascorbate
G 2315
A 2448
1 2 3 4 5 6 7
Primer 2468 – 2488
EDTA·Fe(II)
H2O2 , Ascorbate
G 2315
A 2448
8 9 10 11 12
Primer 2853 – 2873
MPE
Fe(II)
MPE·Fe(II)
H2O2 , Ascorbate
G 2701
A 2834
1 2 3 4 5 6 7
Primer 2853 – 2873
EDTA·Fe(II)
H2O2 , Ascorbate
G 2701
A 2834
8 9 10 11 12
Primer 2982 – 3002
MPE
Fe(II)
MPE·Fe(II)
H2O2 , Ascorbate
G 2871
A 2966
1 2 3 4 5 6 7
Primer 2982 – 3002
EDTA·Fe(II)
H2O2 , Ascorbate
G 2871
A 2966
8 9 10 11 12

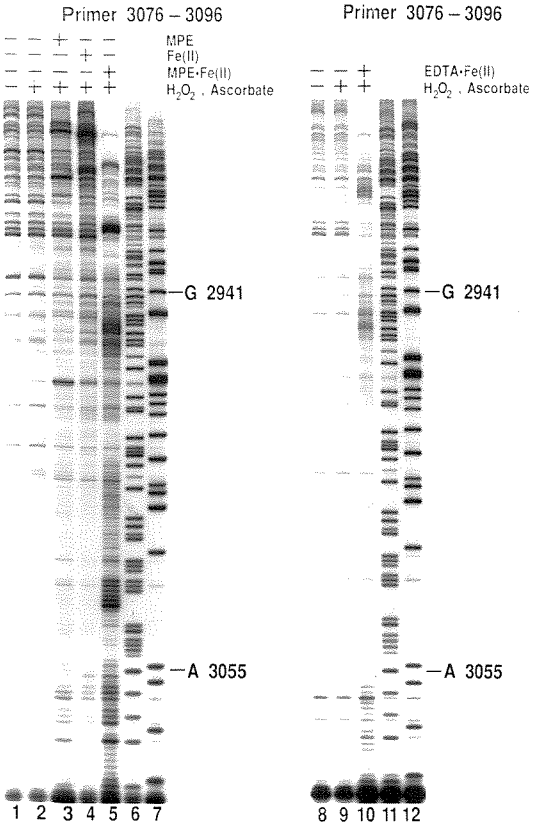
Primer 3076 – 3096
MPE
Fe(II)
MPE·Fe(II)
H_2O_2 , Ascorbate
G 2941
A 3055
1 2 3 4 5 6 7

Primer 3076 – 3096
EDTA·Fe(II)
H_2O_2 , Ascorbate
G 2941
A 3055
8 9 10 11 12

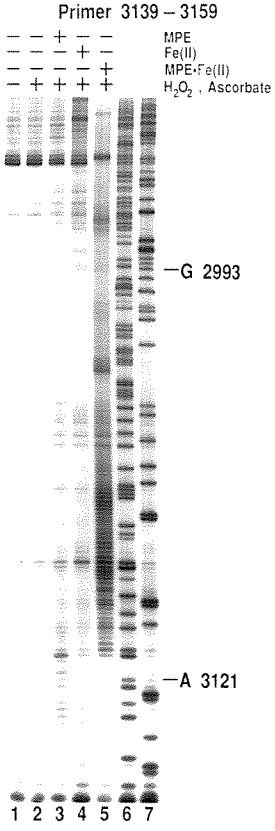
Primer 3139 – 3159
MPE
Fe(II)
MPE·Fe(II)
H_2O_2 , Ascorbate
G 2993
A 3121
1 2 3 4 5 6 7

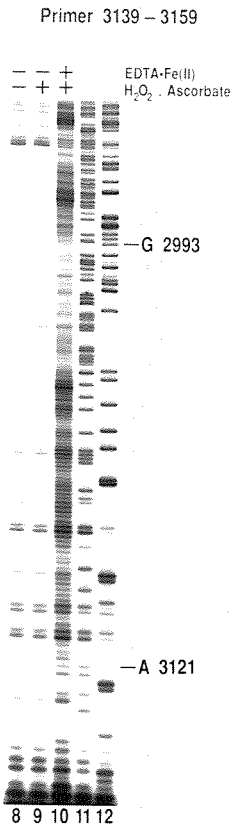
Primer 3139 – 3159
EDTA·Fe(II)
H_2O_2 , Ascorbate
G 2993
A 3121
8 9 10 11 12

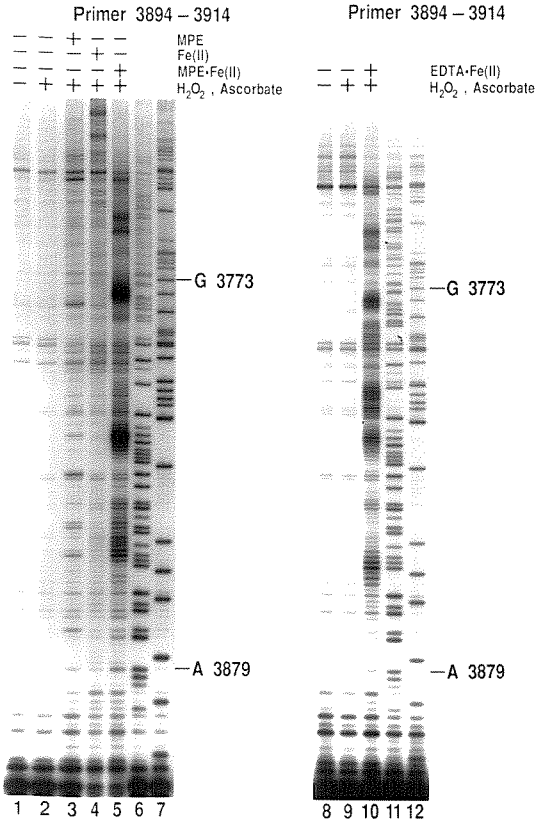
Primer 3894 – 3914
MPE
Fe(II)
MPE·Fe(II)
H_2O_2 , Ascorbate
G 3773
A 3879
1 2 3 4 5 6 7

Primer 3894 – 3914
EDTA·Fe(II)
H_2O_2 , Ascorbate
G 3773
A 3879
8 9 10 11 12

Figure 4. Histrograms of the cleavage data derived from the autoradiograms in Figure 3. (A) 18S rRNA and (B) 28S rRNA. Cleavage sites by MPE•Fe(II) and EDTA•Fe(II) are indicated by arrows above and below the primary sequences, respectively. The heights of the arrows represent the relative cleavage intensities at the indicated bases.

A. 18S rRNA

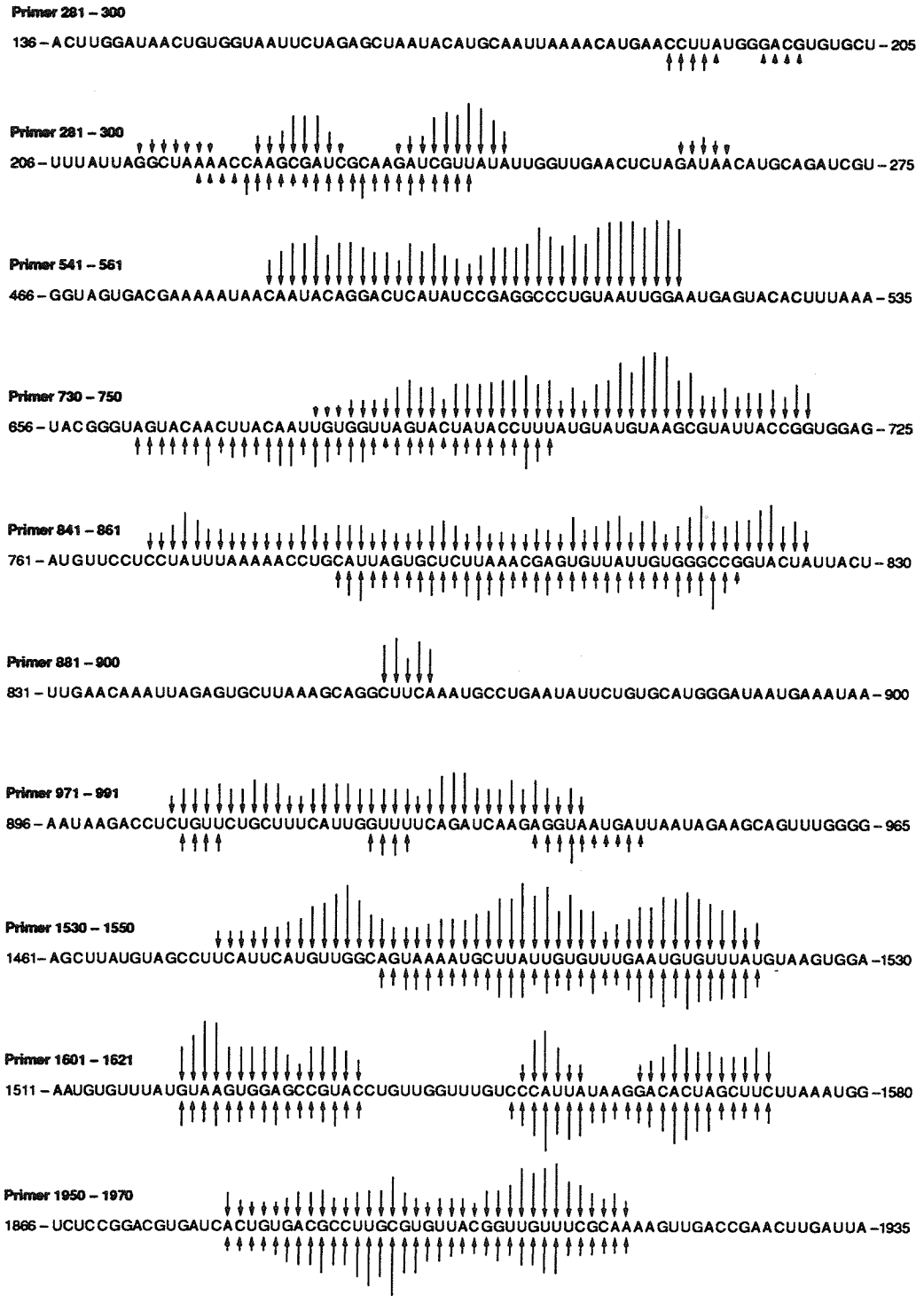
Primer 281 – 300
136 – ACUUGGAUAACUGUGGUAAUUCUAGAGCUAAUACAUGCAAUUAAAACAUGAACCUUAUGGGACGUGUGCU – 205
Primer 281 – 300
206 – UUUAUUAGGCUAAAACCAAGCGAUCGCAAGAUCGUUAUAUUGGUUGAACUCUAGAUAACAUGCAGAUCGU – 275
Primer 541 – 561
466 – GGUAGUGACGAAAAAUAACAAUACAGGACUCAUAUCCGAGGCCCUGUAAUUGGAAUGAGUACACUUUAAA – 535
Primer 730 – 750
656 – UACGGGUAGUACAACUUACAAUUGUGGUUAGUACUAUACCUUUAUGUAUGUAAGCGUAUUACCGGUGGAG – 725
Primer 841 – 861
761 – AUGUUCCUCCUAUUUAAAAACCUGCAUUAGUGCUCUUAAACGAGUGUUAUUGUGGGCCGGUACUAUUACU – 830
Primer 881 – 900
831 – UUGAACAAAUUAGAGUGCUUAAAGCAGGCUUCAAAUGCCUGAAUAUUCUGUGCAUGGGAUAAUGAAAUAA – 900
Primer 971 – 991
896 – AAUAAGACCUCUGUUCUGCUUUCAUUGGUUUUCAGAUCAAGAGGUAAUGAUUAAUAGAAGCAGUUUGGGG – 965
Primer 1530 – 1550
1461 – AGCUUAUGUAGCCUUCAUUCAUGUUGGCAGUAAAAUGCUUAUUGUGUUUGAAUGUGUUUAUGUAAGUGGA – 1530
Primer 1601 – 1621
1511 – AAUGUGUUUAUGUAAGUGGAGCCGUACCUGUUGGUUUGUCCCAUUAUAAGGACACUAGCUUCUUAAAUGG – 1580
Primer 1950 – 1970
1866 – UCUCCGGACGUGAUCACUGUGACGCCUUGCGUGUUACGGUUGUUUCGCAAAAGUUGACCGAACUUGAUUA – 1935

B. 28S rRNA

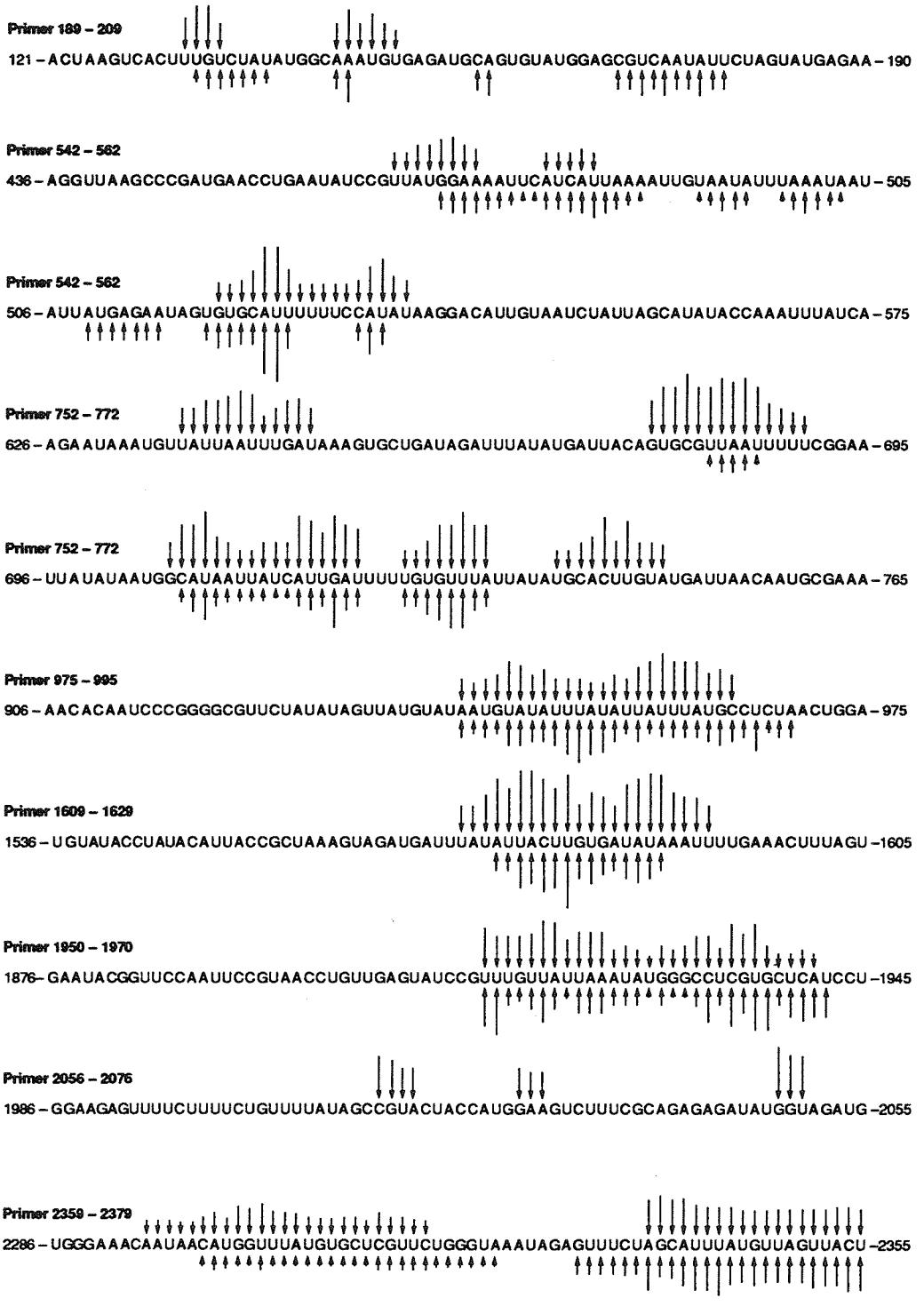
Primer 189 – 209
121 – ACUAAGUCACUUUGUCUAUAUGGCAAAUGUGAGAUGCAGUGUAUGGAGCGUCAAUAUUCUAGUAUGAGAA – 190
Primer 542 – 562
436 – AGGUUAAGCCCGAUGAACCUGAAUAUCCGUUAUGGAAAAUUCAUCAUUAAAAUUGUAAUAUUUAAAUAAU – 505
Primer 542 – 562
506 – AUUAUGAGAAUAGUGUGCAUUUUUUCCAUAUAAGGACAUUGUAAUCUAUUAGCAUAUACCAAAUUUAUCA – 575
Primer 752 – 772
626 – AGAAUAAAUGUUAUUAAUUUGAUAAAGUGCUGAUAGAUUUAUAUGAUUACAGUGCGUUAAUUUUUCGGAA – 695
Primer 752 – 772
696 – UUAUAUAAUGGCAUAAUUAUCAUUGAUUUUUGUGUUUAUUAUAUGCACUUGUAUGAUUAACAAUGCGAAA – 765
Primer 975 – 995
906 – AACACAAUCCCGGGGCGUUCUAUAUAGUUAUGUAUAAUGUAUAUUUAUAUUAUUUAUGCCUCUAACUGGA – 975
Primer 1609 – 1629
1536 – UGUAUACCUAUACAUUACCGCUAAAGUAGAUGAUUUAUAUUACUUGUGAUAUAAAUUUUGAAACUUUAGU – 1605
Primer 1950 – 1970
1876 – GAAUACGGUUCCAAUUCCGUAACCUGUUGAGUAUCCGUUUGUUAUUAAAUAUGGGCCUCGUGCUCAUCCU – 1945
Primer 2056 – 2076
1986 – GGAAGAGUUUUCUUUUCUGUUUUAUAGCCGUACUACCAUGGAAGUCUUUCGCAGAGAGAUAUGGUAGAUG – 2055
Primer 2359 – 2379
2286 – UGGGAAACAAUAACAUGGUUUAUGUGCUCGUUCUGGGUAAAUAGAGUUUCUAGCAUUUAUGUUAGUUACU – 2355

B. 28S rRNA

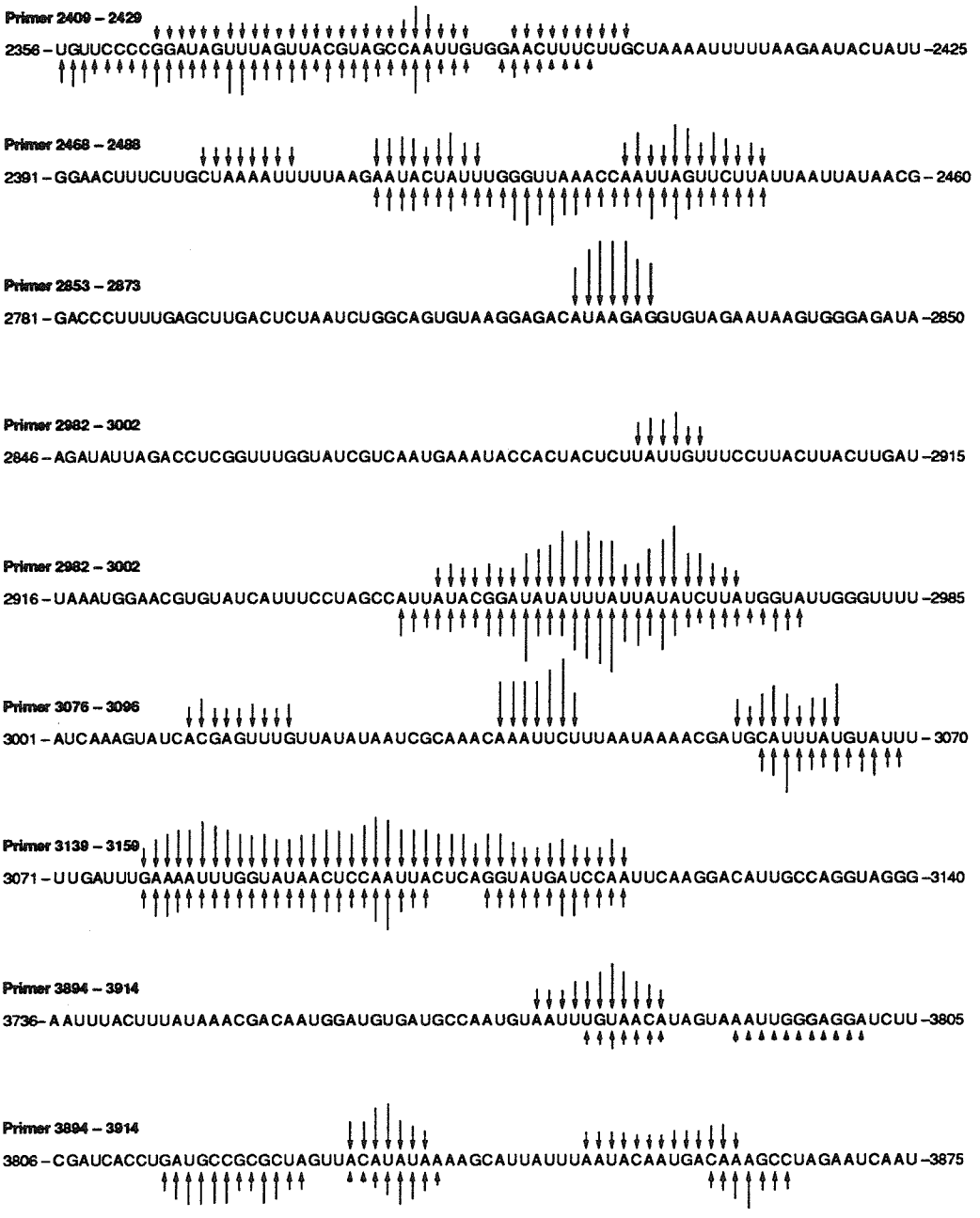
Primer 2409 – 2429
2356 – UGUUCCCCGGAUAGUUUAGUUACGUAGCCAAUUGUGGAACUUUCUUGCUAAAAUUUUUAAGAAUACUAUU –2425
Primer 2468 – 2488
2391 – GGAACUUUCUUGCUAAAAUUUUUAAGAAUACUAUUUGGGUUAAACCAAUUAGUUCUUAUUAAUUAUAACG – 2460
Primer 2853 – 2873
2781 – GACCCUUUUGAGCUUGACUCUAAUCUGGCAGUGUAAGGAGACAUAAGAGGUGUAGAAUAAGUGGGAGAUA –2850
Primer 2982 – 3002
2846 – AGAUAUUAGACCUCGGUUUGGUAUCGUCAAUGAAAUACCACUACUCUUAUUGUUUCCUUACUUACUUGAU –2915
Primer 2982 – 3002
2916 – UAAAUGGAACGUGUAUCAUUUCCUAGCCAUUAUACGGAUAUAUUUAUUAUAUCUUAUGGUAUUGGGUUUU –2985
Primer 3076 – 3096
3001 – AUCAAAGUAUCACGAGUUUGUUAUAUAAUCGCAAACAAAUUCUUUAAUAAAACGAUGCAUUUAUGUAUUU – 3070
Primer 3139 – 3159
3071 – UUGAUUUGAAAAUUUGGUAUAACUCCAAUUACUCAGGUAUGAUCCAAUUCAAGGACAUUGCCAGGUAGGG –3140
Primer 3894 – 3914
3736– AAUUUACUUUAUAAACGACAAUGGAUGUGAUGCCAAUGUAAUUUGUAACAUAGUAAAUUGGGAGGAUCUU –3805
Primer 3894 – 3914
3806 – CGAUCACCUGAUGCCGCGCUAGUUACAUAUAAAAGCAUUAUUUAAUACAAUGACAAAGCCUAGAAUCAAU –3875

Figure 5. Cleavage sites mapped on the secondary structures of (A) 18S and (B) 28S 5′-half and 3′-half rRNAs proposed by Gutell (37, 38). An additional sequence of 25 nucleotides absent in Tautz et al. (33) are presented between G217 and A243 and numbered from A218 to C242 in 28S rRNA (34). Positions of core and expansion segments are indicated according to Hancock et al. (36). Expansion segments are labeled V1 to V7 for 18S rRNA and D1 to D12 for 28S rRNA. Some expansion segments have not been modeled and thus depicted as a block of nucleotides. The region between A1814 and A1858 is processed out of the 28S rRNA gene, yielding the 28Sα and 28Sβ rRNAs. Cleavage sites by both MPE•Fe(II) and EDTA•Fe(II), only by MPE•Fe(II), and only by EDTA•Fe(II) are shown in red, in blue, and in green, respectively.

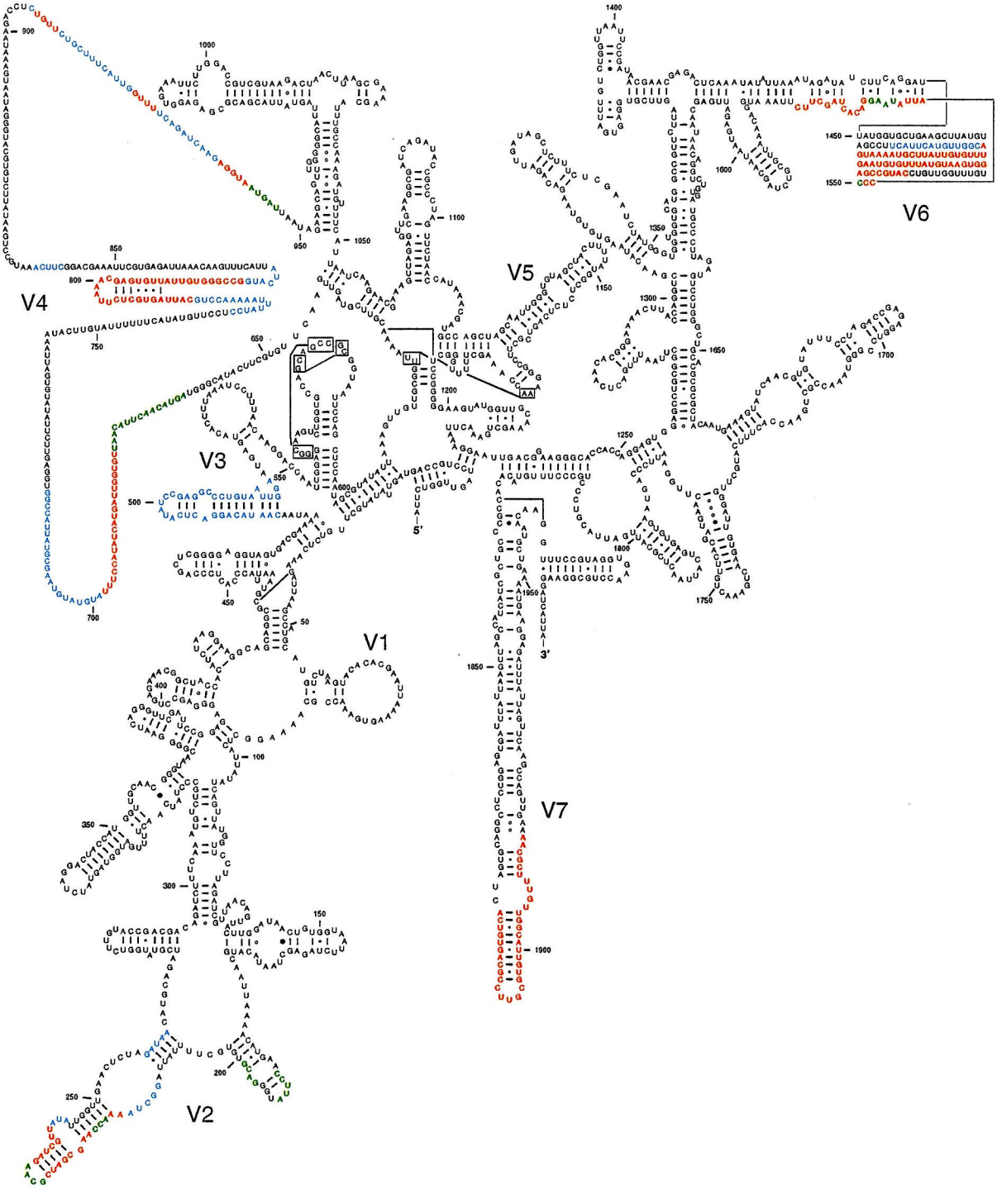
V1
V2
V3
V4
V5
V6
V7
5'
3'

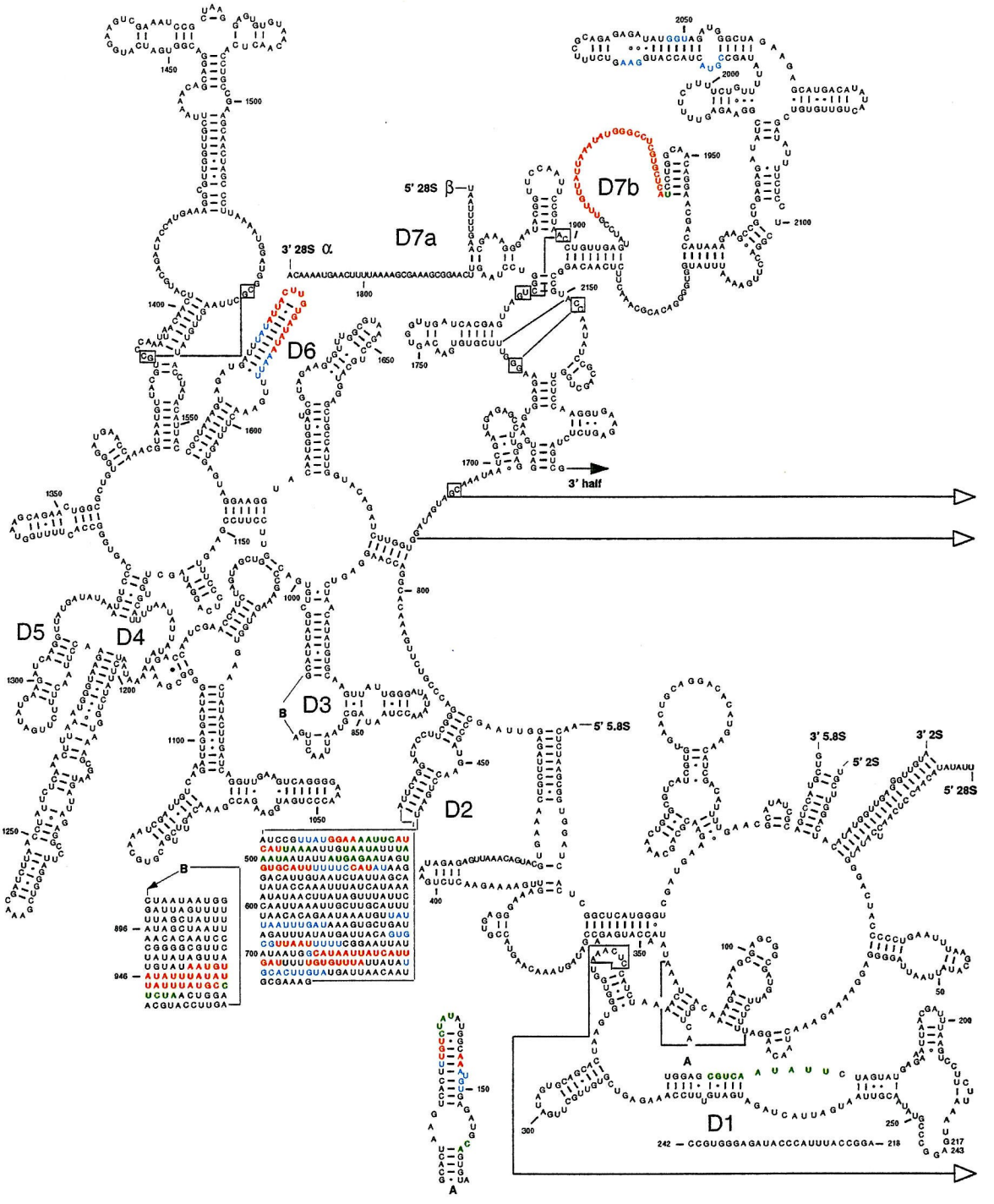
D1
D2
D3
D4
D5
D6
D7a
D7b
5' 28S β
3' 28S α
3' half
5' 5.8S
3' 5.8S
5' 2S
3' 2S
5' 28S

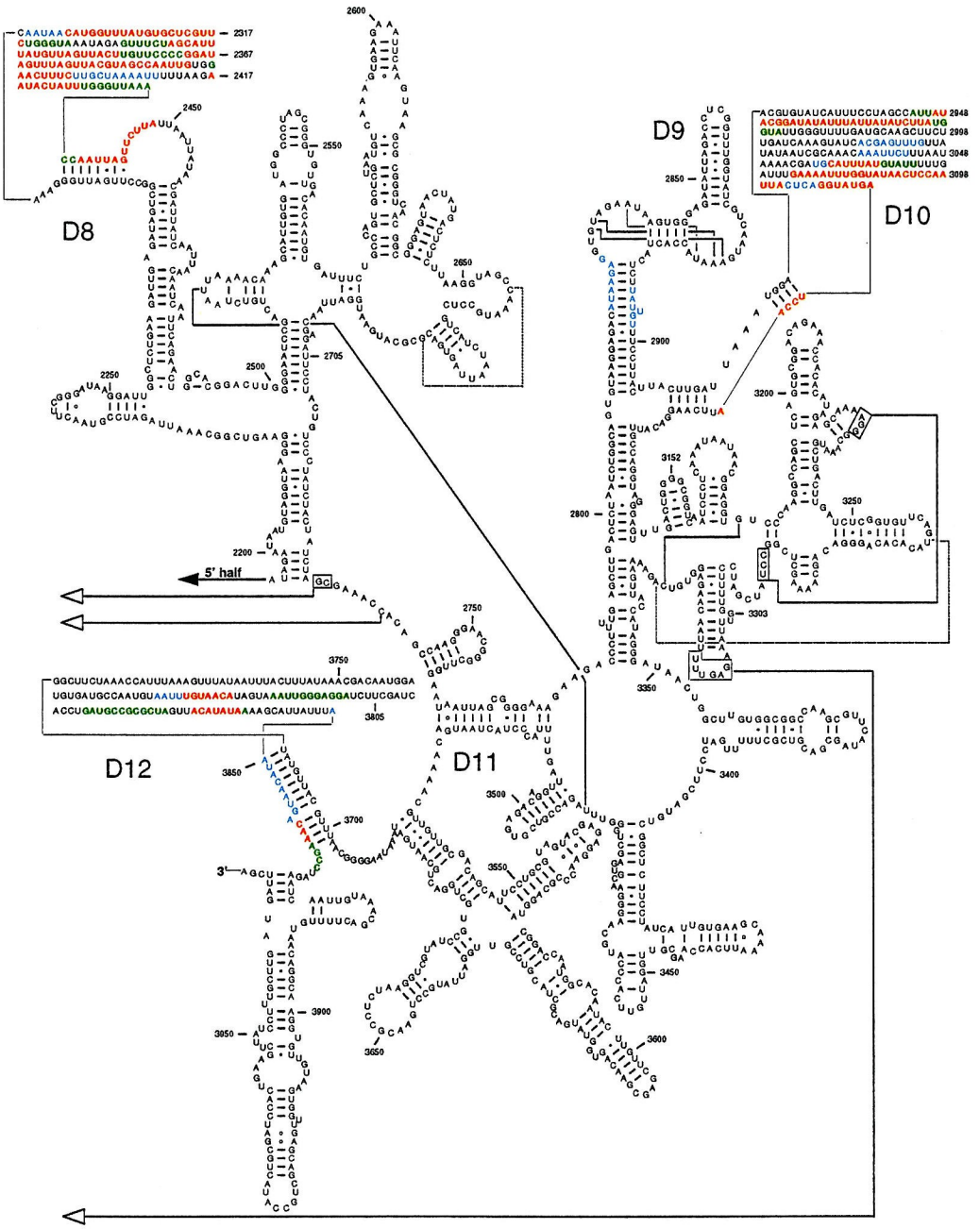
D8
D9
D10
D11
D12
5' half
3'

Figure 6. Schematic representation of (A) 18S and (B) 28S rRNAs. The positions of expansion segments are boxed in dark. Cleavage sites by MPE•Fe(II) and EDTA•Fe(II) are indicated by the black and white boxes, respectively.

A. 18S rRNA

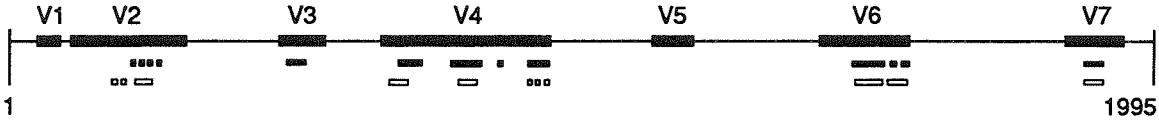

B. 28S rRNA (28Sα & 28Sβ)

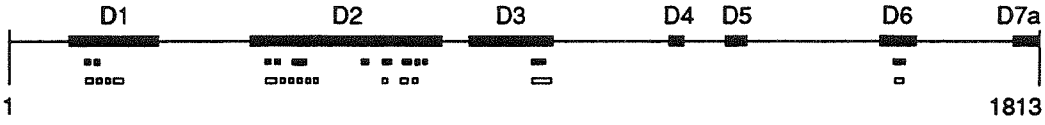

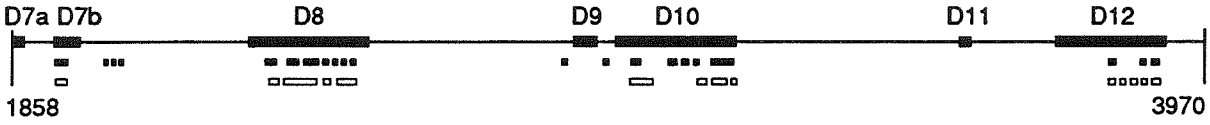

Figure 7. Cleavage sites superimposed on (A and B) two alternative secondary structures of equivalent energy and (C) the other model proposed by Hancock et al. (36) and De Rijk, et al., (42), respectively, in the region located between positions 830 and 946 of the 18S rRNA V4 domain. Filled and open circles indicate cleavage sites by MPE•Fe(II) and EDTA•Fe(II), respectively. Cleavage data favor the models A and C for the 830-946 region.

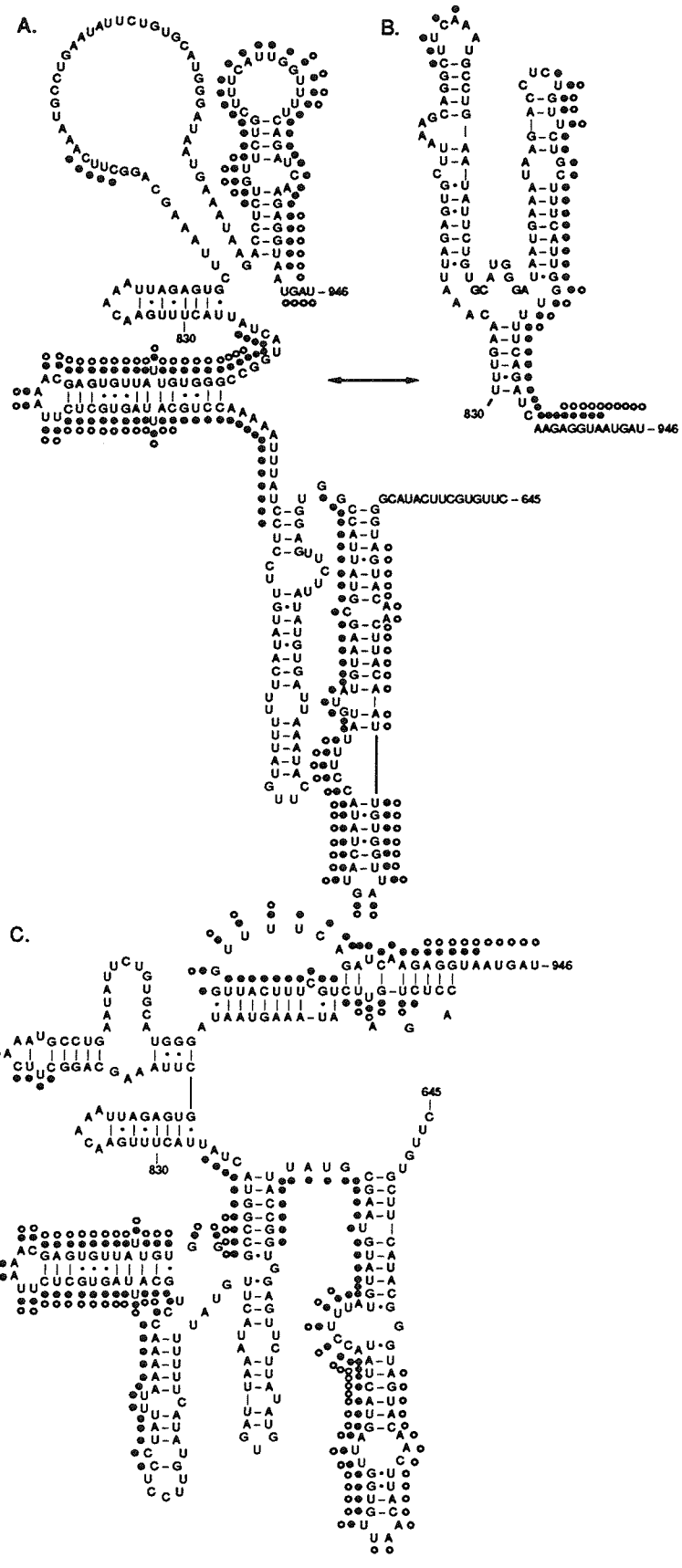
A.
B.
C.
UGAU – 946
830
AAGAGGUAAUGAU – 946
GCAUACUUCGUGUUC – 645
645

Figure 8. Cleavage sites mapped on the secondary structures of (A) 18S and (B) 28S rRNAs proposed by Hancock et al. (36). Filled and open circles indicate cleavage sites by MPE•Fe(II) and EDTA•Fe(II), respectively.

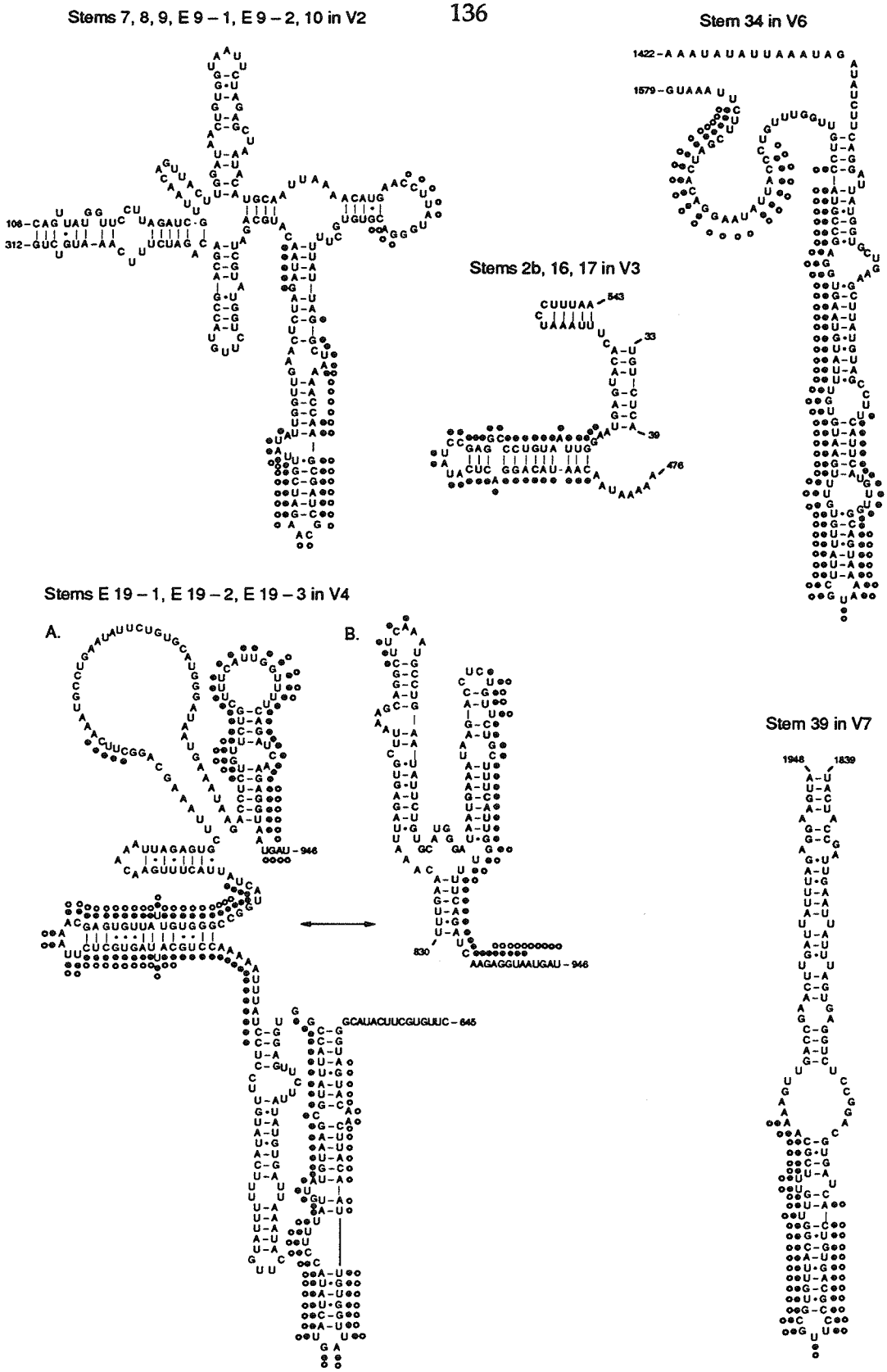
Stems 7, 8, 9, E 9 – 1, E 9 – 2, 10 in V2
Stem 34 in V6
Stems 2b, 16, 17 in V3
Stems E 19 – 1, E 19 – 2, E 19 – 3 in V4
Stem 39 in V7
A.
B.
A. 18S rRNA

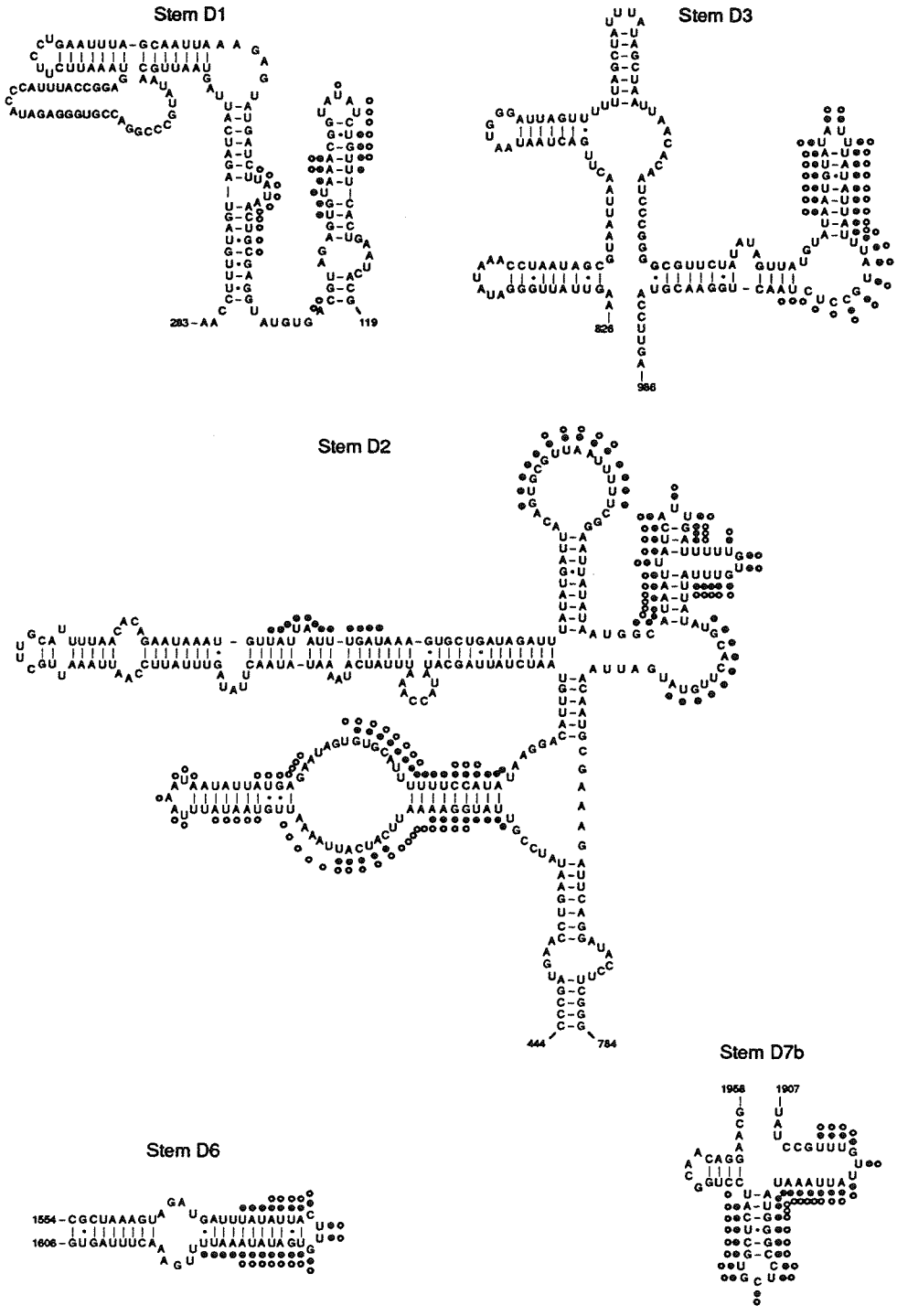

B. 28S rRNA


Stem 44
2065-UUUU UAGCC-GU CUACCAUG
2065-AGAA AUCGG UA-GAUGGUAU

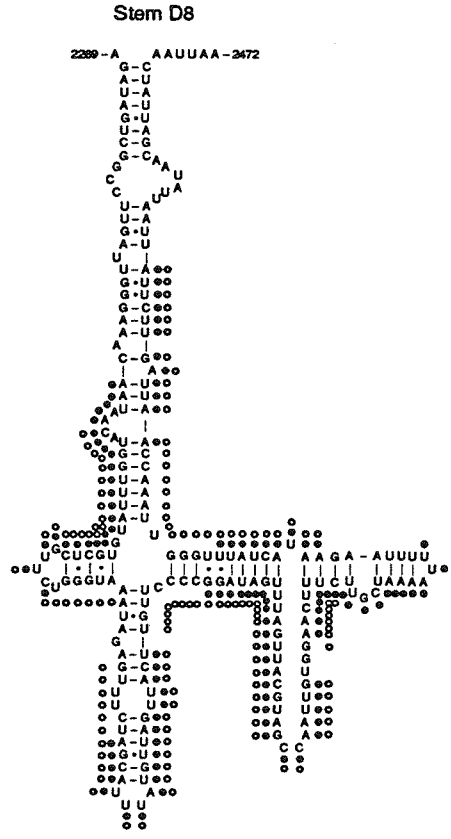
Stem D8
2289-A AAUUAA-2472

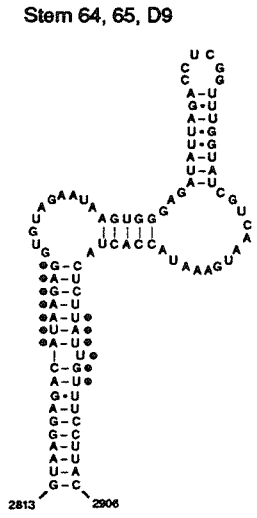
Stem 64, 65, D9
2813
2906

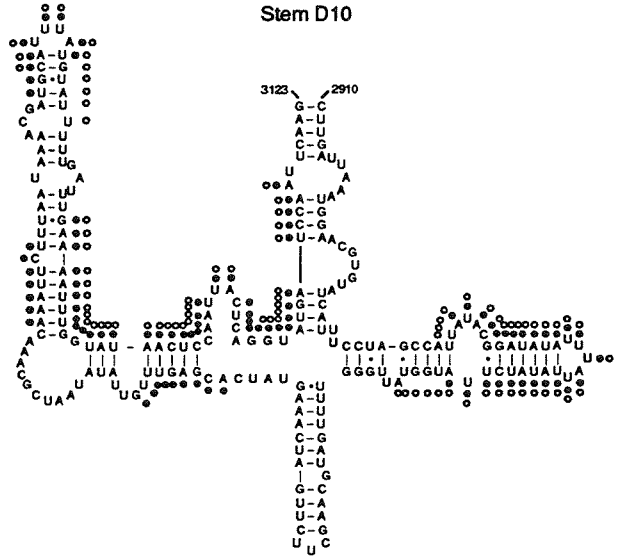
Stem D10
3123
2910

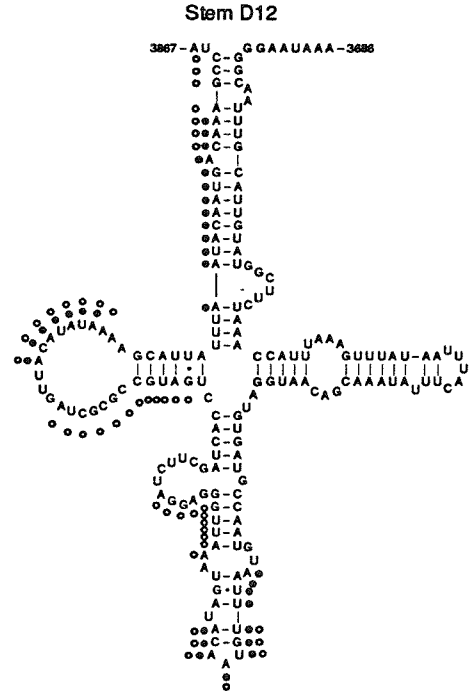
Stem D12
3867-AU GGAAUAAA-3686

B. 28S rRNA